Renewable resources derived hyperbranched polyurethane/ palladium-silver-carbon quantum dot nanocomposite

Highlight

The current chapter describes the performance of nanocomposite of renewable resource derived hyperbranched polyurethane (HPU) with palladium-silver-carbon dot (Pd-Ag@CQD) nanohybrid. The chapter is divided into two sub-chapters. The first sub-chapter, Sub-chapter 5A demonstrates the synthesis and characterization of palladium-silver-carbon dot nanohybrid, along with its catalytic application towards C-C cross coupling reaction. While the second sub-chapter, Sub-chapter 5B, describes fabrication of polyurethane nanocomposite with palladium-silver-carbon dot nanohybrid by *in situ* polymerization using three different nanohybrid loadings (0.5, 1.0 and 2.0 wt%). The fabricated nanocomposite was characterized by various spectroscopic, microscopic and analytical techniques. The nanocomposite displayed significant improvement of mechanical properties like tensile strength (2.2 fold), elongation at break (1.19 fold), toughness (3.0 fold), etc., and thermal stability (above 300 °C) over pristine hyperbranched polyurethane. The nanocomposite showed loading-dependent enhancement of mechanical and thermal properties. The HPU-supported Pd-Ag@CQD nanocomposite displayed exceptional efficiency (100% conversions, 30-60 min) as a robust and recyclable catalyst (upto 10 cycles) for rapid oxidative *ipso*-hydroxylation of aryl boronic acids to yield corresponding phenols.

Sub-chapter 5A: Synthesis, characterization and application of palladium-silver-carbon dot nanohybrid

5A.1.   Introduction

As discussed in the previous chapters, functionalization or modification of nanomaterial presents a way to customize its properties and application. In this regard, carbon nanomaterials are easily modifiable nanomaterials that can be tuned for various applications like electronics, optics, electro-chemical, catalysis and many more [1]. Carbon quantum dot (CQD) is a promising class of carbon nanomaterial that can be effortlessly functionalized or modified to suit an appropriate application. It is composed of amorphous to poorly crystalline carbon cores (predominantly graphitic sp^2 domains) with sizes varying from 2 nm to 10 nm [2]. CQD displays remarkable optical property, owing to its size and excitation wavelength-dependent photoluminescent features, which is unprecedented in most carbon nanomaterials and make them a sought-after commodity [3]. Apart from optical property, CQD exhibit a plethora of attractive properties such as excellent aqueous dispersibility, high chemical stability, good conductivity, low toxicity, biocompatibility, photostability, simple synthetic routes, etc. which offer a wide scope of applicability [2, 3]. However, even though CQD show all the hallmarks of a functional nanomaterial, its potential in the domains of catalytic applications in synthetic organic chemistry remains largely unexplored as compared to other carbon based nanomaterial like carbon nanotubes and graphene. In recent times, nanocatalysis is being widely applied in promoting synthetic organic transformations. These catalysts generally consists of nano-dimensional active components (metal/metal oxides) dispersed over a solid support. The catalytic activity, selectivity and stability of these nanocatalysts mainly depend upon their shape, size, composition and structure [4]. These nano-dimensional particles enhance the surface area of the catalyst, thereby increasing the chances of contact between the reactants and the catalyst. Moreover, their heterogeneous nature makes them relatively easily separable from the reaction mixture and thereby facilitating easy product isolation.

Now, carbon-carbon (C-C) cross couplings are one of the most relevant research topics in current synthetic chemistry. These coupling reactions provide a significant tool for the construction of many important compounds [5]. In this context, the pioneering efforts of Suzuki, Heck and Negishi towards palladium-catalyzed C-C cross coupling reactions are the benchmark for modern synthetic organic chemistry [6]. The Suzuki–Miyaura cross coupling reaction is arguably one of the most widely applied C-C bond formation reactions, till date. The aforementioned reaction provides a potent synthetic pathway for preparing

biaryl compounds, which are generally used in fields of natural products, pharmaceuticals, agro-chemicals and polymers [7]. Traditional Suzuki-Miyaura cross coupling reaction utilizes homogeneous palladium complexes with ligands (like phosphine) as catalysts [8, 9]. Despite high activity and selectivity of these catalytic systems, challenges associated with their recovery and recyclability, limit their utility in industrial process. Further, challenges in preparation, cost and use of toxic ligands (e. g. phosphine) confine the aptness of such catalysts in large-scale applications [10]. In this milieu, palladium based nanocatalysts presents a promising avenue to address these setbacks as one of the most exciting alternative catalysts in the field of C—C cross coupling reactions owing to their high activity and selectivity, compared to the conventional catalysts [11, 12]. As a matter of fact, recent reports on Pd nanoparticles catalyzed C-C cross couplings still suggest its crucial importance in this scenario [13-19]. However, major drawbacks of such nano-catalysts include aggregation of Pd nanoparticles, need for additives and stabilizers that hamper the overall reaction process. In this juncture, CQD represent an interesting choice of support, due to its high surface functionality, chemical stability in various media and inertness to supported metals. As such CQD can function as sites of nucleation and growth of nanoparticles, along with playing a pivotal role in stabilization of the metal nanoparticles.

In this purview, the synthesis of a nanohybrid system of Pd-Ag hybrid nanoparticles supported over CQDs (Pd-Ag@CQD) was reported by a facile UV light-driven reduction process using CQDs as the green reductant and stabilizer. The synthesized nanohybrid was characterized by using UV-Vis, FT-IR, EDX and TEM analyses. The Pd-Ag@CQD nanohybrid was employed as heterogeneous catalyst for promoting Suzuki-Miyaura cross coupling reactions of aryl boronic acids with aryl bromides and aryl chlorides under ligand-free and ambient conditions. The catalytic activity and proficiency of the nanohybrid were explored within the ambit of Suzuki-Miyaura cross coupling reaction.

5A.2.   Experimental

5A.2.1.   Materials

Glucose ($C_6H_{12}O_6$) was used as the precursor for preparation of carbon quantum dots. It is a monosaccharide, appearing as colorless amorphous solid with molar mass of 180.15 g mol^{-1}, density of 0.909 g cm^{-3} and melting point of 146 °C. Glucose (98% purity) was procured from Merck, India and used as received.

Palladium acetate (Pd(OAc)$_2$) was used as a precursor for the synthesis of palladium-silver-carbon quantum dot nanohybrid. It is a brownish metal salt with molecular weight of 224.5 g mol^{-1} and solubility in most organic solvents. Palladium acetate

(98% purity) was obtained from Sigma Aldrich, USA and used as received.

Silver nitrate (AgNO$_3$) was used as a precursor for the synthesis of palladium-silver-carbon quantum dot nanohybrid. It is a colorless crystalline salt with molar mass of 169.87 g mol^{-1} and density of 4.35 g cm^{-3}. Silver nitrate (98% purity) was obtained from Merck, India and used as received.

Ammonia solution of same grade and specification as mentioned in Chapter 3 (Section 3.2.1) was used to maintain a basic pH during the preparation of carbon quantum dots.

Phenyl boronic acid and its derivatives (SRL, India, and Alfa Aesar, India), and aryl bromide and its derivatives (Merck, India; Loba Chemie, India and Alfa Aesar, India) were used as substrates in the Suzuki-Miyaura C-C cross coupling reactions. Silica gel G and silica gel GF 254 (SRL, India) were used for performing thin-layer chromatography (TLC) to monitor the catalytic reactions. Silica gel 60-120 mesh (SRL, India) was used for column chromatographic purification of the crude products. Other chemicals and solvents used in the catalytic reactions include were of reagent grade and purchased from Merck, India.

5A.2.2.   Methods

5A.2.2.1.   Preparation of CQD

CQDs were prepared by a facile microwave-assisted hydrothermal process using glucose as an inexpensive, green and bio-based precursor, with slight modification of an earlier report [20]. In brief, 0.5 g of glucose was dissolved in 50 mL of deionized water in a 100 mL conical flask. A few drops of aqueous ammonia (25%) were added to the solution flask and sealed with a cotton plug. The solution flask was transferred to a domestic microwave oven operating at 600 W for 30 min. The color of the solution changed from colorless to dark brown, indicating the formation of CQDs. The as-formed CQDs were filtered and centrifuged at 6000 rpm for 30 min to separate the particle suspension. The water dispersed CQDs were collected, sonicated (acoustic power density 460 W/cm^2, 60 amplitude) for 10 min and stored under ambient conditions. The concentration of CQDs was 24 mg/mL.

5A.2.2.2.   Synthesis of Pd-Ag@CQD nanohybrid

Pd-Ag@CQD was synthesized by a facile UV-light assisted reduction process by employing CQDs as bio-based reducing as well as stabilizing agent. In a typical experiment, 5 mL of 10 mM Pd(OAc)$_2$ solution and 5 mL of 10 mM AgNO$_3$ solution in ethanol were taken in a round-bottomed flask. 10 mL of as-prepared CQDs (concentration of CQDs was 24 mg/mL) was added to the reaction mixture and it was stirred under UV light at a wavelength of 365 nm for 1 h. The formation of the Pd-Ag@CQD nanohybrid was indicated by change in the

color of the solution from greenish brown to metallic brown, along with the disappearance of the green luminescence of CQDs with advancing reaction time. The nanohybrid was collected, centrifuged at 5000 rpm and washed five times with ethanol/water to remove the excess metal salts and unbound CQDs. The obtained nanohybrid was dispersed in ethanol by ultrasonication and stored under ambient conditions. For structural analysis, the nanohybrid was oven-dried at 45 °C for 24 h under vacuum.

5A.2.2.3.   General procedure for Suzuki-Miyaura C-C cross coupling reaction

Aryl boronic acid (0.255 mmol) and aryl halide (0.25 mmol) were taken in a 50 mL round-bottomed flask and dissolved in 2 mL of EtOH-H_2O (1:1) as the solvent. To this reaction mixture, a 2 mL ethanolic dispersion of 5 wt% Pd-Ag@CQD nanohybrid (with respect to aryl boronic acid) was added, followed by addition of K_2CO_3 (1.0 mmol). The reactants were stirred under room temperature and the progress of the reaction was monitored by TLC. After completion of the reaction, the catalyst was separated from the reaction mixture by centrifugation at 5000 rpm, washed five times with ethanol/water and dried under vacuum. The crude reaction mixture was extracted with ethyl acetate (10 ml x 3), dried over anhydrous Na_2SO_4 followed by drying under reduced pressure. Isolation of the desired product was achieved by column chromatography using hexane and ethyl acetate as the eluent. The products were identified by ^{1}H and ^{13}C NMR spectroscopic analyses.

5A.2.3.   Characterization

UV-Vis, FT-IR, XRD, TEM and EDX analyses of the nanohybrid were conducted using the same instruments, same specifications and same conditions as described in Chapter 3 (Section 3.2.3). ^{1}H and ^{13}C NMR characterization of the isolated products were recorded by the same instrument and under the same conditions as mentioned in Chapter 2 (Section 2.2.3).

Surface area analysis of the nanohybrid was done by BET surface area and pore size analyzer (Model: 1000E, Quantachrome, USA). Metal leaching detection analysis of the nanohybrid was determined by inductively coupled plasma mass spectrometry (ICP-MS) (Model: NexION 2000, Perkin Elmer, USA). Yield of the products was determined from Gas chromatography (GC) analysis (Model: GC 2010, CIC, India).

5A.3.   Results and discussion

5A.3.1.   Synthesis and characterization of Pd-Ag@CQD nanohybrid

Bimetallic Pd-Ag@CQD nanohybrid was synthesized by *in situ* reduction of Pd^{2+} and Ag^+ ions with as-prepared CQDs through UV-irradiation assisted one-step wet chemical protocol, as depicted in **Scheme 5A.1**.
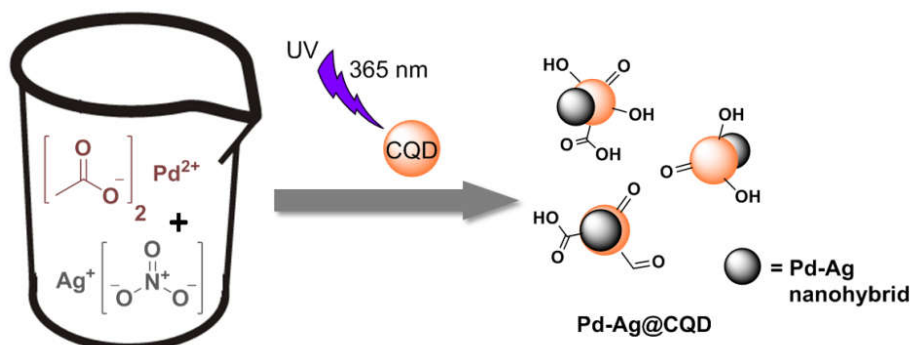
Scheme 5A.1. Synthesis of Pd-Ag@CQD nanohybrid.

It is widely reported that CQDs are capable of reducing metal salts [21-23]. In the current process, CQDs acted as both reducing as well as stabilizing agent. As reported earlier, the surface of CQDs are enriched with diverse polar functionalities such as alkoxyl, hydroxyl, epoxy, aldehydic carbonyl, carboxylic, *etc.* groups [3]. These surface functionalities facilitated the complexation of Pd^{2+} and Ag^+ ions with CQDs and subsequently helped in their reduction to Pd^0 and Ag^0. In addition, CQDs promoted nucleation-oriented growth of these nanoparticles on their surfaces and helped in their stabilization. The reduction process was greatly augmented by the excellent electron-releasing ability of photo-excited CQDs under UV radiation (λ_{exc}=365 nm), leading to dramatic decrease in reduction time. It is demonstrated earlier that photo-excited CQDs can serve as both electron donors and electron acceptors, owing to its photo-ripening capability [24, 25]. Further evidence for the reduction of Pd^{2+} and Ag^+ ions by CQDs was obtained by observing the dramatic quenching of the signatory fluorescence emissions of CQDs. This UV-light assisted fast reduction process was validated by control experiments conducted under dark and visible light, both of which recorded longer duration. Various literatures suggested the role of peripheral polar moieties, especially hydroxyl groups and aldehydic groups in the reduction of metal ions [26, 27]. In this study, presumably aldehydic, alkoxyl, epoxy and hydroxyl groups of CQDs played pivotal role in simultaneous reduction of both Pd^{2+} and Ag^+ ions. Details of the reduction mechanism and formation of the nanohybrid have been provided in **Scheme 5A.2**.
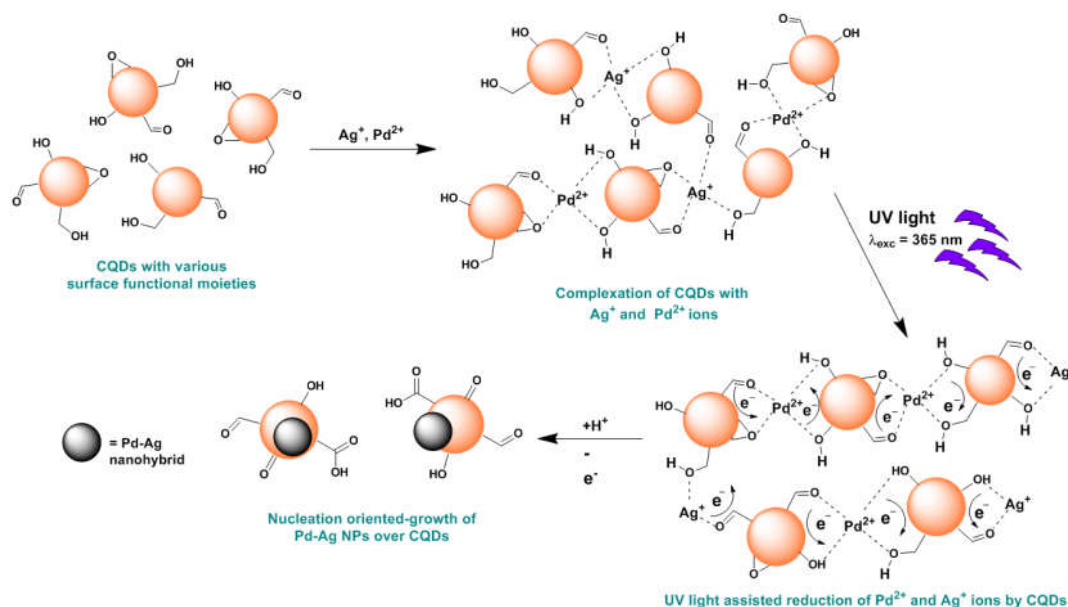
Scheme 5A.2. Mechanism of UV-light assisted reduction and subsequent formation of Pd-Ag@CQD nanohybrid.

UV-Vis study suggested the formation of Pd-Ag@CQD nanohybrid, considering the changes in absorbance from its precursors (**Figure 5A.1.a**). The characteristic absorbance peaks of CQD at 220 nm and 280 nm were either obscured or diminished, along with the absorbance peak of Pd^{2+} ion at 282 nm [16, 20]. Further, the appearance of a continuous absorbance with a weak shoulder between 300 nm and 380 nm attributed to Pd nanoparticles (Pd NPs), followed by a broad peak at 420 nm corresponding to surface plasmon resonance of Ag nanoparticles (Ag NPs) pointed towards the presence of bimetallic Pd-Ag hybrid phase. Such strong but broad surface plasmon peaks are well known in the case of various metal nanoparticles. The absorbance appears over a wide range of 200–1200 nm [28]. These results strongly indicated the role of CQDs as the reducing agent, in formation of the nanohybrid and supported the proposed reduction and formation mechanism involving nucleation and formation of Pd-Ag nanohybrid over on the surface of CQDs. FT-IR analysis further revealed key changes in the surface functionalities of CQDs before (i), during (ii) and after (iii) the formation of Pd-Ag@CQD nanohybrid (**Figure 5A.1.b**). The broad O-H stretching band of CQD, due to extensive H-bonding between the hydroxyl moieties, underwent further broadening during the complexation with Pd^{2+} and Ag^+. Ultimately, this broad O-H band underwent sharpening at 3400 cm^{-1} after formation of the nanohybrid, which indicated the strengthening of the hydroxyl functional groups, possibly stabilizing the Pd-Ag hybrid particles. The C-H stretching bands underwent similar transition during the process, before finally sharpening at 2926cm^{-1} and 2853 cm^{-1} after the formation of the

nanohybrid. Similarly, the C=O (carbonyl) stretching band of CQD endured intensification during the complexation, along with more intensification and minute shifting from 1650 cm^{-1} to 1670 cm^{-1} after formation of the nanohybrid. This plausibly indicated the oxidation of alkoxyl and hydroxyl groups to carbonyl groups on reduction of Pd^{2+} and Ag^{+}. The change in O-H bending band of CQD after formation of the nanohybrid seen at 1360 cm^{-1} further demonstrated the change in hydroxyl functional groups due to presence of the Pd-Ag hybrid particles. Further, the sharp C-O (alkoxyl) stretching band at 1044 cm^{-1} and the oxirane C-O-C stretching band at 886 cm^{-1} of CQDs diminished in due course of complexation and formation of the nanohybrid, undergoing transformation to C=O groups as described before. These changes in intensity and shifting of the band positions in the nanohybrid clearly indicated the strong interactions between CQDs and the bimetallic Pd-Ag hybrid phase. Similar observations were reported by Dey et al. [21] and Shen et al. [23]. These prominent observations pointed towards the contribution of alkoxyl, carbonyl, oxirane and hydroxyl groups in the nanohybrid formation, and thereby provided ample evidence in favor of the presumed reduction and nanohybrid formation mechanism. EDX analysis confirmed the presence of elements like C, O, Pd and Ag in the nanohybrid, with corresponding wt% values of 42.35, 29.78, 17.72 and 10.15, respectively (**Figure 5A.1.c**). XRD analysis results gave interesting evidence regarding the physical structure of nanohybrid (**Figure 5A.1.d**). The nanohybrid displayed the characteristic broad peak of CQDs centered at 2θ = 23° (*d*-spacing of 3.7 Å), indicating the presence of CQDs. Moreover, the nanohybrid exhibited five sharp diffractions indexed as (111), (200), (220), (311) and (222) planes of a face-centered-cubic (fcc) lattice with corresponding peaks at 2θ = 38.2° (*d*-spacing of 2.29 Å), 44.5° (*d*-spacing of 1.98 Å), 64.6° (*d*-spacing of 1.40 Å), 77.5° (*d*-spacing of 1.19 Å) and 81.8° (*d*-spacing of 1.14 Å) respectively. Pd NPs and Ag NPs are known to exhibit the typical face-centered-cubic (fcc) lattice of Pd and Ag metal [14]. Surprisingly, no characteristic diffraction peaks for pure Pd or Ag were observed for the nanohybrid. This phenomenon suggested that Ag entered into the Pd crystal lattice, merging together to form a single crystalline Pd-Ag hybrid phase possibly during nucleation-oriented growth over CQDs [29, 30].
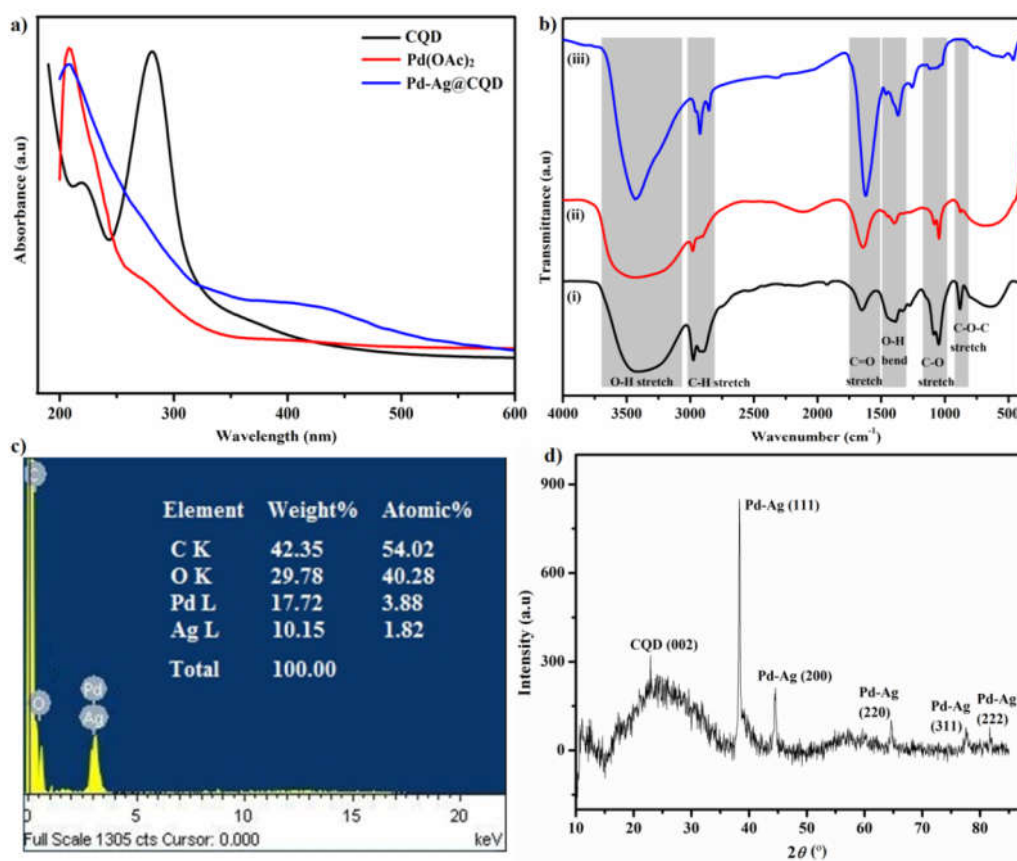
Figure 5A.1. a) UV spectra of CQD, Pd(OAc)$_2$ and Pd-Ag@CQD nanohybrid, **b)** FT-IR spectra of (i) CQD, (ii)Pd^{2+}-Ag$^+$-CQD complex and (iii) Pd-Ag@CQD nanohybrid, **c)** EDX map of Pd-Ag@CQD nanohybrid, and **d)** XRD patterns of Pd-Ag@CQD nanohybrid.

Morphological characteristics of the nanohybrid including shape, size and particle distribution envisioned by TEM analysis, and confirmed the presence of Pd-Ag nanohybrid particles supported over CQDs. TEM images displayed near-spherical morphology and uniform particle distribution of the nanohybrid, albeit some amount of agglomeration (**Figure 5A.2.a**). The Pd-Ag nanohybrid particles (in red circles) nucleated upon CQDs (in yellow circles), thereby forming a stable and supportive nanohybrid system (**Figure 5A.2.b**). Statistical analysis revealed that the size distribution lies between 2-6 nm and the largest fraction of particles possessed size in the range of 3-5 nm (**Figure 5A.2.c**). HRTEM images of Pd-Ag@CQD further showed the presence of lattice fringes (**Figure 5A.2.d** and **5A.2.e**). Conversion of selected area (in yellow and red squares) into corresponding IFFT images revealed different inter-planar distances (inset). The inter-planar distance of 0.364 nm was attributed to lattice planes of CQDs, which is close to the (002) crystallographic plane of CQDs, while the inter-planar distances of 0.185 nm and 0.145 nm were attributed to lattice planes of Pd-Ag nanohybrid phase, which is close to (200) and (220) planes of Pd-

Ag hybrid [29, 30]. Selected area electron diffraction (SAED) patterns of the nanohybrid (**Figure 5A.2.f**) are in good agreement with the crystalline Pd-Ag nanohybrid phase, which were also consistent with powdered X-ray diffraction (XRD) pattern results.
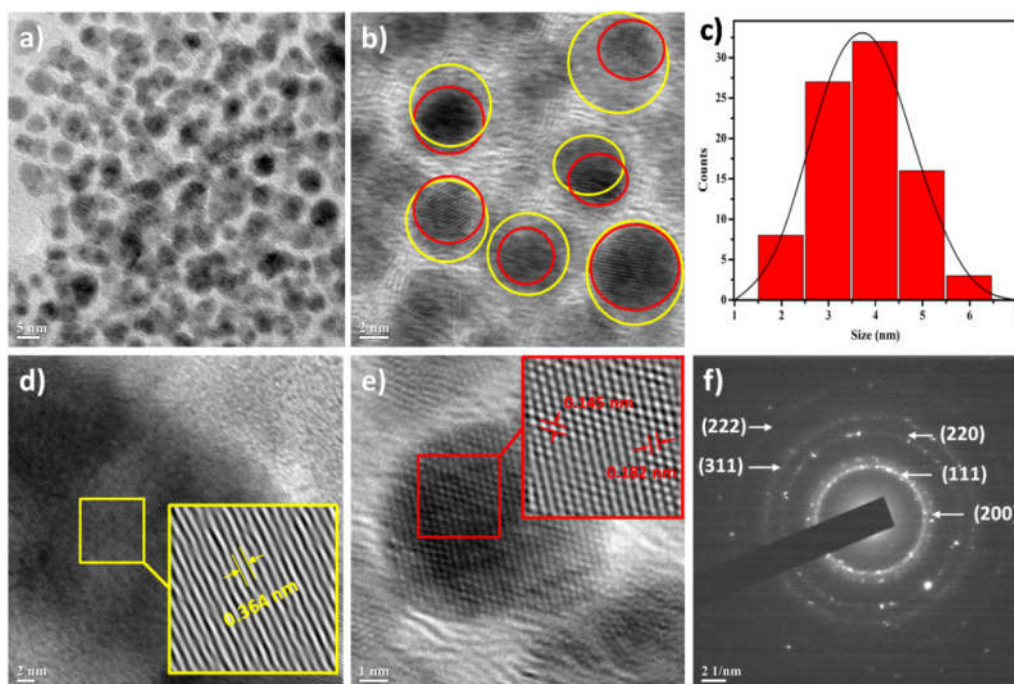

Figure 5A.2. a)-b) TEM images of Pd-Ag@CQD, **c)** size distribution of Pd-Ag@CQ, **d)** HRTEM of CQD phase (inset: IFFT image of selected area of CQD phase), **e)** HRTEM of Pd-Ag nanohybrid phase (inset: IFFT image of selected area of Pd-Ag hybrid phase), and **f)** SAED pattern of Pd-Ag@CQD.

5A.3.2.   Catalytic application of Pd-Ag@CQD nanohybrid in Suzuki-Miyaura C-C cross coupling reaction

The catalytic activity of Pd-Ag@CQD nanohybrid was evaluated in the Suzuki-Miyaura cross coupling reaction. For this purpose, the coupling of 4-ethylphenylboronic acid with 4-bromoanisole was chosen as the model reaction using ethanol-water (1:1) as the solvent system and K_2CO_3 as the base. 1 wt% of the Pd-Ag@CQD nanohybrid, with respect to 4-ethylphenylboronic acid, was employed as the catalyst. The reactions were performed at room temperature under aerobic conditions, without the addition of any ligands or additives (**Scheme 5A.3**). The reaction afforded 4-ethyl-4'-methoxy-1,1'-biphenyl with70% yield in 4 h. For this reaction, ethanol/water mixture (1:1) provided a highly polar co-solvent system in which the substrates were easily homogenized and thus acts as a stable dispersion medium for the nanohybrid catalyst. Moreover, the choice of ethanol/water

solvent offered a neat and green reaction medium. In similar lines, the choice of K_2CO_3 presented a mild, inexpensive, effective base necessary for the cross coupling reaction.
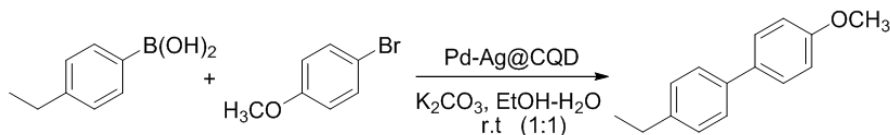
Scheme 5A.3. Model reaction for Pd-Ag@CQD catalyzed Suzuki-Miyaura cross coupling.

To study the effect of catalyst loading on the reaction rate and its efficiency, optimization of the catalyst loading was performed using the model reaction and the results are summarized in **Table 5A.1**.

Table 5A.1. Effect of catalyst loading on Suzuki-Miyaura coupling reaction

Entry	Catalyst loading[a] (wt%)	Time (h)	Yield[b] (%)
1	-	12	-
2	1	4	70
3	2.5	3	85
4	5	1	94
5	7.5	1	94
6	10	1	89

Reaction conditions: 4-ethylphenylboronic acid (0.255 mmol, 0.0379 g), 4-bromoanisole (0.25 mmol, 0.0467 g), K_2CO_3 (1.0 mmol, 0.138 g), EtOH-H_2O (4 ml). [a]wt% with respect to 4-ethylphenylboronic acid. [b]isolated yield.

From this study, it was observed that the catalyst loading is essential for the reaction to proceed (Table 5A.1, Entry 1). Also, it was seen that the catalyst loading affected the reaction rate, in correlation to reaction time and product yield (Table 5A.1, Entry 2-5). Further, it was found that catalytic loading of 5 wt% was the optimized amount for the coupling reaction (Table 5A.1, Entry 4), as further increase in catalyst loading to 7.5 wt% did not have any substantial increment in reaction rate and its efficiency (Table 5A.1, Entry 5). Catalytic loading of 10 wt% eventually led to the decrease in the yield, with some amount of agglomeration observed in the reaction medium (Table 5A.1, Entry 6). This also may be caused by adsorption of some amount of reactants on the surface of the catalyst. In order to determine the applicability and limitation of the current procedure, reactions of different aryl boronic acid derivatives with substituted/unsubstituted aryl bromides and aryl chlorides were examined using the optimized conditions. Aryl bromides/chlorides

were chosen for this purpose as activation of C-Br or C-Cl bonds are tougher than C-I bonds [6]. The results are summarized in **Table 5A.2**.

Table 5A.2. Substrate study for Pd-Ag@CQD catalyzed Suzuki-Miyaura coupling reaction
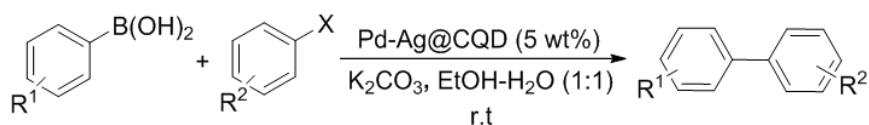
Entry	R^1	R^2	X	Time (h)	Yield^a (%)
1a	H	H	4-Br	1	97
1b	H	$4-OCH_3$	4-Br	1	94
1c	H	$4-NO_2$	4-Br	1.2	90
1d	CH_2CH_3	H	4-Br	1	92
1e	CH_2CH_3	$4-OCH_3$	4-Br	1	94
1f	$3-NO_2$	H	4-Br	1.4	90
1g	$3-CF_3$	$4-OCH_3$	4-Br	1.8	83
1h	$3-NO_2$	$4-NO_2$	4-Br	3	74
1i	2-naphthyl	$4-OCH_3$	4-Br	1	92
1j	$4-OCH_3$	4-OH	4-Br	1	90
1k	H	H	4-Cl	24	25
1l	CH_2CH_3	H	4-Cl	16	30

Reaction conditions: aryl boronic acid (0.255 mmol), aryl halide (0.25 mmol), K_2CO_3 (1.0 mmol, 0.138 g), EtOH-H_2O (4 ml), Pd-Ag@CQD (5 wt% with respect to aryl boronic acid). ^{a}isolated yield, purified by column chromatography and authenticated by NMR analyses (Page 5-18–5-30).

From the substrate study, it was observed that rate of the Suzuki-Miyaura cross coupling reaction depends on the nature of substituents and their inductive effects on both the aryl halides and aryl boronic acids. The presence of electron releasing substituents on the aryl boronic acid as well as on aryl halides required less time to complete, whereas, those with electron withdrawing substituents took a little longer duration for completion. This may be due to the presence of polar electron releasing moieties on the surface of nanohybrid catalyst (from CQDs), which facilitated better interactions with the substrates having electron releasing groups than that of those with electron withdrawing groups. Borah et al. [16], as well as Dey et al. [21], reported comparable observations regarding the effect of

substituents. In most of the cases, cross-coupling products were exclusively encountered and homo-coupling product was either not observed or did not exceed 3% in some cases.

The reusability of the catalyst is very important from the perspective of green and sustainable chemistry. Accordingly, the catalyst was screened for reusability by employing the model reaction for consecutive runs (**Figure 5A.3**). The procedure afforded completion of the reaction in comparable reaction time and product yield during first three runs, as that for fresh catalyst. The catalyst was found to be reusable up to third run without any loss of the catalytic activity. However, the catalyst demonstrated some amount of agglomeration in the reaction medium after the fourth run, with slight loss in catalytic activity as manifested by decrease in product yield. This slight loss of activity can be attributed to the agglomeration of the nanohybrid, leading to deactivation of catalytic system after several runs of the reaction and recovery process. Similar observations were made by Moussa et al. [14], Borah et al. [16], and Dey et al. [21] regarding agglomeration of nanoparticles in the reaction medium on subsequent catalytic cycles.
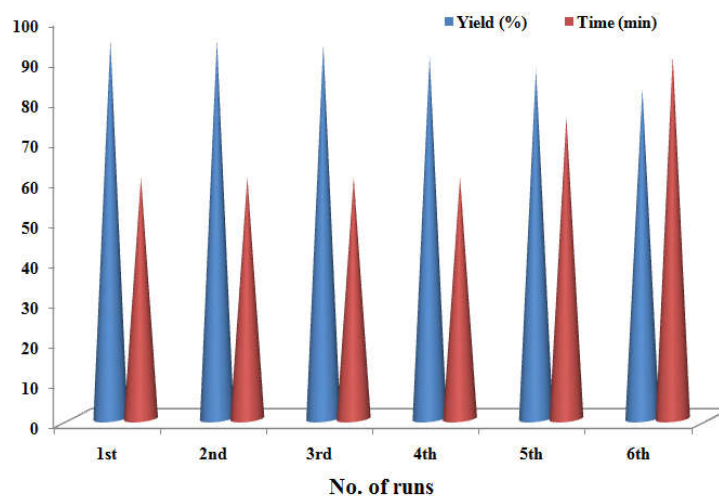
Figure 5A.3. Catalyst reusability, in terms of yield and time.

In order to verify any change in the structure and morphology after undergoing several runs, the recovered catalyst was analyzed by XRD. The results, in general, hinted towards intact state and structure of the catalyst, as supported by the appearance of previously observed diffraction patterns for the Pd-Ag@CQD nanohybrid (**Figure 5A.4.a**). Also, the EDX study of the recovered catalyst displayed almost the same elemental composition as seen before (**Figure 5A.4.b**). In addition, the leaching of Pd and Ag in the reaction medium was studied by ICP analysis. The study disclosed the leakage of 0.871 ppm Pd and 0.520 ppm Ag in the reaction mixture, amounting to loss of 0.058% Pd and 0.034% Ag from the total amount of catalyst. These results suggested the presence of trace amounts

of Pd and Ag in the reaction medium; but since the amount was less than 1 ppm, the leakage can be treated as very minute. Calculations of turnover number (TON) and turnover frequency (TOF) revealed the highest TON and TOF of 752.3 and 12.53 min^{-1} for Pd-Ag@CQD catalyzed cross coupling reaction.
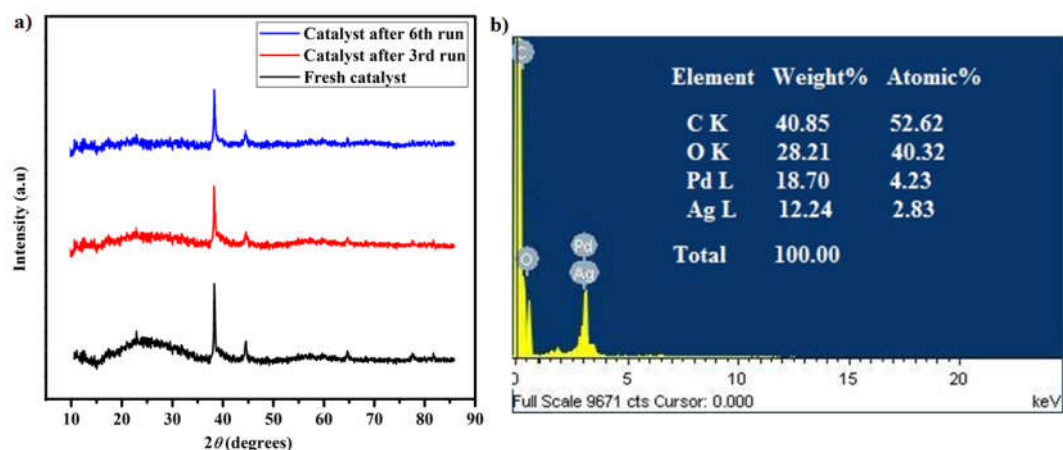
Figure 5A.4. a) XRD patterns of recovered catalyst, and **b)** EDX map of recovered catalyst.

The mechanism of the C-C cross coupling reactions catalyzed by heterogeneous palladium catalysts is a subject of great scientific interest, as to identify the exact species responsible for the catalysis [7]. However, it is widely accepted that the mechanism follows a heterogeneous catalytic cycle. To test the heterogeneity of the catalyst, the model reaction was again performed under the optimized reaction conditions and the yield monitored by GC after a definite interval of time (**Figure 5A.5.a**). After 0.5 h, an isolated yield of 65% was obtained, following which the reaction mixture was carefully filtered off and the filtrate was
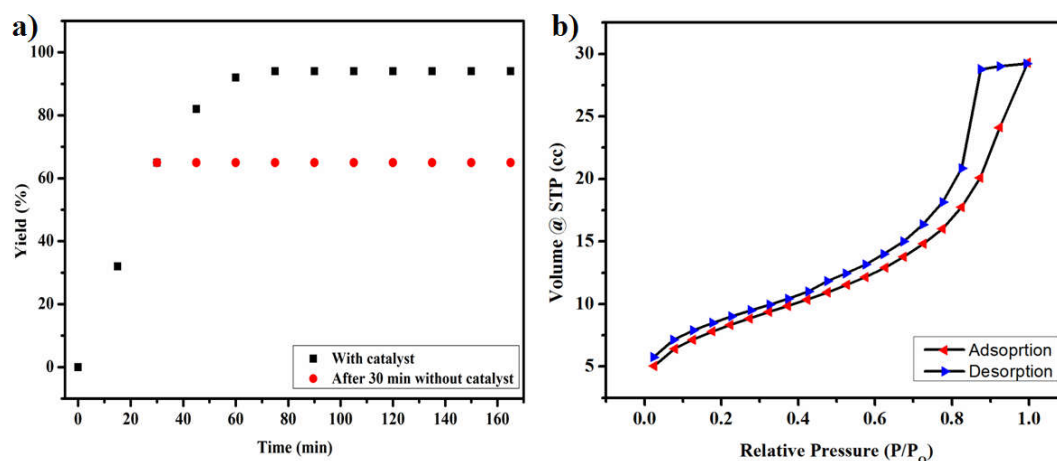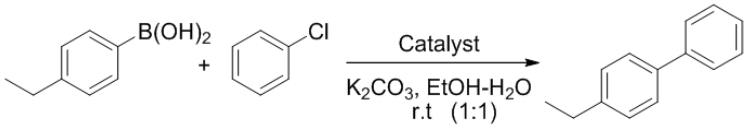
Figure 5A.5. a) Hot filtration test for heterogeneity of the catalyst and, **b)** N$_2$ adsorption-desorption isotherm of the catalyst.

allowed to react for an additional 12 h. However, no significant increase in the yield of the cross-coupled product was observed, which suggested the heterogeneity of the catalyst. Additionally, surface area analysis of the nanohybrid by BET measurements revealed a very high surface area of 674.327 $m^2 g^{-1}$ of the nanohybrid. The corresponding N_2 adsorption-desorption isotherm of the nanohybrid (**Figure 5A.5.b**) catalyst displayed a type V isotherm with a hysteresis loop, very typical of mesoporous materials.

From the catalyst optimization study and substrate study, it was seen that the Suzuki-Miyaura cross coupling reaction was greatly enhanced by Pd-Ag@CQD nanohybrid in terms of reaction time and yield. In order to explain the basis of this enhancement, i.e. the role of the components in the nanohybrid system, the reaction was emulated with the different variants of the catalyst *viz.* CQDs, AgNP, PdNPs and the results are summarized in the **Table 5A.3.** For this purpose, the Suzuki-Miyaura cross coupling reaction of aryl boronic acid derivative and aryl chloride was chosen to be the model reaction. This is because, since the reaction with aryl bromides were comparatively faster and easier, the toughest reaction conditions i.e. with aryl chlorides were emulated for better understanding of the role of the catalyst in the cross coupling reaction. From the study, it was observed that the reaction did not proceed in the presence of only CQDs as the catalyst (Entry 1). The similar observation was made when only AgNPs were used in catalytic amounts (Entry 2). Both of these initial observations can be attributed to the inability of CQDs and AgNPs to singlehandedly catalyze the reaction. On the other hand, when only PdNPs were used, the reaction proceeded sluggishly with very low yield of 16% (Entry 3). This can be accredited to the difficulty in activation of C-Cl bond of aryl chloride under the current reaction conditions. Hence, this outcome necessitates the presence of palladium for the reaction to proceed. Again, when both PdNPs and AgNPs were used in tandem, slight better yield of 22% was recorded (Entry 4). This pointed towards the role of AgNPs in assisting PdNPs for catalyzing the reaction and signified the catalytic enhancement brought about by the combination of the two. The reaction was not successful with combination of AgNP and CQDs (Entry 5), as observed earlier. However, the combination of PdNPs and CQDs afforded better results with reduced reaction time and an increased yield of 20% (Entry 6). Hence, the presence of CQDs in tandem with PdNPs resulted in the catalytic enhancement of the reaction too. Now, when PdNPs, AgNPs and CQDs were used together, the reaction time decreased further and the yield of 25% was recorded (Entry 7). The outcome suggested the synergistic ability of CQDs and AgNPs in assisting PdNPs in the catalytic enhancement of the cross coupling reaction. This result was comparable to Pd-Ag@CQD nanohybrid system, which recorded the minimum time with maximum yield (Entry 8).

Table 5A.3. Study of the role of components of the nanohybrid for Suzuki-Miyaura cross coupling

Entry	Catalyst	Time (h)	Yield (%)[a]
1	CQDs[d]	24	NR
2	AgNPs[c]	24	NR
3	PdNPs[b]	32	16
4	PdNPs[b]+AgNPs[c]	32	22
5	AgNPs[c]+CQDs[d]	24	NR
6	PdNPs[b]+CQDs[d]	24	20
7	PdNPs[b]+AgNPs[c]+CQDs[d]	22	25
8	Pd-Ag@CQD[b]	16	30

[a]Isolated yield. [b]5wt% with respect to phenyl boronic acid derivative. [c]5wt% with respect to phenyl boronic acid derivative. [d]2 wt% with respect to phenyl boronic acid derivative.

Hence, it can be suggested that Ag and CQD played a pivotal role in stabilization and activation of Pd in the nanohybrid, thereby providing crucial assistance during the catalytic process. The integration of Pd with Ag in the nanohybrid augmented the activity of Pd, by virtue of synergistic metal-metal interactions and thereby making energetic electron transfer process feasible between them [31]. Additionally, CQDs with its surface functional moieties served as the reaction surface by means of secondary interactions like π-π interactions, H-bonding, etc. with the reactants, especially during the oxidative addition and transmetallation steps (**Scheme 5A.4**). The rate-determining step in the Suzuki–Miyaura cross coupling reaction, the oxidative addition step, may be accelerated by the activated Pd species, leading to the enrichment of inherent catalytic activity of the reaction. Furthermore, the energy released during electron transfer to the surrounding environment probably contributed to the enhancement of catalytic activity [31]. Thus, overall these observations clearly exhibited that the enhanced activity in the Suzuki Miyaura cross coupling reaction might be attributed to the synergistic effect between Pd-Ag hybrid nanoparticles adjacently existing with each other, supported over CQDs.
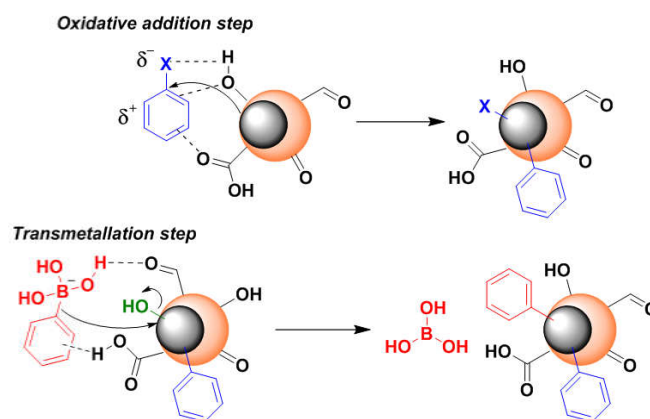
Scheme 5A.4. Synergistic role of Pd-Ag@CQD nanohybrid in the Suzuki-Miyaura cross coupling reaction.

5A.4.   Conclusion

Photo-activated CQDs can be used as the reducing and stabilizing agent for synthesis of Pd-Ag@CQD nanohybrid by a facile and expeditious single step protocol. Structural analyses confirmed the formidable structural integration of CQDs with Pd-Ag hybrid nanoparticles in the nanohybrid system. Most interestingly, the Pd-Ag@CQD nanohybrid served as an effective heterogeneous catalyst for Suzuki Miyaura cross coupling reaction under normal atmosphere and ligand-free conditions. The synergistic action of the components in the nanohybrid induced catalytic enhancement of the cross coupling reaction, in terms of short reaction time and high yield. The heterogeneous nature of the nanohybrid enabled catalyst recovery and reusability.

NMR spectral data of the products of Table 5A.2

1,1'-biphenyl (Table 5A.2, Entry 1a)
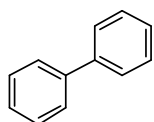
^{1}H NMR (400 MHz, CDCl$_3$): δ_H(ppm) 7.62 (m, 4H), 7.47 (m, 4H), 7.37 (m, 2H); ^{13}C NMR (100 MHz, CDCl$_3$): δ_C (ppm) 141.34, 128.88, 127.37, 127.29.

4-methoxy-1,1'-biphenyl (Table 5A.2, Entry 1b)
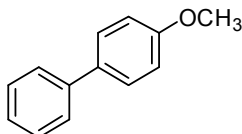
^{1}H NMR (400 MHz, CDCl$_3$): δ_H (ppm) 7.55 (t, *J* = 8 Hz, 4H), 7.42 (t, *J* =8 Hz, 2H), 7.32 (m, 1H) 6.99 (d, *J* = 8 Hz, 2H), 3.85 (s, 3H); ^{13}C NMR (100 MHz, CDCl$_3$): δ_C (ppm) 159.22, 140.91, 133.86, 128.83, 128.26, 128.27, 126.84, 126.76, 114.29, 55.44.

4-nitro-1,1'-biphenyl (Table 5A.2, Entry 1c)
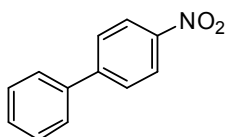
^{1}H NMR (400 MHz, CDCl$_3$): δ_H (ppm) 8.30 (m, 1H), 7.91(m, 4H), 7.73 (m, 1H), 7.61 (m, 1H), 7.47 (m, 2H); ^{13}C NMR (100 MHz, CDCl$_3$): δ_C 147.71, 138.78, 138.74, 129.23, 128.99, 127.87, 127.46, 124.96, 124.94, 124.92, 124.18, 102.72, 100.00.

4-ethyl-1,1'-biphenyl (Table 5A.2, Entry 1d)
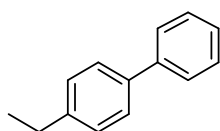
^{1}H NMR (400 MHz, CDCl$_3$): δ_H (ppm) 7.60 (m, 2H), 7.54 (m, 2H), 7.45 (m, 2H), 7.31 (m, 3H), 2.72 (q, *J* = 8 Hz, 2H), 1.30 (t, *J* = 8 Hz, 3H); ^{13}C NMR (100 MHz, CDCl$_3$): δ_C (ppm)143.51, 141.30, 138.72, 128.83, 128.42, 127.20, 127.14, 127.09, 28.64, 15.75.

4-ethyl-4'-methoxy-1,1'-biphenyl (Table 5A.2, Entry 1e)
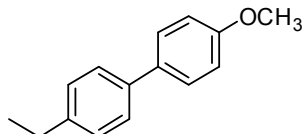
^{1}H NMR (400 MHz, CDCl$_3$): δ_H (ppm) 7.56 (m, 4H), 7.30 (d, *J* =8 Hz, 2H), 7.01 (m, 2H), 3.88 (s, 3H), 2.74 (q, *J* = 8 Hz, 2H), 1.33 (t, *J* = 8 Hz, 3H); ^{13}C NMR (100 MHz, CDCl$_3$): δ_C (ppm) 159.01, 142.84, 138.31, 133.87, 128.33, 128.08, 128.08, 126.75, 114.23, 55.42, 28.56, 15.71.

3-nitro-1,1'-biphenyl (Table 5A.2, Entry 1f)
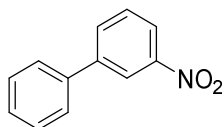
^{1}H NMR (400 MHz, CDCl$_3$) δ_H (ppm) 8.45 (s, 1H), 8.19 (d,*J* = 8 Hz, 1H), 7.91 (d,*J* = 8 Hz, 1H), 7.61 (m, 3H), 7.48 (m, 2H), 7.43 (m, 1H);^{13}C NMR (100 Hz, CDCl$_3$) δ_C(ppm) 148.83, 142.97, 138.76, 133.12, 129.79, 129.25, 128.63, 127.25, 127.23, 122.12, 122.05.

### 4'-methoxy-3-(trifluoromethyl)-1,1'-biphenyl (Table 5A.2, Entry 1g)
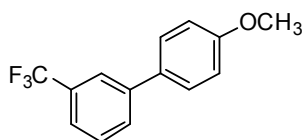
^{1}H NMR (400 MHz, CDCl$_3$): δ_H (ppm)7.79 (s, 1H), 7.72 (d, J = 8 Hz, 1H), 7.53(m, 4H), 7.00 (m, 2H), 3.86 (s, 3H); ^{13}C NMR (100 MHz, CDCl$_3$) δ_C (ppm) 159.80, 141.68, 132.30, 131.66, 131.34, 131.02, 130.71, 130.01, 129.26, 128.33, 123.57, 123.53, 123.49, 123.39, 123.35, 123.31, 114.51, 55.44.
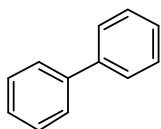
3,4'-nitro-1,1'-biphenyl (Table 5A.2, Entry 1h)
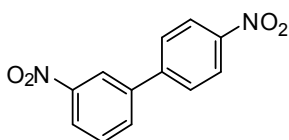
^{1}H NMR (400 MHz, CDCl$_3$): δ_H (ppm) 8.48 (s, 1H), 8.35 (m, 2H), 8.29 (m, 1H), 7.95 (m, 1H), 7.79 (m, 2H), 7.69 (t, J = 8.0 Hz, 1H); ^{13}C NMR (100 MHz, NMR (400 MHz, CDCl$_3$): δ_C (ppm)147.71, 138.74, 129.23, 128.99, 127.87, 127.46, 124.94, 124.92, 124.18, 102.72, 100.00.

2-(4-methoxyphenyl)naphthalene (Table 5A.2, Entry 1i)
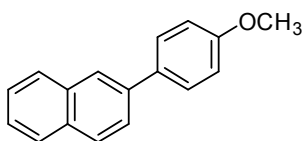
^{1}H NMR (400 MHz, CDCl$_3$): δ_H (ppm) 7.99 (s, 1H), 7.87 (m, 3H), 7.71 (dd, *J* =8 Hz, 1H), 7.65 (m, 2H), 7.47 (m, 2H), 7.02 (m,2H) 3.87 (s, 3H); ^{13}C NMR (100 MHz, CDCl$_3$): δ_C (ppm) 159.32, 133.83, 133.71, 132.39, 128.55, 128.52, 128.44, 128.14, 127.71, 126.33, 125.74, 125.53, 125.12, 114.40. 55.48.

4'-methoxy-(1,1'-biphenyl)-4-ol (Table 5A.2, Entry 1j)
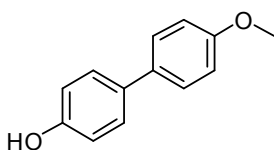
^{1}H NMR (400 MHz, CDCl$_3$): δ_H (ppm) 7.44 (m, 4H), 7.04 – 6.89 (m, 2H), 6.90 – 6.80 (m, 2H), 4.85 (s, 1H), 3.83 (s, 3H); ^{13}C NMR (100 MHz, CDCl$_3$): δ_C (ppm) 158.68, 154.57, 133.53, 133.51, 128.05, 127.73, 115.38, 114.17, 55.16.
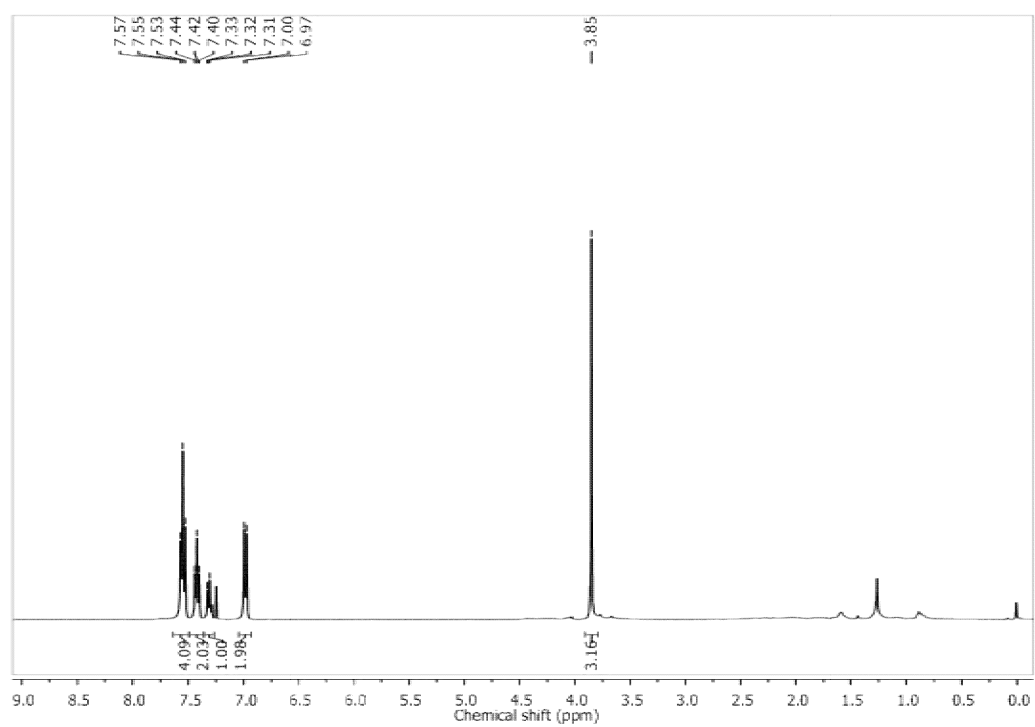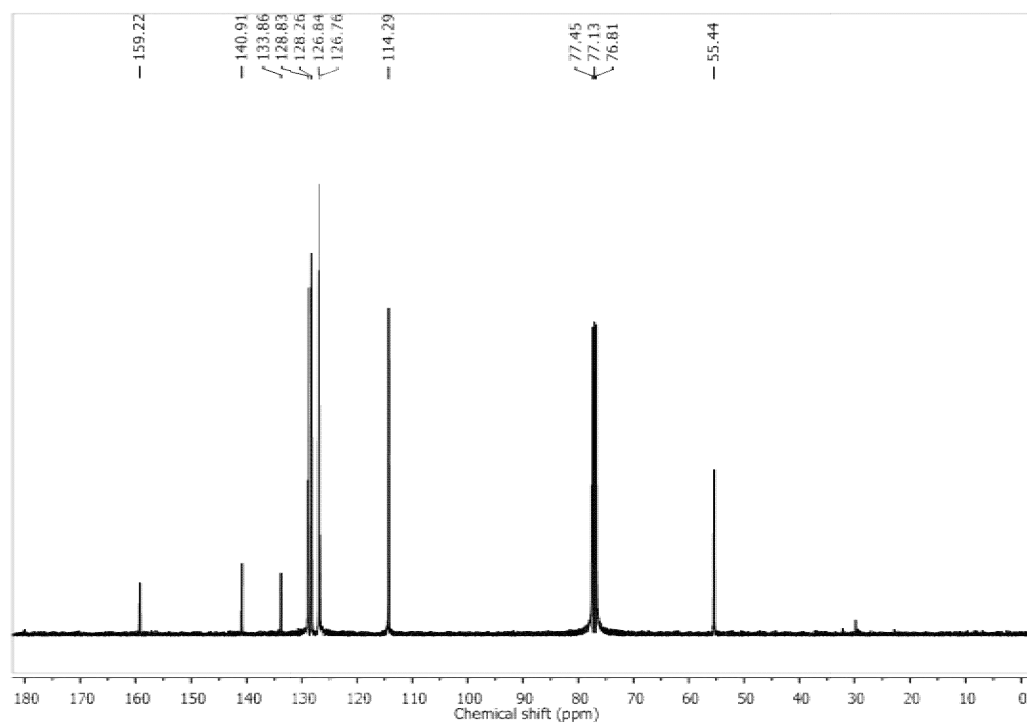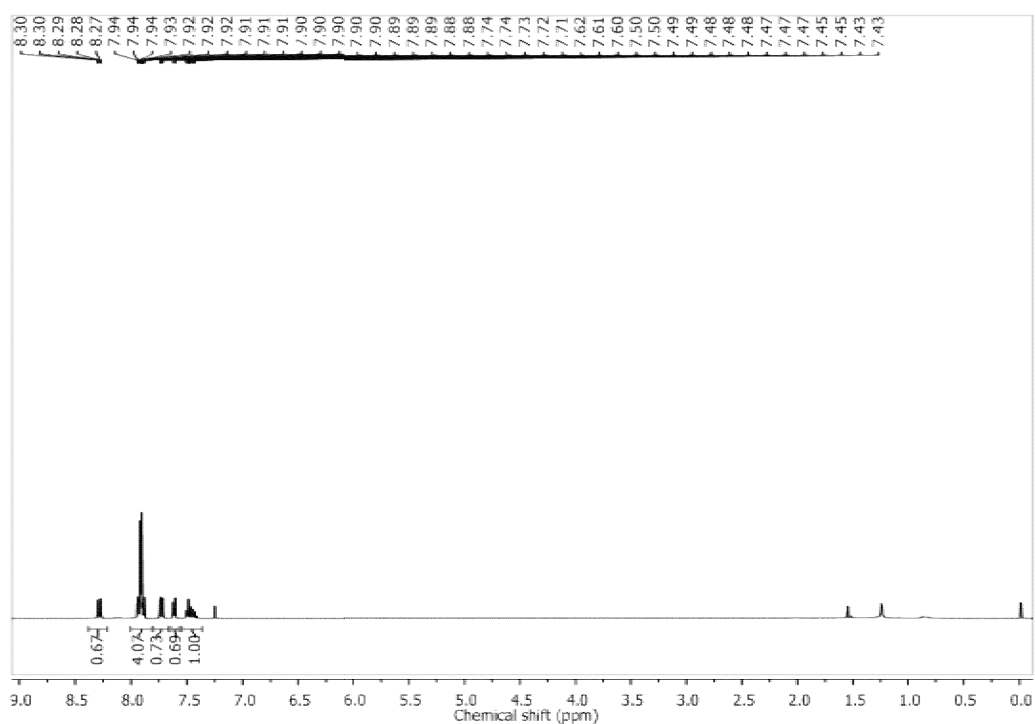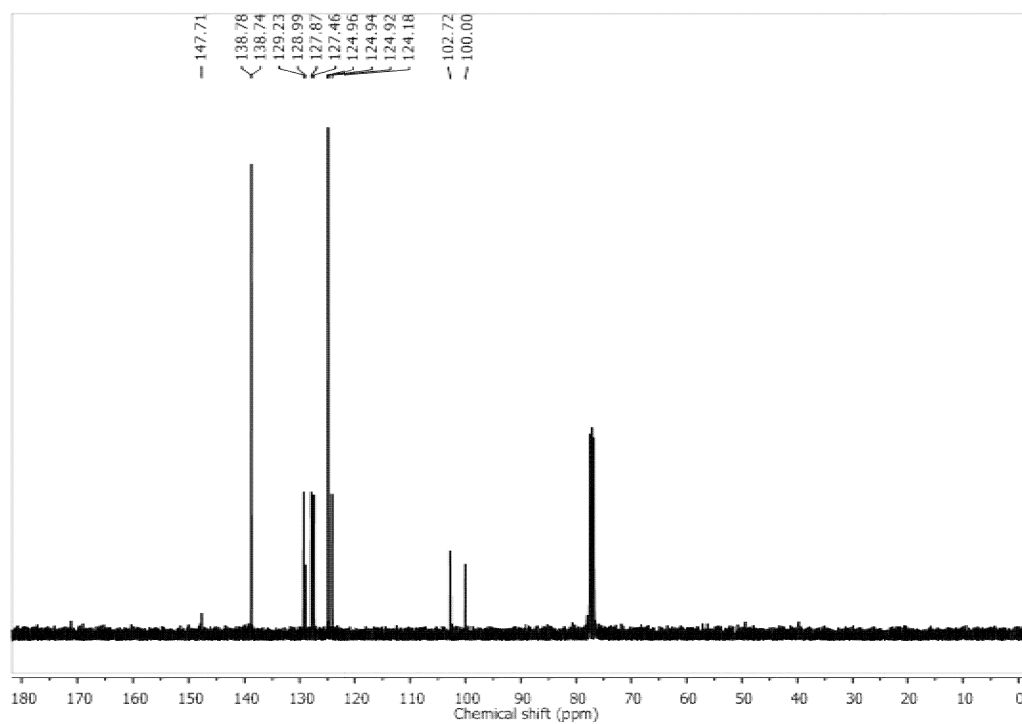
1,1'-biphenyl (Table 5A.2, Entry 1k)

^{1}H NMR (400 MHz, CDCl$_3$): δ_H (ppm) 7.61 (m, 4H), 7.46 (m, 4H), 7.37 (m, 2H).

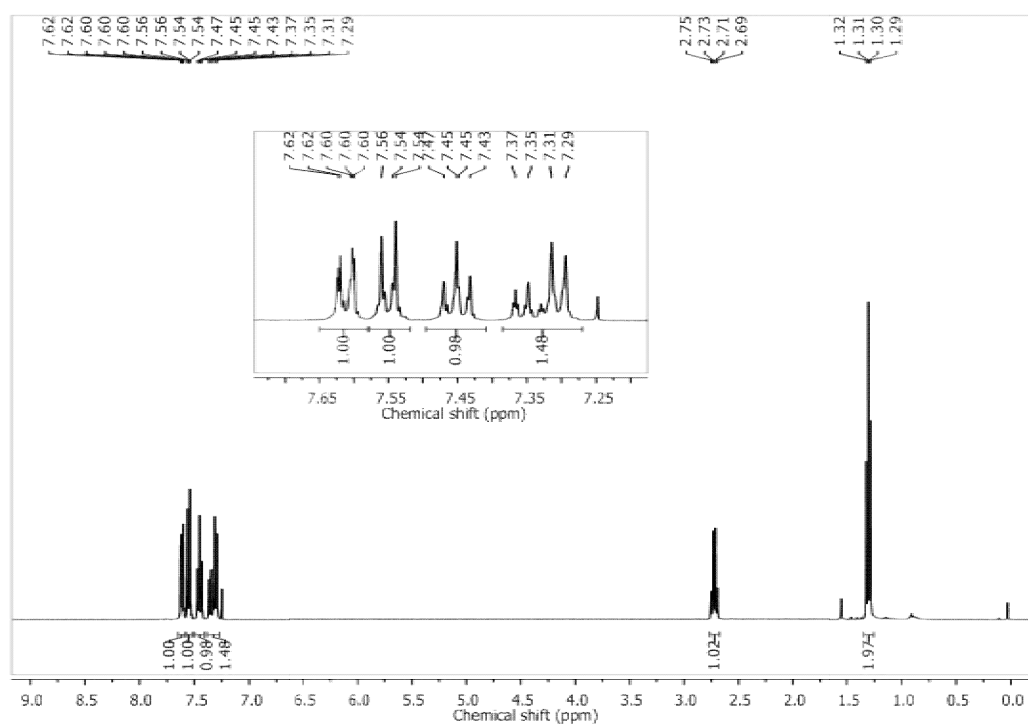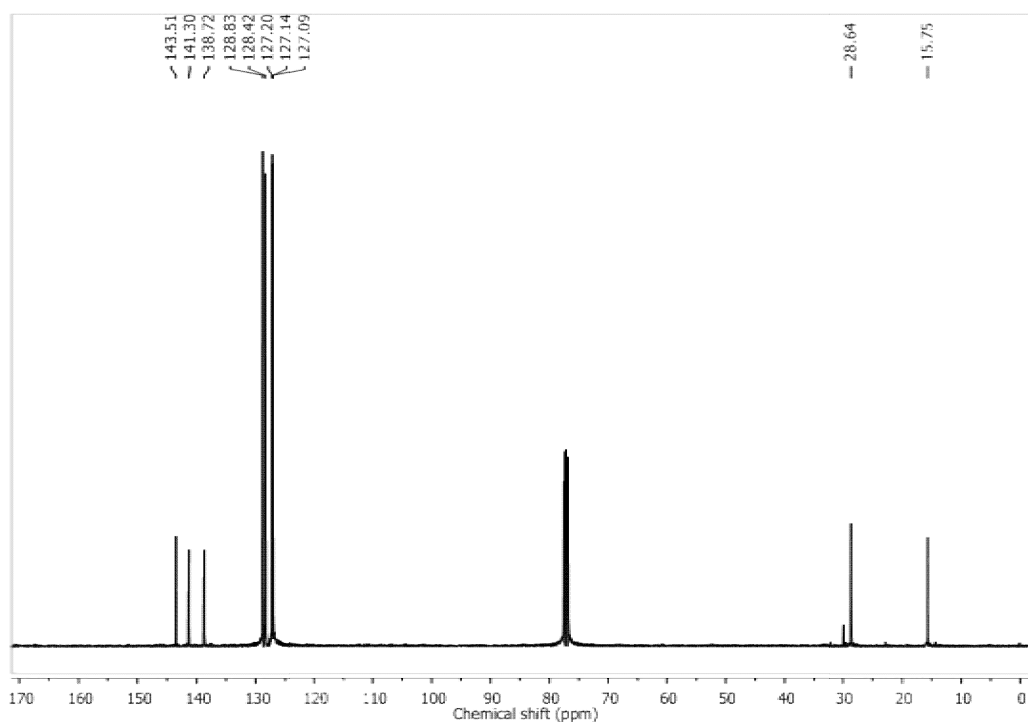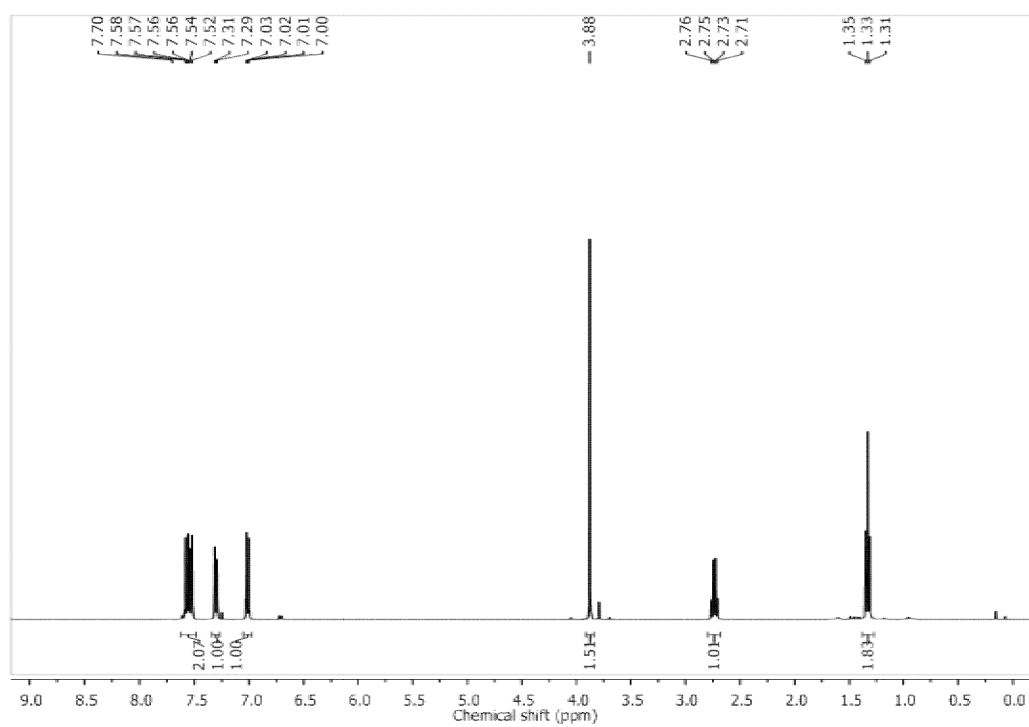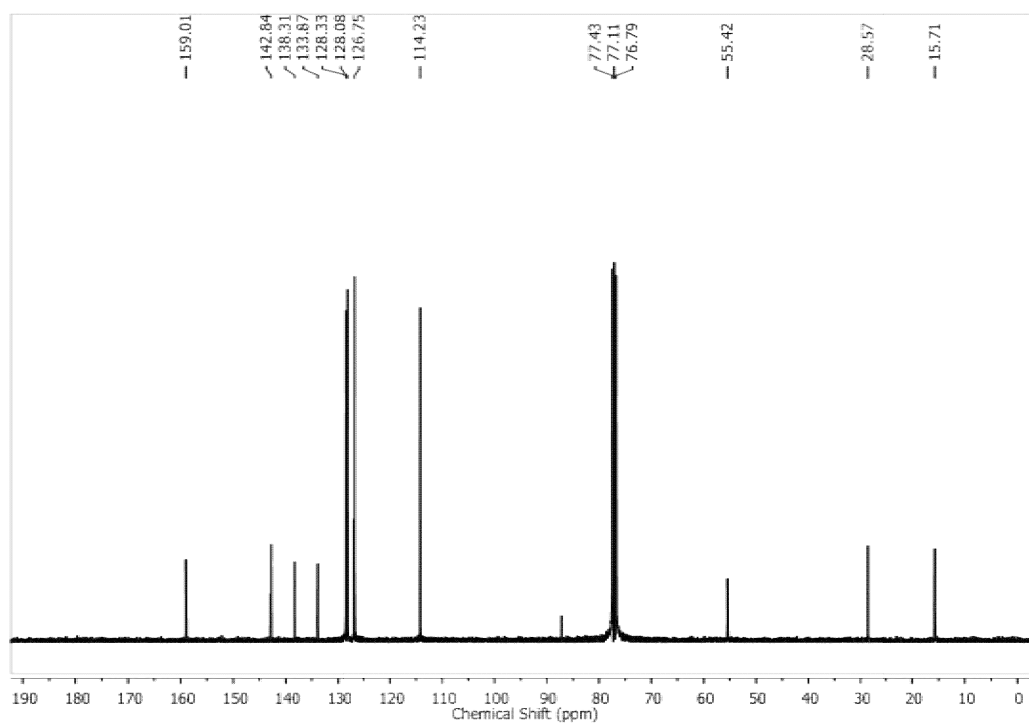### 4-methoxy-1,1'-biphenyl (Table 5A.2, Entry 1l)
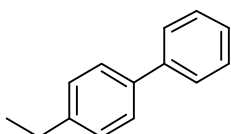
^{1}H NMR (400 MHz, CDCl$_3$): δ_H (ppm) 7.57 (t, *J* = 8 Hz, 4H), 7.40 (t, *J* =8 Hz, 2H), 7.31 (m, 1H), 6.97 (d, *J* = 8 Hz, 2H), 3.85 (s, 3H).
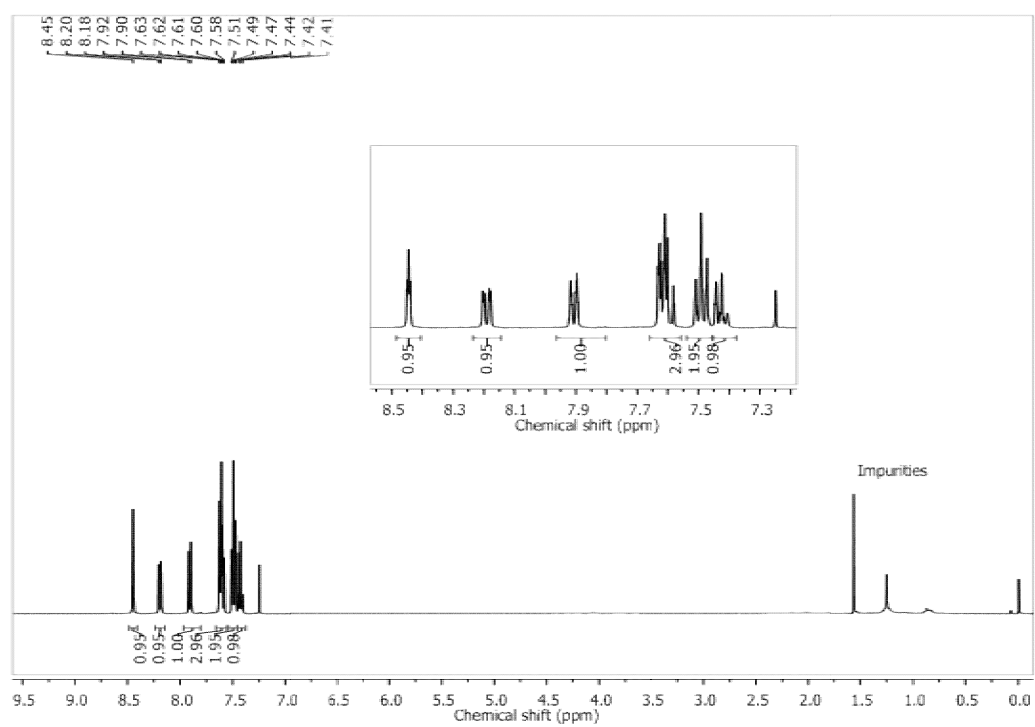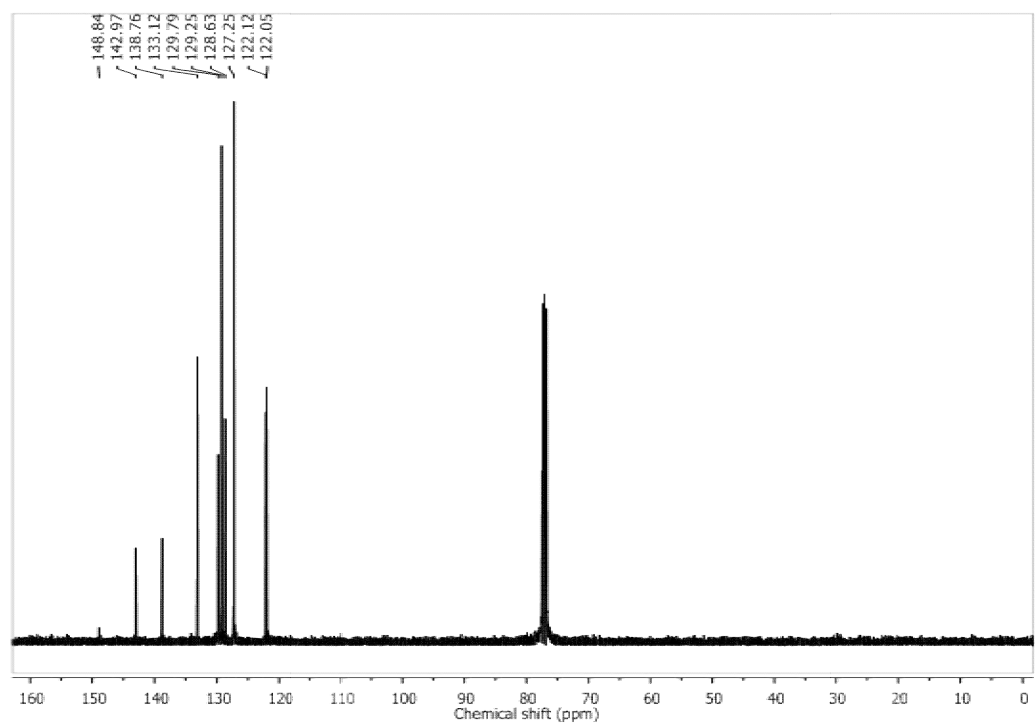
¹H NMR spectrum of 1,1'-biphenyl (Table 5A.2, Entry 1a):
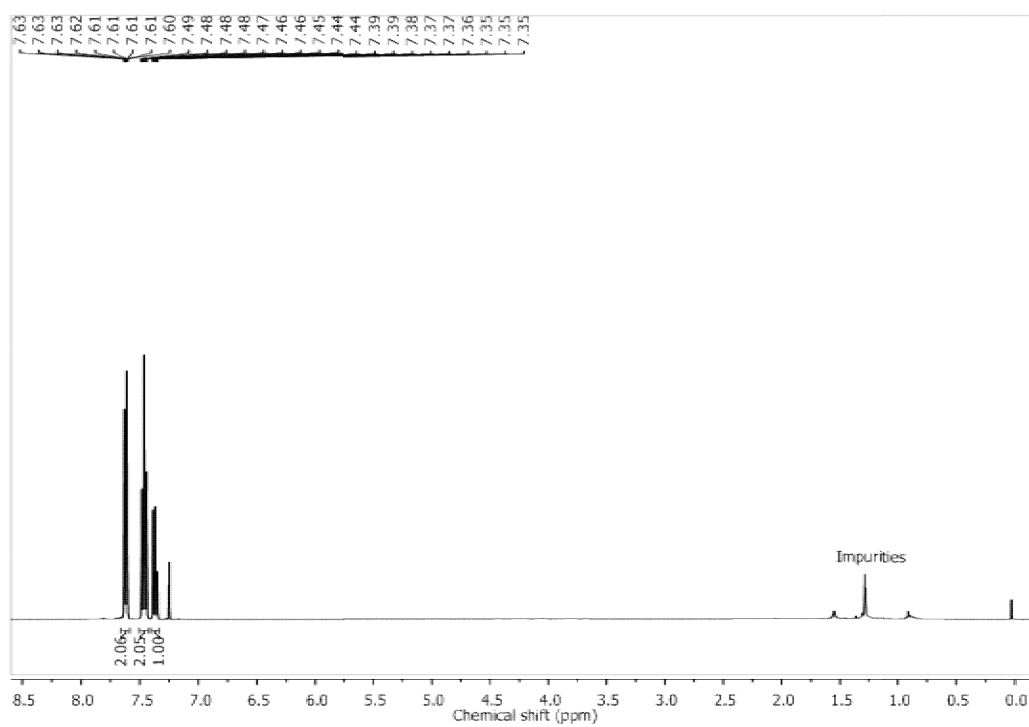
¹³C NMR spectrum of 1,1'-biphenyl (Table 5A.2, Entry 1a):
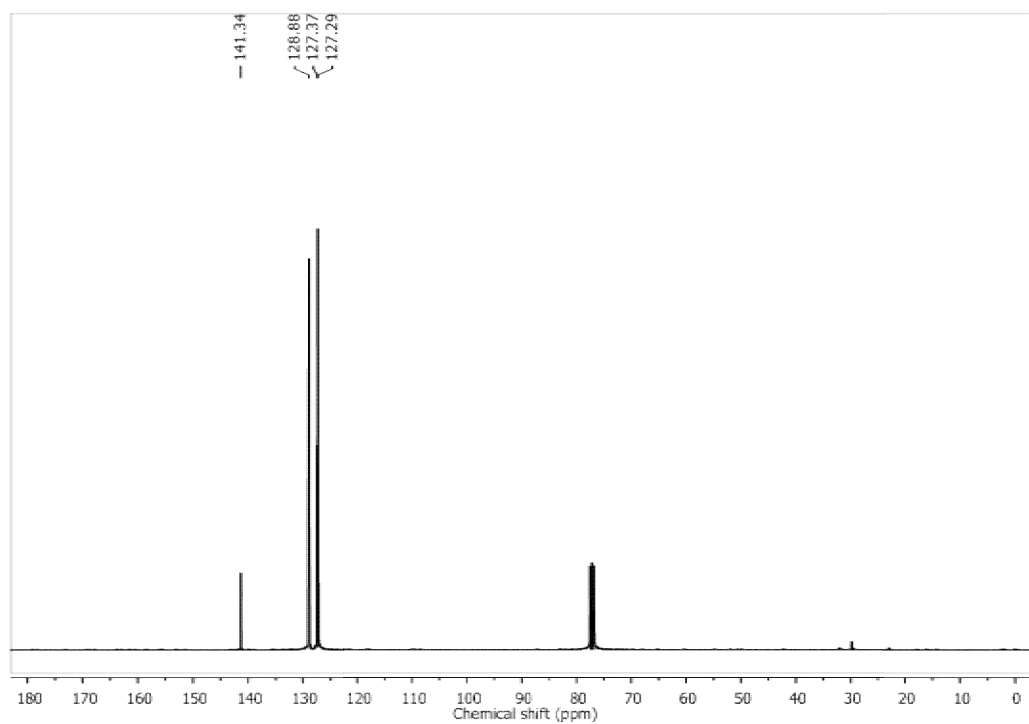
^{1}H NMR spectrum of 4-methoxy-1,1'-biphenyl (Table 5A.2, Entry 1b):

^{13}C NMR spectrum of 4-methoxy-1,1'-biphenyl (Table 5A.2, Entry 1b):
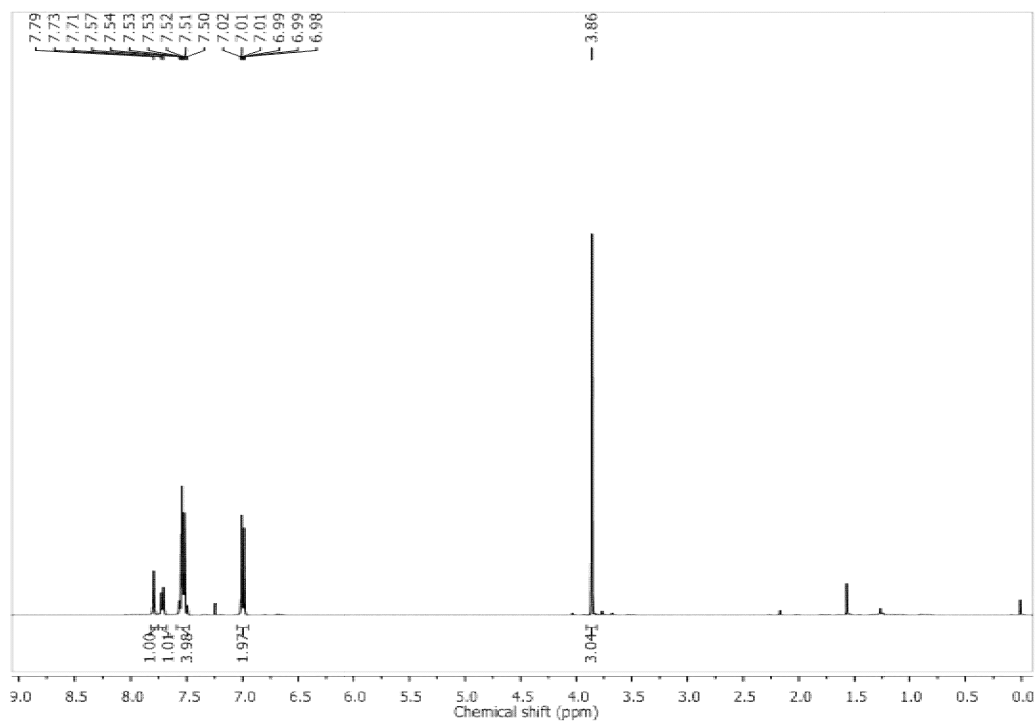
¹H NMR spectrum of 4-nitro-1,1'-biphenyl (Table 5A.2, Entry 1c):

¹³C NMR spectrum of 4-nitro-1,1'-biphenyl (Table 5A.2, Entry 1c):

¹H NMR spectrum of 4-ethyl-1,1'-biphenyl (Table 5A.2, Entry 1d):

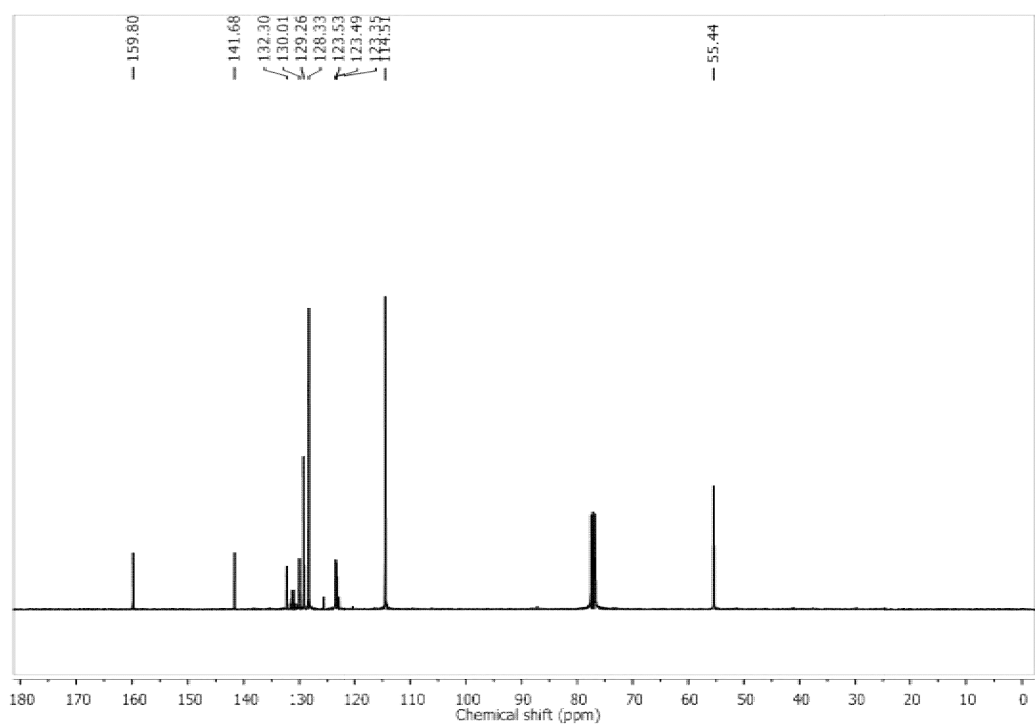**¹³C NMR spectrum of 4-ethyl-1,1'-biphenyl (Table 5A.2, Entry 1d):**

¹H NMR spectrum of 4-ethyl-4'-methoxy-1,1'-biphenyl (Table 5A.2, Entry 1e):

¹³C NMR spectrum of 4-ethyl-4'-methoxy-1,1'-biphenyl (Table 5A.2, Entry 1e):
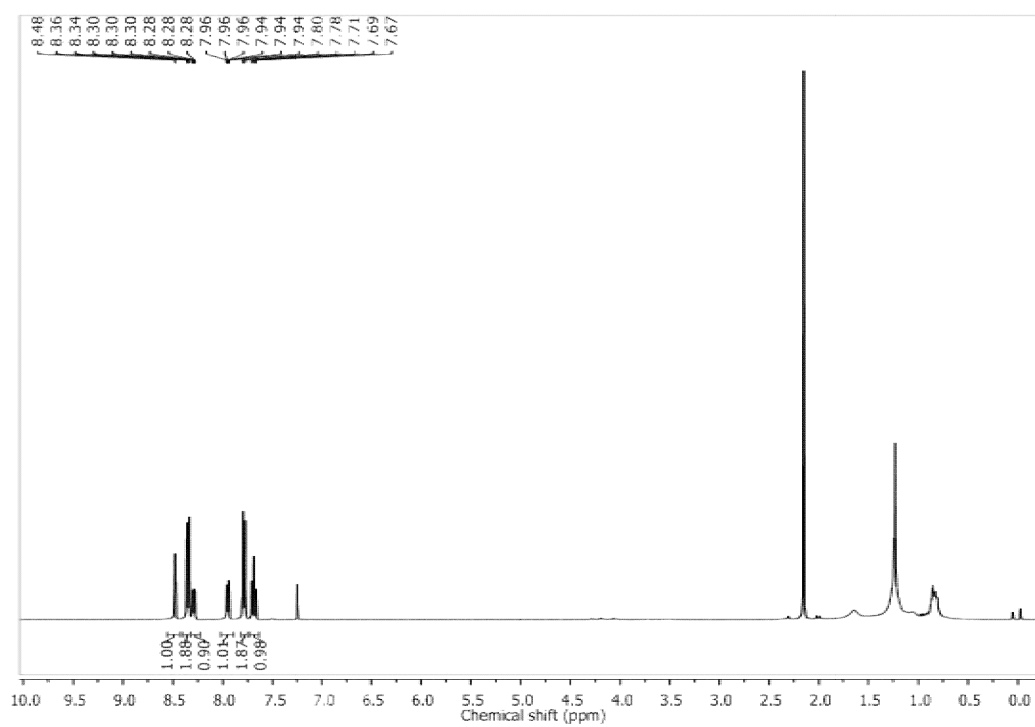
¹H NMR spectrum of 3-nitro-1,1'-biphenyl (Table 5A.2, Entry 1f):

¹³C NMR spectrum of 3-nitro-1,1'-biphenyl (Table 5A.2, Entry 1f):

¹H NMR spectrum of 4'-methoxy-3-(trifluoromethyl)-1,1'-biphenyl (Table 5A.2, Entry 1g):

¹³C NMR spectrum of 4'-methoxy-3-(trifluoromethyl)-1,1'-biphenyl (Table 5A.2, Entry 1g):
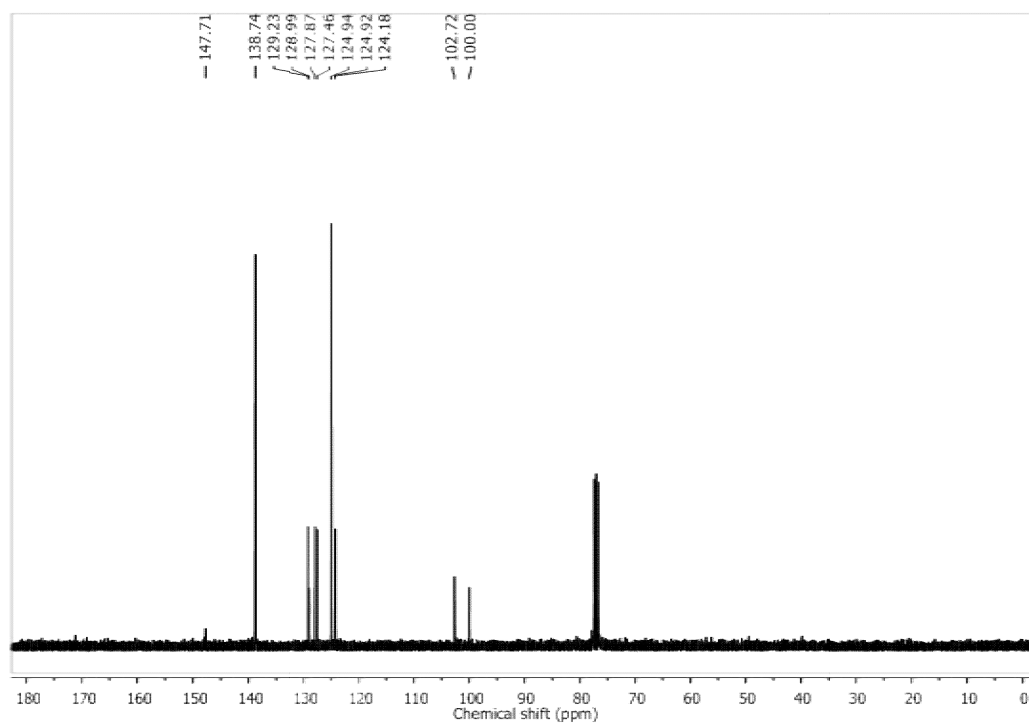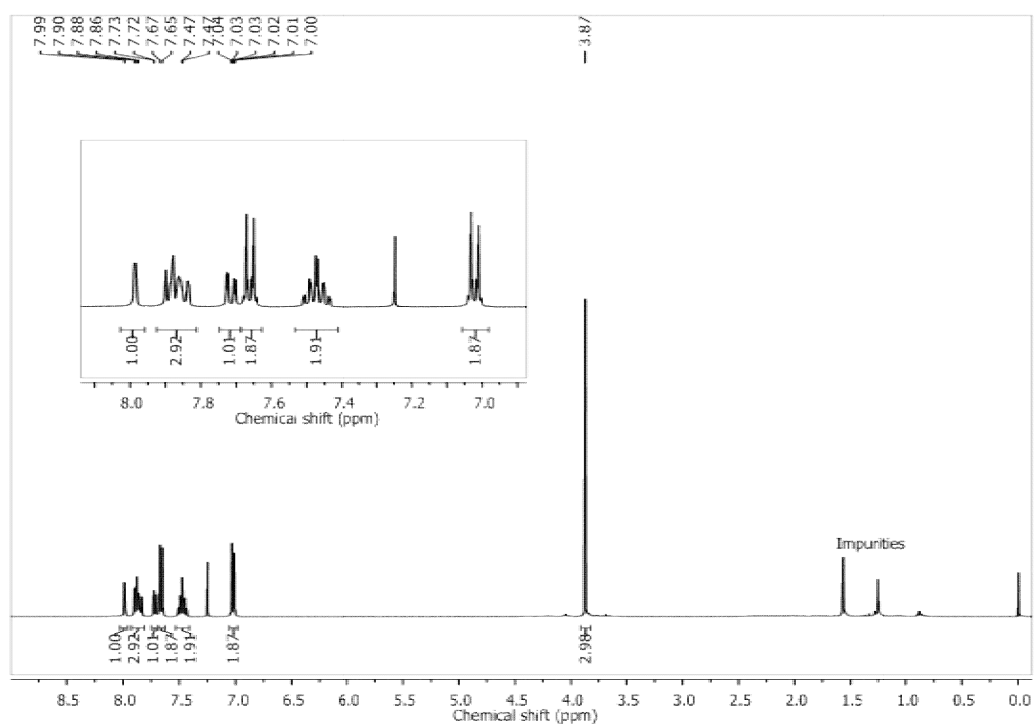
¹H NMR spectrum of 3,4'-nitro-1,1'-biphenyl (Table 5A.2, Entry 1h):

¹³C NMR spectrum of 3,4'-nitro-1,1'-biphenyl (Table 5A.2, Entry 1h):

¹H NMR spectrum of 2-(4-methoxyphenyl)naphthalene (Table 5A.2, Entry 1i):

¹³C NMR spectrum of 2-(4-methoxyphenyl)naphthalene (Table 5A.2, Entry 1i):
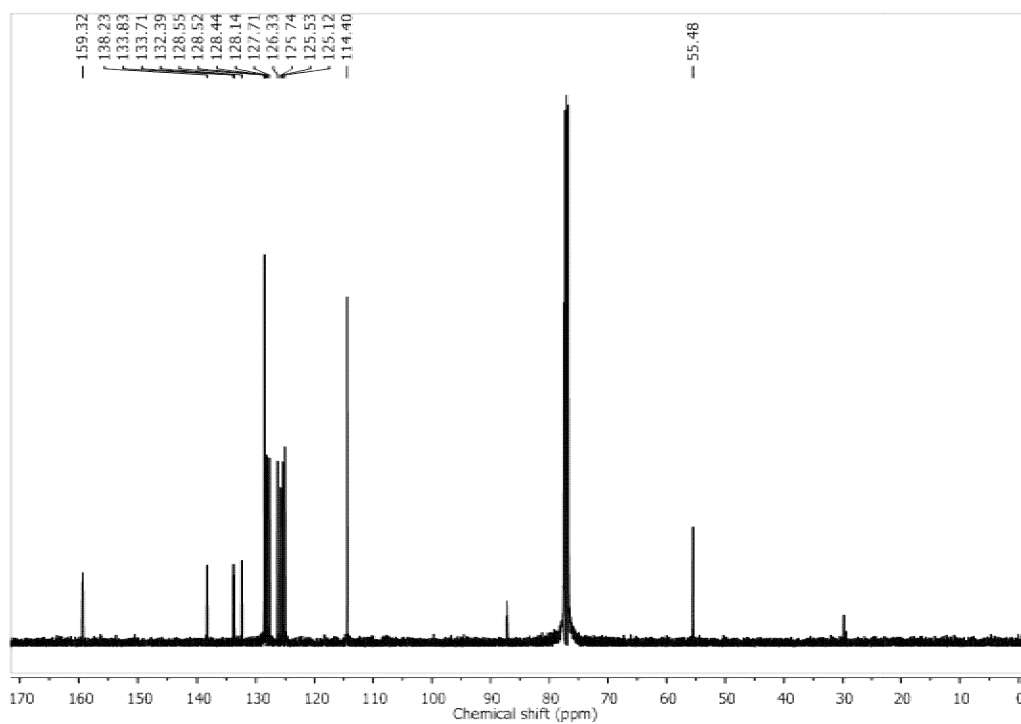
¹H NMR spectrum of 4'-methoxy-(1,1'-biphenyl)-4-ol (Table 5A.2, Entry 1j):
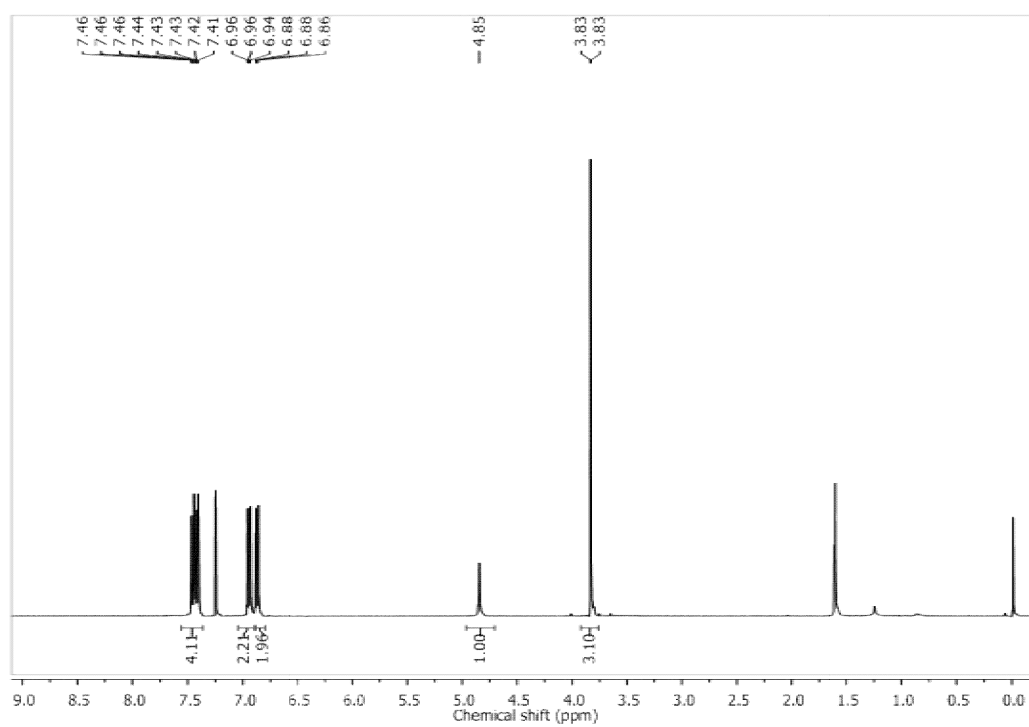
¹³C NMR spectrum of 4'-methoxy-(1,1'-biphenyl)-4-ol (Table 5A.2, Entry 1j):
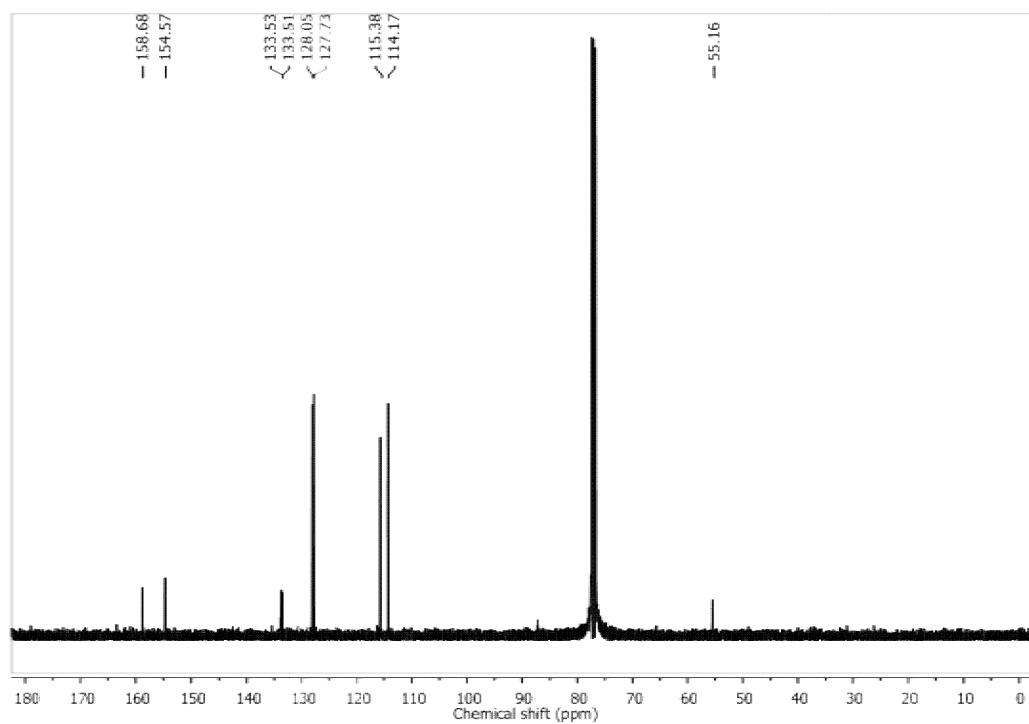
^{1}H NMR spectrum of 1,1'-biphenyl (Table 5A.2, Entry 1k):
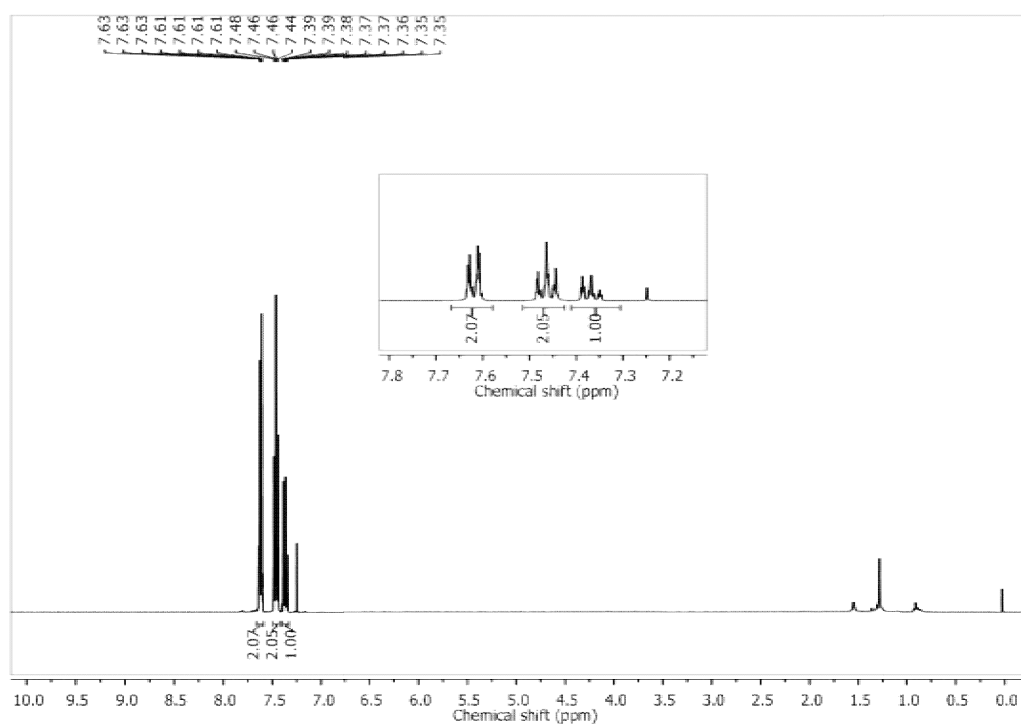
^{1}H NMR spectrum of 4-methoxy-1,1'-biphenyl (Table 5A.2, Entry 1l):
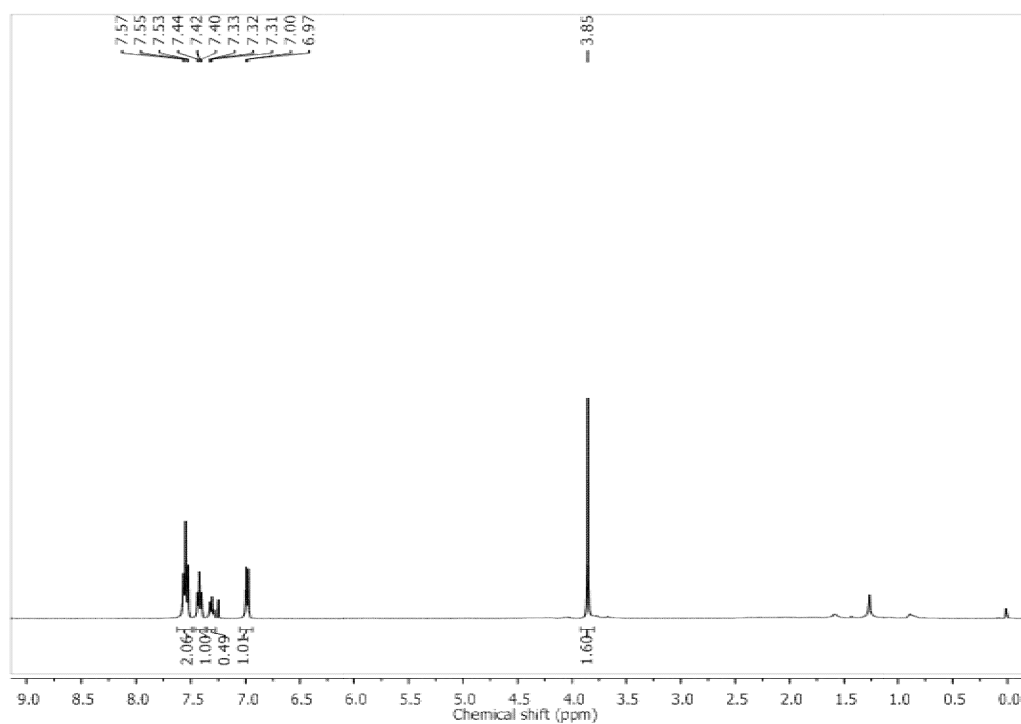
References

[1]   Dai, L. *Carbon Nanotechnology: Recent Developments in Chemistry, Physics, Materials Science and Device Applications*. Elsevier Inc., Amsterdam, 2006.

[2]   Lim, S. Y., Shen, W., and Gao, Z. Carbon quantum dots and their applications. *Chemical Society Reviews*, 44(1):362-381, 2015.

[3]   Wang, Y. and Hu, A. Carbon quantum dots: synthesis, properties and applications. *Journal of Materials Chemistry C*, 2(34):6921-6939, 2014.

[4]   Philippot, K. and Serp, P. Concept in nanocatalysis. In Serp, P., and Philippot, K., editors, *Nanomaterials in Catalysis*, pages 1-12, John Wiley & Sons, Weinheim, 2013.

[5]   Corey, E. J. and Cheng, X. M. *The Logic of Chemical Synthesis*. John Wiley & Sons, New York, 1989.

[6]   Hiyama, T. and Shirakawa, E. Overview of other palladium-catalyzed cross-coupling protocols, In Negishi, E. I. and De Meijere, A., editors, *Handbook of Organopalladium Chemistry for Organic Synthesis*, pages 285-309, John Wiley & Sons, Weinheim, 2002.

[7]   Magano, J. and Dunetz, J. R. Large-scale applications of transition metal-catalyzed couplings for the synthesis of pharmaceuticals. *Chemical Reviews*, 111(3):2177-2250, 2011.

[8]   Suzuki, K., Hori, Y., Nishikawa, T., and Kobayashi, T. A novel (2,2-diarylvinyl) phosphine/palladium catalyst for effective aromatic amination. *Advanced Synthesis & Catalysis*, 349(13):2089-2091, 2007.

[9]   Martin, R. and Buchwald, S. L. Palladium-catalyzed Suzuki–Miyaura cross-coupling reactions employing dialkylbiaryl phosphine ligands. *Accounts of Chemical Research*, 41(11):1461-1473, 2008.

[10]   Hagen, J. *Industrial Catalysis: A Practical Approach*, John Wiley & Sons, Weinheim, 2006.

[11]   Rai, R. K., Tyagi, D., Gupta, K., and Singh, S. K. Activated nanostructured bimetallic catalysts for C–C coupling reactions: recent progress. *Catalysis Science & Technol*ogy, 6(10):3341-3361, 2016.

[12]   Bej, A., Ghosh, K., Sarkar, A., and Knight, D. W. Palladium nanoparticles in the catalysis of coupling reactions. *RSC Advances*, 6(14):11446-11453, 2016.

[13]   Chen, X. C., Hou, Y. Q., Wang, H., Gao, Y., and He, J. H. Facile deposition of Pd nanoparticles on carbon nanotube microparticles and their catalytic activity for Suzuki coupling reactions. *Journal of Physical Chemistry C*, 112(22):8172-8176, 2008.

[14]   Moussa, S., Siamaki, A. R., Gupton, B. F., and El-Shall, M. S. Pd-partially reduced graphene oxide catalysts (Pd/PRGO): laser synthesis of Pd nanoparticles supported on PRGO nanosheets for carbon–carbon cross coupling reactions. *ACS Catalysis*, 2(1):145-154, 2011.

[15]   García-Suárez, E. J., Lara, P., García, A. B., Ojeda, M., Luque, R., and Philippot, K. Efficient and recyclable carbon-supported Pd nanocatalysts for the Suzuki–Miyaura reaction in aqueous-based media: microwave vs conventional heating. *Applied Cataysis A: General*, 468:59-67, 2013.

[16]   Borah, R. K., Saikia, H. J., Das, V. K., Bora, U., and Thakur, A. J. Biosynthesis of poly (ethylene glycol)-supported palladium nanoparticles using *Colocasia esculenta* leaf extract and their catalytic activity for Suzuki–Miyaura cross-coupling reactions. *RSC Advances*, 5(89):72453-72457, 2015.

[17]   Puthiaraj, P. and Ahn, W. S. Highly active palladium nanoparticles immobilized on NH_2-MIL-125 as efficient and recyclable catalysts for Suzuki–Miyaura cross coupling reaction. *Catalysis Communication*, 65:91-95, 2015.

[18]   Gholinejad, M., Seyedhamzeh, M., Razeghi, M., Najera, C., and Kompany-Zareh, M. Iron oxide nanoparticles modified with carbon quantum nanodots for the stabilization of palladium nanoparticles: an efficient catalyst for the Suzuki reaction in aqueous media under mild conditions. *ChemCatChem*, 8(2):441-447, 2016.

[19]   Lebaschi, S., Hekmati, M., and Veisi, H. Green synthesis of palladium nanoparticles mediated by black tea leaves (*Camellia sinensis*) extract: catalytic activity in the reduction of 4-nitrophenol and Suzuki-Miyaura coupling reaction under ligand-free conditions. *Journal of Colloid and Interface Science*, 485:223-231, 2017.

[20]   Tang, L., Ji, R., Cao, X., Lin, J., Jiang, H., Li, X., Teng, K. S., Luk, C. M., Zeng, S., Hao, J., and Lau, S.P. Deep ultraviolet photoluminescence of water-soluble self-passivated graphene quantum dots. *ACS Nano*, 6(6):5102-5110, 2012.

[21]   Dey, D., Bhattacharya, T., Majumdar, B., Mandani, S., Sharma, B., and Sarma, T. K. Carbon dot reduced palladium nanoparticles as active catalysts for carbon–carbon bond formation. *Dalton Transactions*, 42(38):13821-13825, 2013.

[22]   Gholinejad, M., Najera, C., Hamed, F., Seyedhamzeh, M., Bahrami, M., and Kompany-Zareh, M. Green synthesis of carbon quantum dots from vanillin for modification of magnetite nanoparticles and formation of palladium nanoparticles: efficient catalyst for Suzuki reaction. *Tetrahedron*, 73(38):5585-5592, 2017.

[23]   Shen, L., Chen, M., Hu, L., Chen, X., and Wang, J. Growth and stabilization of silver nanoparticles on carbon dots and sensing application. *Langmuir*, 29(52):16135-16140, 2013.

[24]   Wang, X., Cao, L., Lu, F., Meziani, M. J., Li, H., Qi, G., Zhou, B., Harruff, B. A., Kermarrec, F., and Sun, Y. P. Photoinduced electron transfers with carbon dots. *Chemical Communications*, 25:3774-3776, 2009.

[25]   Xu, J., Sahu, S., Cao, L., Anilkumar, P., Tackett, K. N., Qian, H., Bunker, C. E., Guliants, E. A., Parenzan, A., and Sun, Y. P. Carbon nanoparticles as chromophores for photon harvesting and photoconversion. *ChemPhysChem*, 12(18):3604-3608, 2011.

[26]   De, B., Voit, B., and Karak, N. Carbon dot reduced Cu_2O nanohybrid/hyperbranched epoxy nanocomposite: mechanical, thermal and photocatalytic activity. *RSC Advances*, 4(102):58453-58459, 2014.

[27]   Duarah, R., Singh, Y. P., Gupta, P., Mandal, B. B., and Karak, N. High performance bio-based hyperbranched polyurethane/carbon dot-silver nanocomposite: a rapid self-expandable stent. *Biofabrication*, 8(4):045013, 2016.

[28]   Nadagouda, M. N. and Varma, R. S. Green synthesis of silver and palladium nanoparticles at room temperature using coffee and tea extract. *Green Chemistry*, 10(8):859-862, 2008.

[29]   Kakaei, K. and Dorraji, M. One-pot synthesis of palladium silver nanoparticles decorated reduced graphene oxide and their application for ethanol oxidation in alkaline media. *Electrochimica Acta*, 143:207-215, 2014.

[30]   Li, L., Chen, M., Huang, G., Yang, N., Zhang, L., Wang, H., Liu, Y., Wang, W., and Gao, J. A green method to prepare Pd–Ag nanoparticles supported on reduced graphene oxide and their electrochemical catalysis of methanol and ethanol oxidation. *Journal of Power Sources*, 263:13-21, 2014.

[31]   Verma, P., Kuwahara, Y., Mori, K., and Yamashita, H. Synthesis and characterization of a Pd/Ag bimetallic nanocatalyst on SBA-15 mesoporous silica as a plasmonic catalyst. *Journal of Materials Chemistry A*, 3(37):18889-18897, 2015.

Sub-chapter 5B: Renewable resources derived hyperbranched polyurethane/palladium-silver-carbon quantum dot nanocomposite

5B.1.   Introduction

The previous two chapters discussed the potential of GO and rGO based carbon nanomaterials as suitable reinforcing agents for renewable resource based HPU, emboldening their corresponding nanocomposites with significant property enhancements as well as imparting smart attributes. However, as advantageous as it seems, difficulties in processing and risk of agglomeration of nanomaterial during mass-scale production and at higher loadings are some pertinent issues that needs to be addressed. In this juncture, CQD presents a suitable option as a nano-reinforcing material. As discussed in the previous sub-chapter, CQD is exciting class of carbon nanomaterials, predominantly of zero dimensions. CQD not only offer plethora of attractive properties [1-3], their facile preparative routes by using non toxic chemicals and bio-based precursors make them a valuable commodity [2, 3]. Most importantly, CQD possess high surface functionality, owing to the presence of various surface passivating functional groups, chemical stability in different chemical media and inertness to supported metals [2], which makes them apt nano-reinforcing materials in polymer matrices. Moreover, their zero-dimensional qualities considerably reduce the processing difficulties and risk of agglomeration at higher loadings.

Of late, polymer nanocomposites are being employed for a plethora of in-demand applications; however one such popular instance of catalytic application in direct organic transformations still remains properly unexplored. There are very few reports on utilization of renewable resources based polymer nanocomposites as catalysts [4-6], even though they show prime qualities of a multi-functional and sustainable material. The polymer matrix can be reinforced with suitable nanoparticles to introduce catalytic activity. Such nanoparticles dispersed or immobilized in polymer matrix can offer large number of reactive sites. Further, the reinforced nanocomposite matrix can provide a robust and sustainable reaction surface with polar functionalities in its vicinity that can inherently activate the reacting species, enhance recyclability and minimize leaching or deactivation of catalyst.

Again, in the domains of synthetic organic chemistry, hydroxylation of arenes is one of the most demanding reactions [7], as it generates hydroxyl-arene or phenol motif which is a core unit of many modern pharmaceuticals, agrochemicals, polymers and naturally occurring compounds [8]. Traditional routes in the previous literatures cite nucleophilic substitution of activated aryl halides, Cu-catalyzed conversion of diazoarenes, Pd-catalyzed

conversion of aryl halides for the preparation of phenols [9, 10]. However, these existing routes are marred by harsh reaction conditions, use of excessive amounts of metal salts, additional purification steps. In this context, aryl boronic acids are providing a new avenue for substituting the traditional inactive synthetic precursors. As of now, *ipso*-hydroxylation, a straightforward technique for the conversion of aryl boronic acids to phenol is gaining immense popularity due to easy availability, higher stability and greater functional group diversity of aryl boronic acids. Various protocols for *ipso*-hydroxylation of aryl boronic acids are reported using different catalyst such as biosilica-H_2O_2 [11], I_2-H_2O_2 [12], Al_2O_3-H_2O_2 [13], PEG-H_2O_2 [14], $NaClO_2$ [15], NH_2OH [16], KOH-TBHP [17], $CuSO_4$-Phenantholine [18], H_3BO_4-H_2O_2 [19], WERSA-H_2O_2 [20], Amberlite IR-120 resin [21], supported AgNPs [22], organic hypervalent iodine(III) [23], $PdCl_2$-PPh_3 [24], etc. Despite the near effectiveness of all these existing catalytic protocols for *ipso*-hydroxylation of aryl boronic acids, certain drawbacks such as use of bulk reagents, catalyst, bases, ligands and volatile organic solvents, make it imperative to develop a more viable alternative. Hence, there is a pertinent need to explore more convenient approaches and catalysts for such hydroxylation reactions. In this juncture, use of nano-scale materials, instead of bulk metal ions or salts, can be a good proposition. Nano-scale metal particles are known to display good catalytic properties due to their high surface area, but their long term stability is the problem [25]. The use of both nano-Pd and nano-Ag can be considered an apt choice, as they act as good transient species for hydroxylation reactions [22, 24], and brings down the cost comparatively. Again, surface passivation or decoration of metal nanoparticles over other supports can solve the problem of stability.

In this quest, the fabrication of renewable resource derived HPUNC with bimetallic-cum-carbonaceous Pd-Ag@CQD nanohybrid was reported. The nanocomposite was fabricated with different loading of Pd-Ag@CQD nanohybrid by *in situ* polymerization technique. Various mechanical and thermal properties of the nanocomposites were evaluated in order to ascertain the potency and performance of the nanocomposite. In addition, the nanocomposite was screened for catalytic activity towards oxidative *ipso*-hydroxylation of aryl boronic acids to afford their corresponding phenols.

5B.2.   Experimental

5B.2.1.   Materials

PCL, IPDI, MGE, COMP, xylene and THF were used for the preparation of HPUNC. Molecular sieves were used to store the solvents. All these chemical possess the same grade and

specifications as described in Chapter 2 (Section 2.2.1). Same Pd-Ag@CQD nanohybrid, exactly as described in Chapter 5A (Section 5A.2.3) was used for the fabrication of HPUNC.

Phenyl boronic acid and its derivatives (SRL, India, and Alfa Aesar, India) were used as substrates in the oxidative *ipso*-hydroxylation reaction. Hydrogen peroxide (H_2O_2) of same grade and specifications as mentioned in Chapter 3 (Section 3.2.1) was used as the oxidizing agent in the *ipso*-hydroxylation reaction. Silica gel G, silica gel GF 254 and silica gel 60-120 mesh, of same grade and specification, as described in Sub-Chapter 5A, were used for the monitoring the reaction by TLC and column chromatographic purification of crude products. Other chemicals and solvents used in the catalytic reactions include were of reagent grade and purchased from Merck, India.

5B.2.2.   Methods

5B.2.2.1.   Fabrication of HPU/Pd-Ag@CQD nanocomposite

Fabrication of HPU/Pd-Ag@CQD nanocomposite was accomplished by an *in situ* polymerization technique, following the same process as described in Chapter 3 (Section 3.2.2.1). Only in this case, a stable dispersion of Pd-Ag@CQD nanohybrid (in dry THF) was incorporated in the second step of the polymerization reaction under constant mechanical agitation.

HPUNCs with different weight percentages of Pd-Ag@CQD, *viz.* 0.5 wt%, 1.0 wt% and 2.0 wt% were prepared and encoded as HPUNC0.5, HPUNC1.0 and HPUNC2.0, respectively. In the same way, pristine HPU was prepared without using Pd-Ag@CQD nanohybrid for comparison purpose. Pristine HPU is equivalent to HPU3, as described in Chapter 2 and used as the matrix.

5B.2.2.2.   Sample preparation for performance study

Samples of HPU/Pd-Ag@CQD nanocomposite were prepared by the same process as HPU, as described in Chapter 2 (Section 2.2.2.3). All analysis and testing were performed using bulk HPUNC samples without any further purification. For catalytic application, the processed HPU/Pd-Ag@CQD nanocomposite thin films were cut into fine pieces and used directly as catalyst.

5B.2.2.3.   General procedure for oxidative *ipso*-hydroxylation of aryl boronic acid

Aryl boronic acid (1 equivalent, 0.121 g) was taken in a round-bottomed flask with addition of H_2O (2 mL). Finely cut thin films of HPUNC (5 wt% with respect to aryl boronic acid) as catalyst were added to the flask, followed by addition of 30% H_2O_2 (5 equivalent, 0.17 g,

0.15 mL). The reaction was carried out at room temperature and the progress of the reaction monitored by TLC. After completion of the reaction, the HPUNC catalyst was recovered from the reaction mixture by simple filtration. The crude reaction mixture was then extracted with ethyl acetate (2 x 10 mL) and dried over anhydrous Na_2SO_4, followed by drying under reduced pressure. The crude product was purified by column chromatography using hexane and ethyl acetate as eluent. The purified products were identified by ^1H and ^{13}C NMR spectroscopy.

5B.2.3.   Characterization

FT-IR, XRD, TEM, TGA and DSC analyses of the HPUNC were conducted using the same instruments, same specifications and same conditions as described in Chapter 3 (Section 3.2.3). ^1H and ^{13}C NMR spectra of the isolated products were recorded by the same instrument and under the same conditions as mentioned in Chapter 2 (Section 2.2.3). Surface area analysis of the nanocomposite was determined by the same BET instrument and under same conditions as mentioned in Chapter 5A (Section 5A.2.3).

Various mechanical testing of the HPUNC films *viz.* tensile strength, elongation at break, scratch hardness, impact resistance, etc. were performed by the same instruments and under the same conditions as described in Chapter 2 (Section 2.2.3).

5B.3.   Results and discussion

5B.3.1.   Fabrication   and   characterization   of   HPU/Pd-Ag@CQD nanocomposite

Bio-derived HPU/Pd-Ag@CQD were fabricated by *in situ* polymerization technique using 0.5 wt%, 1.0 wt% and 2.0 wt% loading of the nanohybrid. In general, immobilization of metallic nanoparticles in polymer matrix is difficult, mostly due to poor dispersibility in the matrix, stemming from agglomeration of nanoparticles [26]. In this context, dispersion of Pd-Ag@CQD nanohybrid was found to be suitable as CQD contains multi-functionalities moieties by means of various surface passivating functional groups. These multi-functional groups interacted with the polymer matrix possibly by physico-chemical interactions, resulting in dispersion of the nanohybrid in the matrix [27-29]. The nanohybrid played the role of nano-reinforcing agent by incorporating itself with the molecular chains of the polymer matrix. In fact, both the HPU matrix and the nanohybrid complimented each other in forming a mutually compatible and homogeneous nanocomposite system (**Scheme 5B.1**).
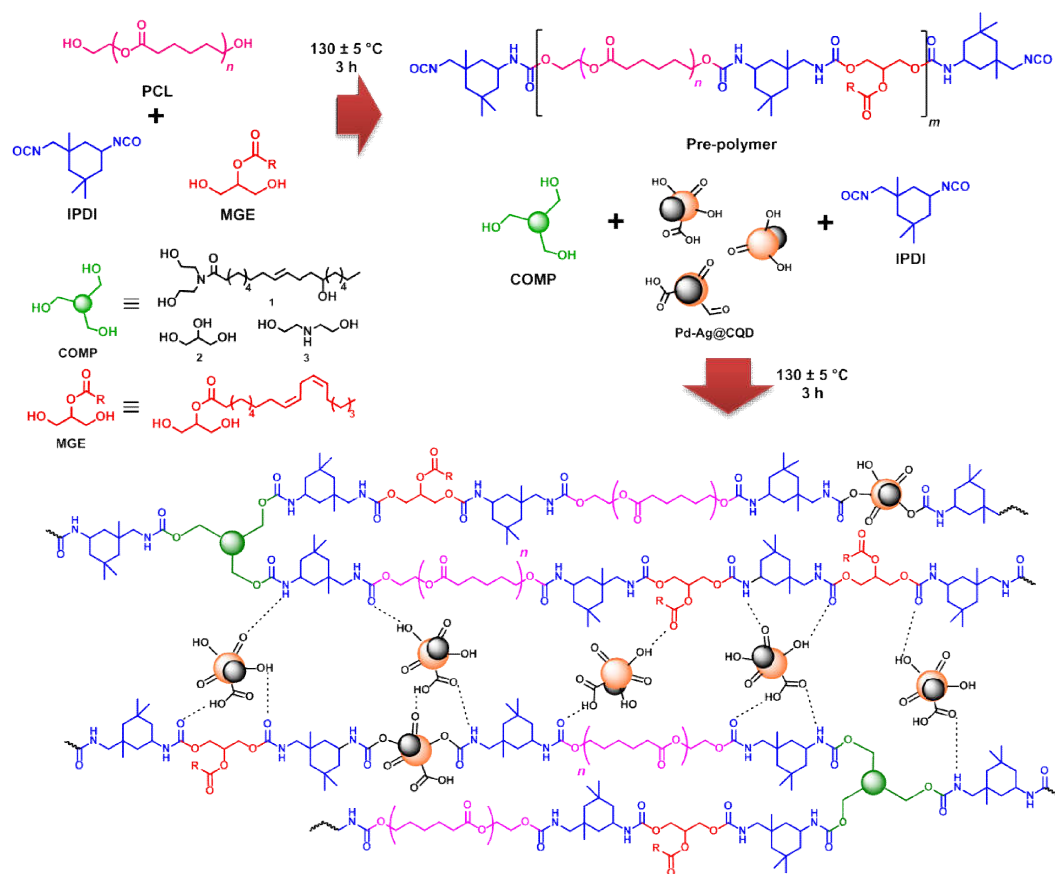
Scheme 5B.1. Fabrication of HPU/Pd-Ag@CQD nanocomposite.

FT-IR study of the nanocomposites revealed the presence of functional moieties associated with structure of polyurethanes (**Figure 5B.1.a**). The N-H stretching band appeared at 3436 cm^{-1}, overlapping with O-H stretching band. The C=O (amide linkage of urethane) stretching band appeared at 1636 cm^{-1} along with the C-O stretching band at 1030 cm^{-1}. Other notable frequencies include the C-H (asymmetric and symmetric) stretching band at 2924 cm^{-1} and 2857 cm^{-1}, C=O (ester of bio-based moieties) stretching band at 1735 cm^{-1}, C-H bending at 1438 cm^{-1}, the C-N stretching band that overlapped with C-O band at 1030 cm^{-1}, C-O-C stretching at 936 cm^{-1} and the N-H deformation band at 610 cm^{-1}. The FT-IR results were consistent with the functional groups of HPU matrix as observed in prior art [30]. Notably, there were no bands observed for Pd-Ag@CQD nanohybrid, which can be attributed to very small amount of nanohybrid (0.5-2.0 wt% with respect to HPU) dispersed in the HPU matrix. XRD patterns of HPUNCs showed the presence of crystallinity in the nanocomposites (**Figure 5B.1.b**). The nanocomposites showed two distinct peaks at 2θ = 21.3° (*d*-spacing of 4.16 Å) and 2θ = 23.6° (*d*-spacing of 3.76 Å) corresponding to the (200) and (110) planes of the PCL moiety respectively, which constitute the soft segments of HPU matrix [31, 32]. In addition, increase in peak intensity of PCL moiety with increasing

nanohybrid loading was observed. This indicated the increase in the crystallinity of the nanocomposite with nanohybrid loading, due to the good nano-reinforcing ability of the nanohybrid [29, 33]. The Pd-Ag@CQD nanohybrid enhanced the crystallinity of the polymer matrix through various physicochemical interactions that strengthened the polymer matrix. Calculation of the percentage of crystallinity of HPUNCs confirmed this observation with corresponding values of 20.6 % (0.5 wt%), 21.6 % (1.0 wt%) and 22.4 % (2.0 wt%). Furthermore, no peaks were observed for the Pd-Ag@CQD nanohybrid. This may be due to the presence of very small amount of nanohybrid (0.5-2 wt% with respect to HPU) present in the polymer matrix.
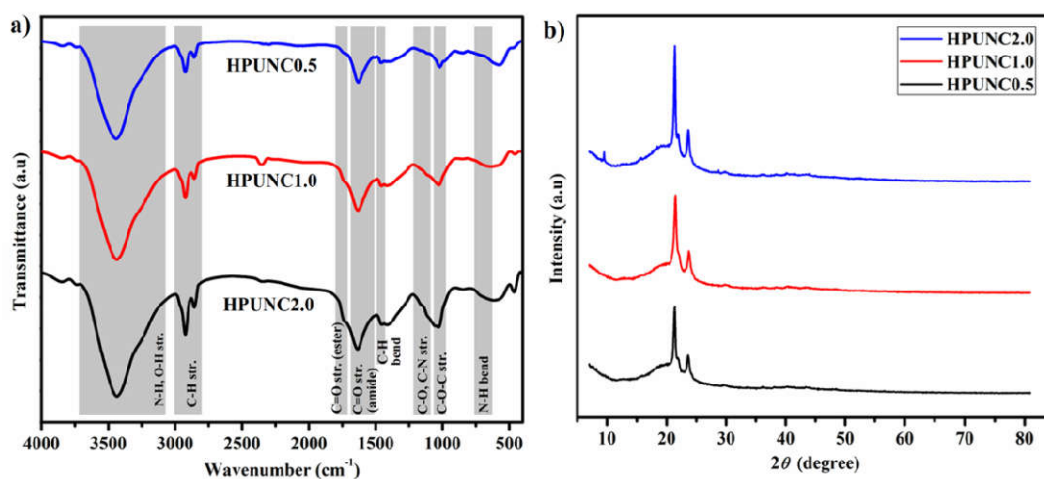
Figure 5B.1. a) FT-IR spectra, and **b)** XRD patterns of HPUNCs.

TEM analysis of HPUNC2.0 revealed network-like polydispersion of the nanohybrid in the HPU matrix, which can be attributed to the good nucleating ability of the CQDs (**Figure 5B.2.a and 5B.2.b**). By the virtue of its surface passivating functional groups, CQDs interacted with molecular chains of HPU, reinforcing the matrix in the process [27-29]. TEM images displayed the presence of Pd-Ag hybrid phase over CQDs and preservation of the near-spherical morphology of the nanohybrid as reported in our previous report [34]. High resolution TEM (HRTEM) images showed the polydispersion of Pd-Ag@CQD nanohybrid in HPU matrix as well as presence of lattice fringes of the nanohybrid (**Figure 5B.2.c** and **5B.2.d**). Conversion of selected areas (in red and yellow squares) into corresponding IFFT images showed interplanar distances of CQD phase (0.360 nm) and Pd-Ag hybrid phase (0.182 nm and 0.145 nm), which were in good agreement with our previous report [34]. The quantum confinement effect of the bimetallic-cum-carbonaceous nanohybrid rendered very little variation, in terms of size and morphology. Statistical analysis revealed that the largest fraction of particles size came within the range of 5-5.5 nm (**Figure 5B.2.e**).
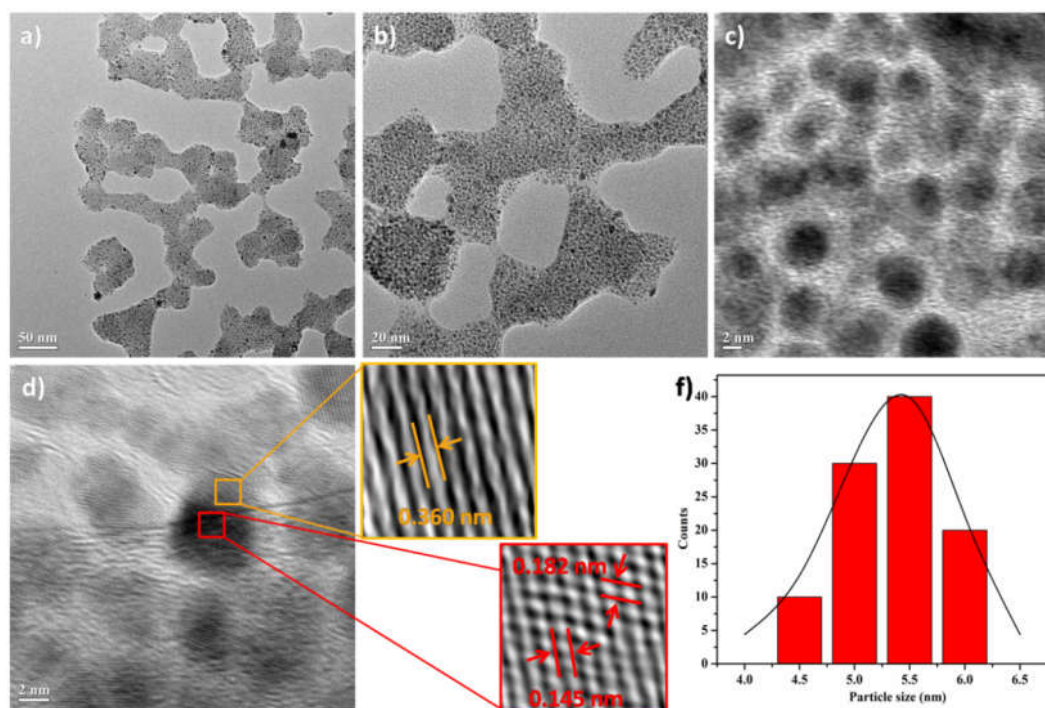
Figure 5B.2. a)-b) TEM images of HPUNC2.0, **c)-d)** HRTEM images of Pd-Ag@CQD in HPUNC2.0 (inset: lattice fringes of CQD and Pd-Ag hybrid phase), and **e)** Particle size distribution of Pd-Ag@CQD in HPUNC2.0.

5B.3.2. Mechanical properties

The mechanical performance of the HPUNCs provided significant insight into the feasibility and quality of the nanocomposites. Primarily, the mechanical properties of pristine HPU were found to be not adequate enough, mostly due to the presence of bio-based aliphatic chain segments [30]. This inadequacy was ably compensated by addition of Pd-Ag@CQD nanohybrid to the HPU matrix. The results demonstrated tremendous enhancement of mechanical properties of HPUNCs *viz.* tensile strength, elongation at break and toughness, even at very low loading of the nanohybrid. Further, all the HPUNCs displayed loading-dependent enhancement of mechanical properties (**Table 5B.1**).

Tensile strength of the HPUNCs showed great improvement by 2.2 fold (maximum), displaying an increasing trend with increase of nanohybrid loading. Elongation at break and flexibility of HPUNCs also enhanced significantly by 1.19 fold (maximum) with increasing amount of nanohybrid in the polymer matrix. In similar lines, the measurement of toughness from stress-strain profiles of the nanocomposites (**Figure 5B.3**) demonstrated vastly improved values upto 3.0 fold (maximum). The nanocomposites further exhibited high values of scratch hardness and impact resistance; however the exact

values of both could not be quantified as they exceeded the limiting values of the instruments used. The improved mechanical performance of the nanocomposites can be attributed mainly to good dispersion and excellent reinforcing ability of nano-scale CQDs [28, 29]. CQDs possess a carbonized core structure and peripheral polar functional moieties, which provided the rigidity and flexibility to the HPU matrix through strong interfacial interactions and multiple secondary interactions [27-29]. Thus, the incorporation of semi-carbonaceous Pd-Ag@CQD nanohybrid was instrumental in the formation of a robust nanocomposite system.

Table 5B.1. Mechanical properties of HPU and its nanocomposites

Parameter	HPU	HPUNC0.5	HPUNC1.0	HPUNC2.0
Tensile strength (MPa)	5.3 ± 0.3	6.3 ± 0.3	8.6 ± 0.2	10.0 ± 0.5
Elongation at break (%)	605 ± 5	628 ± 4	670 ± 5	762 ± 7
Toughness[a] (MJm^{-3})	27.35 ± 0.5	34.96 ± 0.2	52.04 ± 0.3	67.52 ± 0.2
Scratch hardness[b] (kg)	10	>10	>10	>10
Impact strength[c] (kJm^{-1})	>19.02	>18.59	>19.02	>19.02

[a]Calculated by integrating the stress-strain curves. [b]Maximum limit of the instrument is 10 kg. [c]Converted to energy units per thickness of the sample (sample thickness between 0.43-0.45 mm).
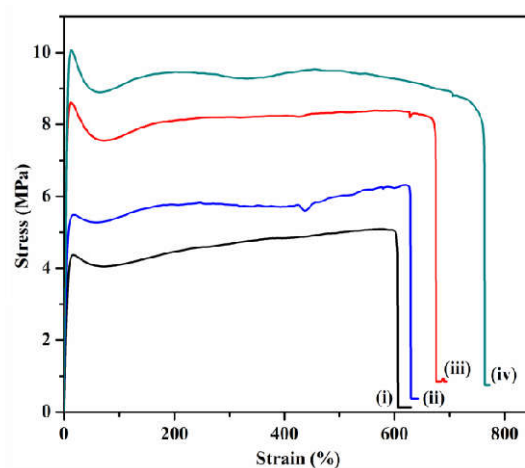

Figure 5B.3. Stress-strain profiles of (i) HPU, (ii) HPUNC0.5, (iii) HPUNC1.0 and (iv) HPUNC2.0.

5B.3.3. Thermal properties

Thermogravimetric analysis (TGA) was performed to study the thermal stability of the HPUNC nanocomposites. The TG thermograms (**Figure 5B.4.a**) and their corresponding dTG curves (**Figure 5B.4.b**) of HPUNCs revealed high thermal degradation temperatures above 300 °C. In addition, all the nanocomposites displayed enhancement of degradation temperatures with increase in nanohybrid loading. This thermal stability can be attributed to the reinforcement of the HPU matrix by bimetallic Pd-Ag@CQD nanohybrid. The nanohybrid occupied the free volume in the HPU matrix, leading to the restriction of the thermal motion of the polymeric chains. This stability was also aided by the presence of bimetallic Pd-Ag hybrid nanoparticles which imparted high thermal resistance to the decomposition and pyrolysis of the HPU matrix. Inclusion of metallic particles and carbon nanomaterials are known to have thermal insulating effect and enhances thermal stability in polymer matrix [29, 35].
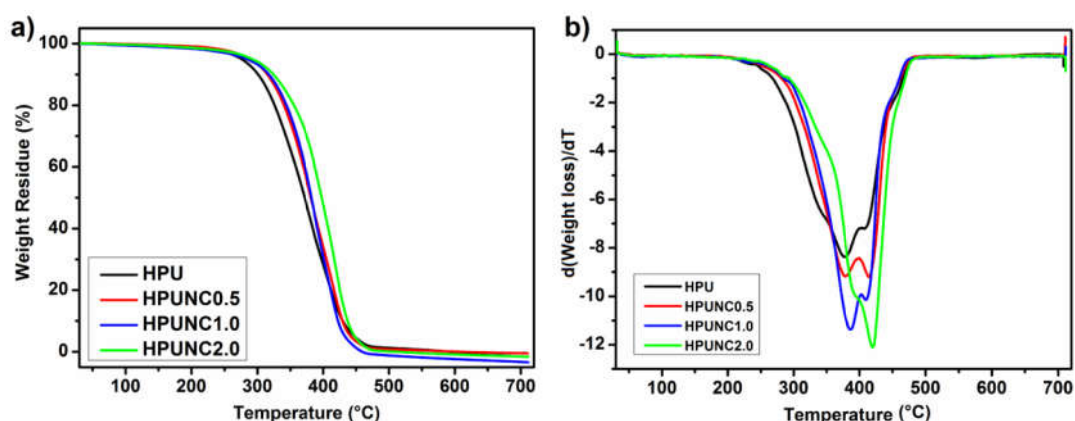
Figure 5B.4. a) TG thermograms, and **b)** dTG curves of HPU and HPUNCs.

Differential scanning calorimetry (DSC) revealed the glass transition temperatures of the polymer segments of the nanocomposites (**Figure 5B.5**). The DSC curves of the nanocomposites demonstrated a weak glass transition temperature (T_g) with very little variation, corresponding to the soft segments of the nanocomposites. At the same time, DSC curves also displayed a comparatively sharp glass transition temperature ($T_{g'}$) corresponding to the hard segments of the nanocomposites, showing an increasing trend with increase in nanomaterial content. This result is in good agreement with the preferential strengthening of the hard segments by the nanohybrid [28, 32]. This selective reinforcement of the hard segments by semi-carbonaceous nanohybrid lead to polymer chain stiffening, which in turn increased the glass transition temperature [28, 33].
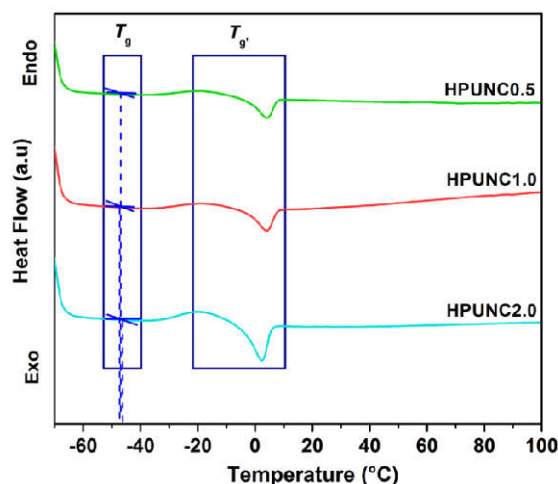
Figure 5B.5. DSC curves of HPUNCs.

5B.3.4.   Catalytic application of HPUNC in oxidative *ipso*-hydroxylation of aryl boronic acids

The catalytic activity of HPUNC was investigated in the oxidative *ipso*-hydroxylation of aryl boronic acids. Initially, phenyl boronic acid (1 mmol) was taken as the model substrate with 30% aq. H_2O_2 (1 mL) as the oxidant and HPUNC (1 wt% with respect to phenyl boronic acid) as the heterogeneous catalyst, to check the viability of the reaction. HPUNC2.0, because of its superior mechanical properties and highest loading of Pd-Ag@CQD nanohybrid (2 wt%) was chosen as the catalyst and simply referred as HPUNC. The reaction was carried out under room temperature and yielded phenol as the sole product. However, during the course of the reaction, a sticky reaction mass was observed in the vessel which was difficult to solubilize and separate the catalyst. In order to tackle this problem, water (2 mL) was chosen as the solvent. The reaction afforded complete conversion of phenyl boronic acid to phenol in aqueous medium. The preliminary investigation of the reaction mixture revealed the sharp odor of phenol and gradual change in color of solution from colorless to the light brown. Surprisingly, no homocoupling product was detected for the reaction. Therefore, in order to identify the best conditions, the conversion of phenyl boronic acid to phenol using 30% aq. H_2O_2 as the oxidant and HPUNC as catalyst in aqueous medium was taken as the model reaction (**Scheme 5B.2**).
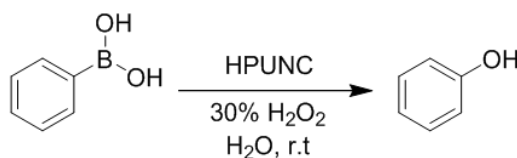
Scheme 5B.2. HPUNC catalyzed *ipso*-hydroxylation of phenyl boronic acid with H_2O_2.

With the purpose of optimizing the catalyst loading (**Table 5B.2**) and the amount of the oxidant (**Table 5B.3**), a series of the model reaction was emulated.

Table 5B.2. Optimization of catalyst loading using model reaction

Entry	Catalyst loading[a]	Time (min)	Conversion (%)
1	-	1440	54
2	1	180	100
3	2	95	100
4	2.5	85	100
5	3	60	100
6	5	30	100
7	7	30	100

Reaction conditions: Phenyl boronic acid (1 equiv., 0.121 g), H_2O_2 (30% aq., 1 mL), H_2O (2 mL), room temperature. [a]wt% with respect to phenyl boronic acid.

Table 5B.3. Optimization of amount of oxidant using model reaction

Entry	Amount of oxidant (mL)	Time (min)	Conversion (%)
1	-	1440	0
2[a]	1	180	100
3[b]	1	60	100
4	1	30	100
5	0.50	30	100
6	0.25	30	100
7	0.15	30	100
8	0.10	120	80
9	0.06	360	60
10	0.03	360	42

Reaction conditions: Phenyl boronic acid (1 equiv., 0.121 g), H_2O (2 mL), room temperature, 5 wt% of catalyst with respect to phenyl boronic acid unless mentioned otherwise. [a]1 wt% catalyst with respect to phenyl boronic acid. [b]3wt% catalyst with respect to phenyl boronic acid.

Initially, it was noticed that the reaction proceeded very sluggishly without the presence of catalyst, recording only 54% conversion after 24 h (Entry 1, Table 5B.2). This exemplified the role of catalyst in effectively enhancing the reaction. Subsequently, the reaction was attempted with different amount of catalyst (Entry 2-7, Table 5B.2), taking 1 mL of 30% aq. H_2O_2 and it was found that 5 wt% HPUNC was sufficient for the rapid

conversion of 1 mmol of phenyl boronic acid (Entry 6 vs 7, Table 5B.2). In similar vein, the reaction was found to not proceed at all in the absence of oxidant (Entry 1, Table 5B.3). Thereafter, the reaction was tried with various amounts of oxidant (Entry 2-10, Table 5B.3), and it was found that taking 0.15 mL (5 equiv.) of oxidant with 5 wt% HPUNC was sufficient for the rapid conversion of 1 mmol of phenyl boronic acid to phenol (Entry 7 vs 8, Table 5B.3).

To determine the scope and limitations of the current process, the optimized reaction conditions were implemented on electronically diverse aryl boronic acids (**Table 5B.4**). The reaction proceeded efficiently with aryl substrates carrying activating and deactivating substituents, recording yields upto 100%. Interestingly, the reaction yielded good results with polynuclear aromatic hydrocarbon (Entry 1d, Table 5B.4), sterically hindered (Entry 1i, Table 5B.4) as well as di-substituted (Entry 1j, Table 5B.4) substrates, respectively. Notably, the substrates with activating substituents afforded better yield and shorter reaction times compared to those with deactivating substituents. This observation can solely be attributed to inductive effects of the substituents on the boronic acid moiety on the *ipso*-position, influencing its reactivity accordingly.

Table 5B.4. Substrate study for oxidative *ipso*-hydroxylation of aryl boronic acids

Entry	R	Time (min)	Yield^a (%)
1a	H	30	100
1b	4-OCH$_3$	30	100
1c	4-Br	45	95
1d	2-naphthyl	30	100
1e	3-NO$_2$	60	90
1f	4-NO$_2$	45	90
1g	4-NH$_2$	30	100
1h	4-CH$_3$CH$_2$	30	100
1i	4-*tert*-butyl	30	100
1j	3,5-OCH$_3$	30	100

Reaction conditions: Phenyl boronic acid derivative (1 equiv., 0.121 g), H$_2$O$_2$ (30% aq., 5 equiv., 0.17 g, 0.15 mL), HPUNC catalyst (5 wt%), H$_2$O (2 mL), room temperature. ^{a}Isolated yield, purified by filter column chromatography and authenticated by NMR analyses (Page 5-50–5-61).

The reusability of a catalyst is an important aspect for an effective chemical protocol as well as the sustainability of the catalyst. In this context, the reusability of HPUNC was studied using the optimized reaction conditions with initially 10 mg (8.3 wt%) of catalyst loading. After completion of each cycle, the catalyst was filtered and washed with hot ethanol, water and then vacuum dried. Surprisingly, the catalyst displayed high efficiency and the reaction afforded excellent conversions even upto 10 cycles, without any significant loss of activity (**Table 5B.5**). This high efficacy of the catalyst can be assigned to the robust nature of the nanocomposite system. The enhanced mechanical properties of the nanocomposite provided longevity to the catalyst, thereby increasing its recyclability. At the same time, the heterogeneity of the catalyst enabled easy recovery by simple filtration. However, a slight loss of the catalyst was observed in the reaction medium after each cycle, that can be attributed to some amount of H_2O_2 oxidizing the HPU matrix during the reaction. However, this loss can be considered miniature compared to the overall amount of catalyst used.

Table 5B.5. Recovery and recyclability of catalyst using model reaction

Entry	Run	Time (min)	Conversion	Amount of catalyst recovered (mg)
1	1st	30	Complete	110
2	2nd	30	Complete	9.99
3	3rd	35	Complete	9.95
4	4th	40	Complete	9.90
5	5th	45	Complete	9.81
6	6th	45	Complete	9.75
7	7th	45	Complete	9.69
8	8th	50	Complete	9.66
9	9th	50	Complete	9.60
10	10th	60	Complete	9.50

Additionally, to further understand the physical aspect of activity of HPUNC catalyst, BET analysis was performed at liquid N_2 temperature. The N_2 adsorption-desorption isotherm of HPUNC resembled type IV with a combination of H1 and H3 hysteresis loop (**Figure 5B.6**). This type of isotherm is typical of mesoporous materials, which can be attributed to the hyperbranched nature of the HPUNC matrix. Also, the BET surface area analysis of HPUNC revealed a high surface area of 188.973 m^2g^{-1}, which was instrumental to the performance of the catalyst.
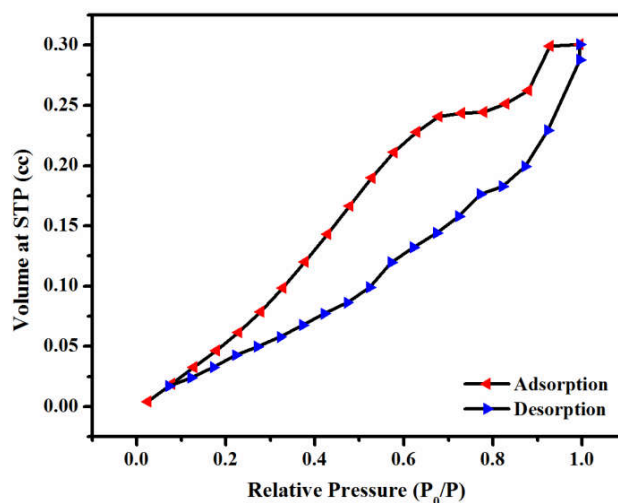
**Figure 5B.6.** N_2 adsorption-desorption isotherm of HPUNC catalyst.

In order to identify the basis of this catalytic activity, the model reaction was emulated with HPU, Pd-Ag@CQD nanohybrid and HPUNCs (**Table 5B.6**). The reaction was found to advance slowly in the presence of 5 wt% HPU, albeit with only upto 70% conversion (Entry 1, Table 5B.6). The presence of the polar functional groups in HPU matrix facilitated the oxidation of phenyl boronic acid by inherently activating the reactants. In better perspective, presence of 5 wt% Pd-Ag@CQD nanohybrid afforded upto 100% conversion within a very short time (Entry 2, Table 5B.6). The presence of Pd-Ag@CQD enhanced the oxidation process by virtue of its nano-dimensional activity. But tedious recovery and agglomeration of bare nanohybrid makes this protocol improbable. Applying the model reaction to HPUNCs provided better results in terms of efficiency, with high product conversion and easy catalyst recovery, although taking different reaction times. HPUNC0.5 afforded upto 80% conversion, however taking up a longer duration (Entry 3, Table 5B.6). Comparatively, HPUNC1.0 showed 90% conversion taking a lesser duration (Entry 4, Table 5B.6). Use of HPUNC2.0 provided the optimum result of complete product conversion within the shortest time (Entry 5, Table 5B.6). This suggested the role of Pd-Ag@CQD nanohybrid loading on the efficiency of the reaction, in terms of reaction time and product conversion. Increase of nanohybrid loading in the HPUNC introduced more amounts of active catalytic sites, thereby enhancing product conversion and rapidly reducing reaction time. Hence, even though both HPU and Pd-Ag@CQD nanohybrid played pivotal roles in the effectiveness of the model reaction, considering issues of protocol efficiency, catalyst recyclability and reusability, HPUNC provided a better route for rapid and effective *ipso*-hydroxylation of aryl boronic acids.

Table 5B.6. Comparison of the components and compositions of HPUNC using model reaction

Entry	Catalyst[a]	Time (min)	Conversion (%)
1	HPU	360	70
2	Pd-Ag@CQD	45	100
3	HPUNC0.5	240	82
4	HPUNC1.0	180	90
5	HPUNC2.0	30	100

[a]5 wt% with respect to phenyl boronic acid.

The exact mechanism for *ipso*-hydroxylation of aryl boronic acid is still not properly recognized. But based on mechanisms found in prior art involving heterogeneous/nano-based catalysts [36-38], a probable mechanism for the reaction is illustrated (**Scheme 5B.3**). Presumably, HPU-supported Pd-Ag@CQD nanohybrid entrapped H_2O_2 molecules on its surface, generating a reactive hydroperoxyl (HOO^-) species. Meanwhile, the supporting HPU matrix served to activate the aryl boronic acid molecules by polar functional moieties through secondary interactions, in its three-dimensional cage-like hyperbranched structure [39]. Subsequently, the aryl boronic acid consumed this hydroperoxyl species following a 1,2-migration of the aryl moiety and subsequent hydrolysis, lead to the formation of hydroxyl-aryl motif or phenol motif [36]. The synergistic combination of Pd-Ag@CQD nanohybrid and HPU matrix imparted dramatic catalytic enhancement, leading to shorter reaction times and high conversions. In overall, good dispersion of Pd-Ag@CQD offered high number of reactive sites and the mechanically reinforced HPU matrix provided a chemically stable heterogeneous reaction surface, manifesting in high catalyst recovery and recyclability.
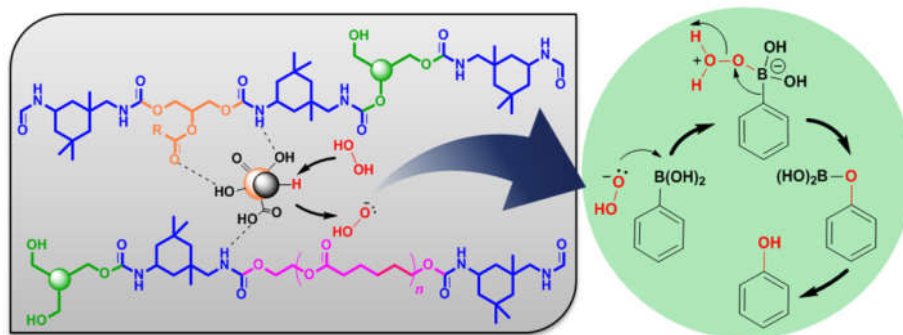
Scheme 5B.3. Probable mechanism of oxidative *ipso*-hydroxylation of aryl boronic acid catalyzed by HPUNC.

5B.4. Conclusion

The current chapter describes the suitability of Pd-Ag@CQD nanohybrid towards fabrication of bio-derived HPUNC by *in situ* polymerization technique. The nanohybrid and the HPU matrix combine effectively to form a well dispersed system, where the nanohybrid plays the role of reinforcing agent. The reinforcement of the HPU matrix ensures high performance of the nanocomposite. The nanocomposite acts as robust, efficient and sustainable catalyst for rapid *ipso*-hydroxylation mediated conversion of aryl boronic acids to phenols under ambient conditions. The nanocomposites possess good potential for future practical applications in material and catalytic technologies.

NMR spectral data of the products of Table 5B.3

Phenol (Table 5B.3, Entry 1a)
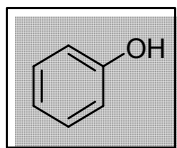
^{1}H NMR (400 MHz, CDCl$_3$): δ 7.44 – 7.06 (m, 2H), 6.99 – 6.90 (m, 1H), 6.90 – 6.80 (m, 2H), 6.39 (s, 1H); ^{13}C NMR (100 MHz, CDCl$_3$): δ 155.47, 129.88, 120.96, 115.54.

4-methoxyphenol (Table 5B.3, Entry 1b)
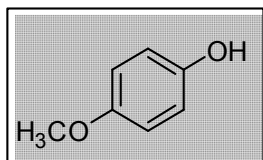
^{1}H NMR (400 MHz, CDCl$_3$) δ 6.77 (s, 4H), 5.94 (s, 1H), 3.75 (s, 3H); ^{13}C NMR (101 MHz, CDCl$_3$) δ 153.57, 149.80, 116.22, 114.99, 55.95.

4-bromophenol (Table 5B.3, Entry 1c)
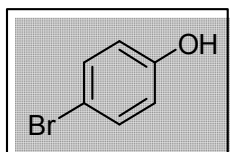
^{1}H NMR (400 MHz, CDCl$_3$) δ 7.31 (m, 2H), 6.77 – 6.62 (m, 2H), 5.61 (s, 1H); ^{13}C NMR (100 MHz, CDCl$_3$) δ 154.77, 132.55, 132.54, 117.32, 112.88.

2-naphthol (Table 5B.3, Entry 1d)
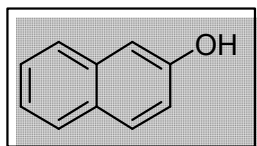
^{1}H NMR (400 MHz, CDCl$_3$): δ 7.81 – 7.71 (m, 1H), 7.67 (d, J = 8.3 Hz, 1H), 7.42 (ddd, J = 8.1, 7.0, 1.0 Hz, 1H), 7.37 – 7.28 (m, 1H), 7.14 (d, J = 2.5 Hz, 1H), 7.09 (dd, J = 8.8, 2.5 Hz, 1H), 4.99 (s, 1H); ^{13}C NMR (100 MHz, CDCl$_3$) δ 153.39, 134.65, 129.95, 129.02, 127.85, 126.62, 126.44, 123.71, 117.79, 109.56.

3-nitrophenol (Table 5B.3, Entry 1e)
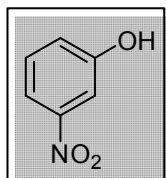
^{1}H NMR (400 MHz, CDCl$_3$) δ 7.84 – 7.76 (m, 1H), 7.69 (t, *J* = 8 Hz, 1H), 7.40 (t, *J* = 8 Hz, 1H), 7.21 – 7.13 (m, 1H), 5.56 (s, 1H); ^{13}C NMR (100 MHz, CDCl$_3$) δ 156.31, 130.39, 122.01, 116.01, 110.61.

4-nitrophenol (Table 5B.3, Entry 1f)
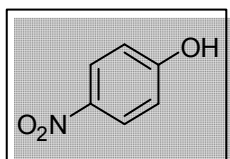
^{1}H NMR (400 MHz, CDCl$_3$) δ 8.17 (d, *J* = 8 Hz, 2H), 6.95 (d, *J* = 8 Hz, 2H), 6.58 (s, 1H); ^{13}C NMR (100 MHz, CDCl$_3$) δ 161.96, 141.38, 126.51, 115.96.

4-aminophenol (Table 5B.3, Entry 1g)
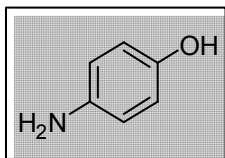
^{1}H NMR (400 MHz, DMSO-d$_6$) δ 8.31 (s, 1H), 6.54 – 6.28 (m, 4H), 4.33 (s, 2H); ^{13}C NMR (101 MHz, DMSO-d$_6$) δ 148.74, 141.16, 116.06, 115.77.
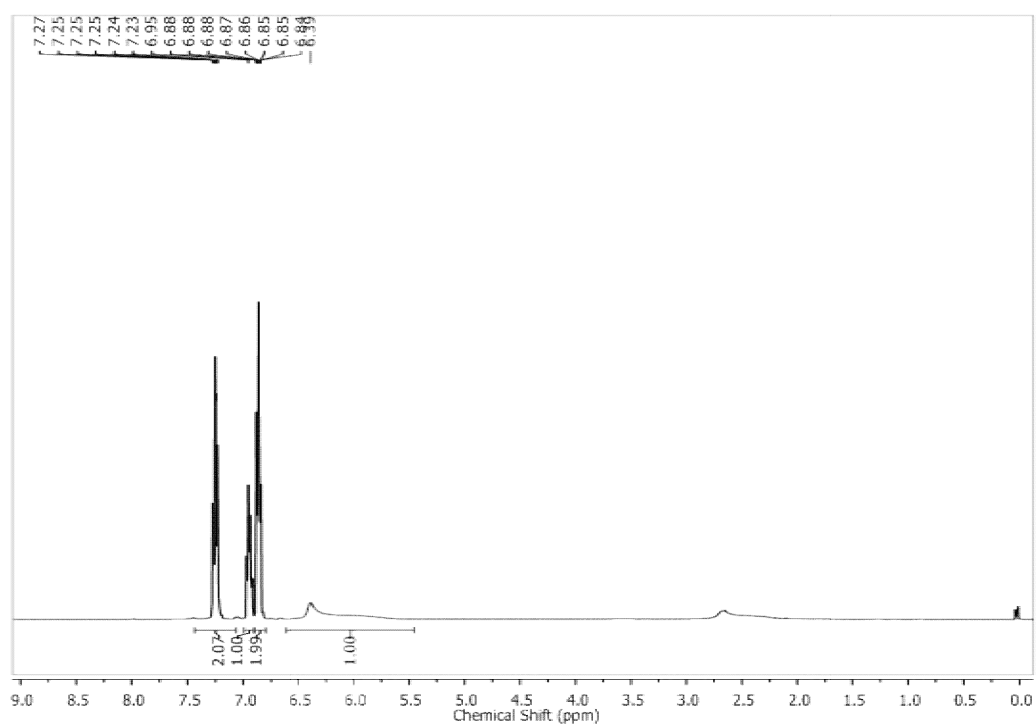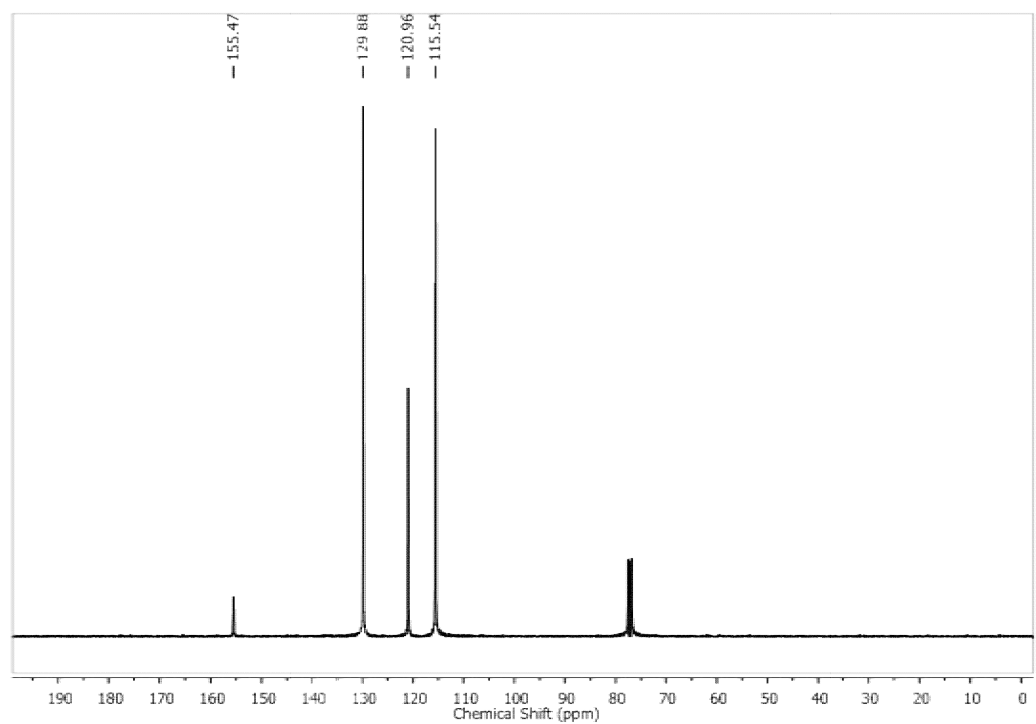
4-ethylphenol (Table 5B.3, Entry 1h)
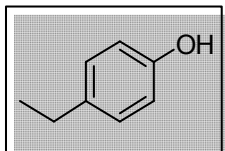
^{1}H NMR (400 MHz, CDCl$_3$) δ 7.05 (m, 2H), 6.76 (m, 2H), 5.46 (s, 1H), 2.56 (q, *J* = 8 Hz, 2H), 1.19 (t, *J* = 8 Hz, 3H); ^{13}C NMR (101 MHz, CDCl$_3$) δ 153.82, 136.29, 128.92, 115.22, 28.05, 15.97.
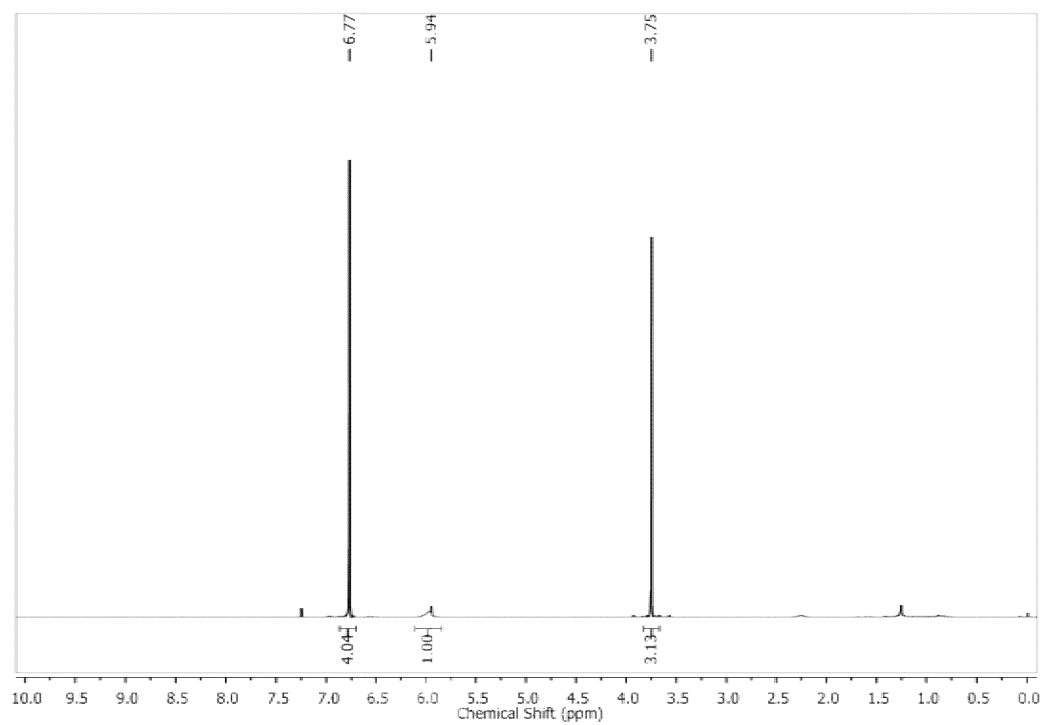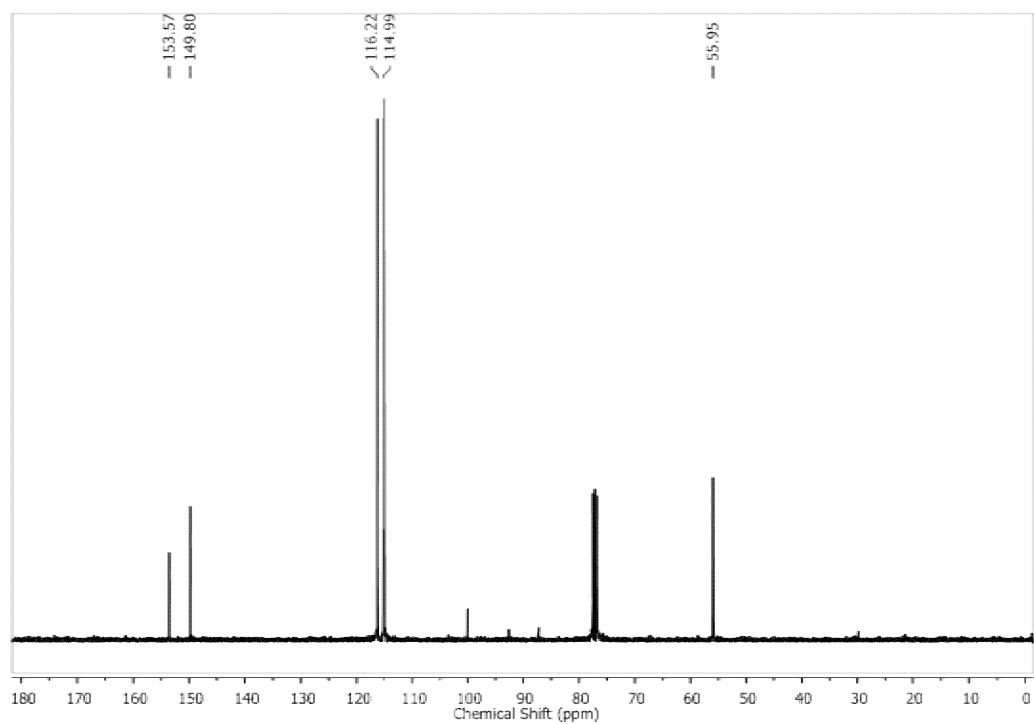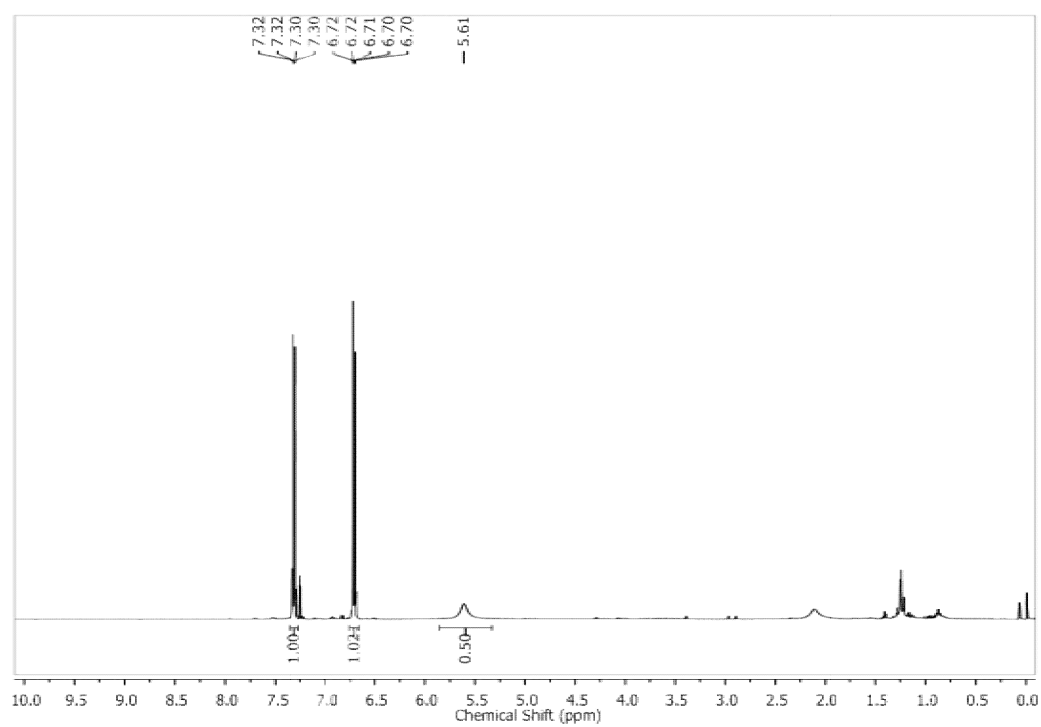
4-*tert*-butylphenol (Table 5B.3, Entry 1i)
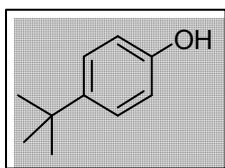
^{1}H NMR (400 MHz, CDCl$_3$) δ 7.27 (m, 2H), 6.83 (m, 2H), 5.88 (s, 1H), 1.33 – 1.30 (m, 9H); ^{13}C NMR (100 MHz, CDCl$_3$); ^{13}C NMR (100 MHz, CDCl$_3$) δ 152.98, 143.81, 126.65, 115.04, 34.23, 34.21, 31.67.

**3,5-dimethoxyphenol (Table 5B.3, Entry 1j)**
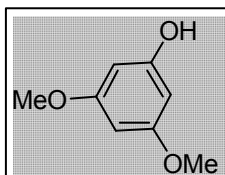
^{1}H NMR (400 MHz, CDCl$_3$) δ 6.67 – 6.53 (m, 1H), 6.47 (dd, *J* = 1.2, 0.6 Hz, 2H), 5.11 (s, 1H), 2.27 (s, 6H); ^{13}C NMR (100 MHz, CDCl$_3$) δ 155.42, 139.67, 122.69, 113.15, 21.35.
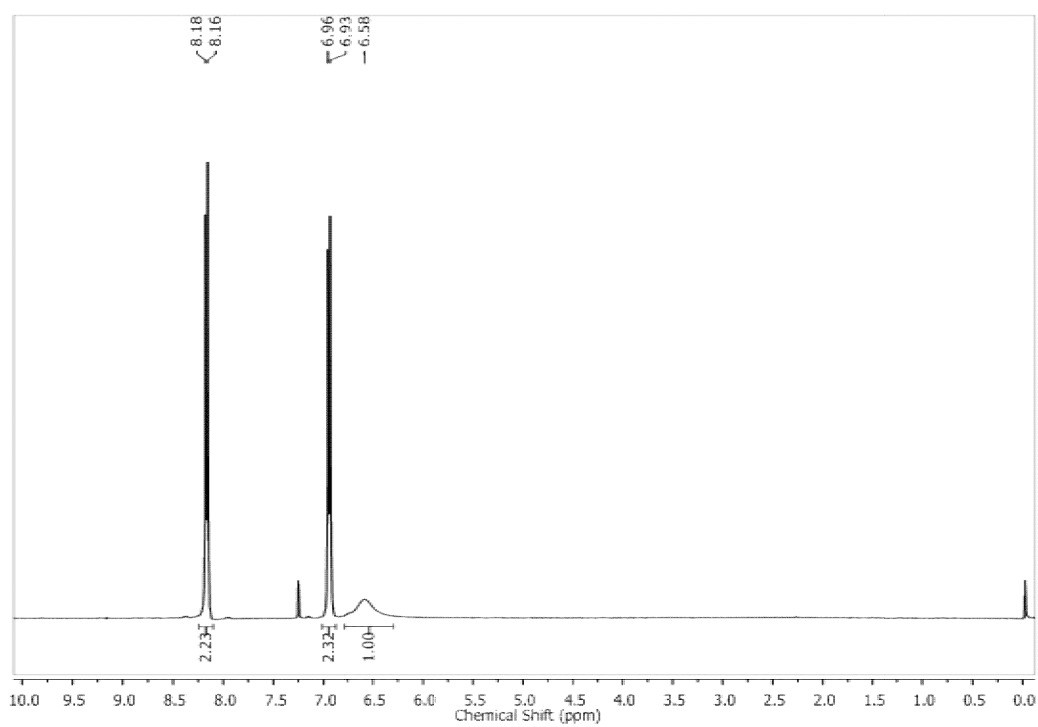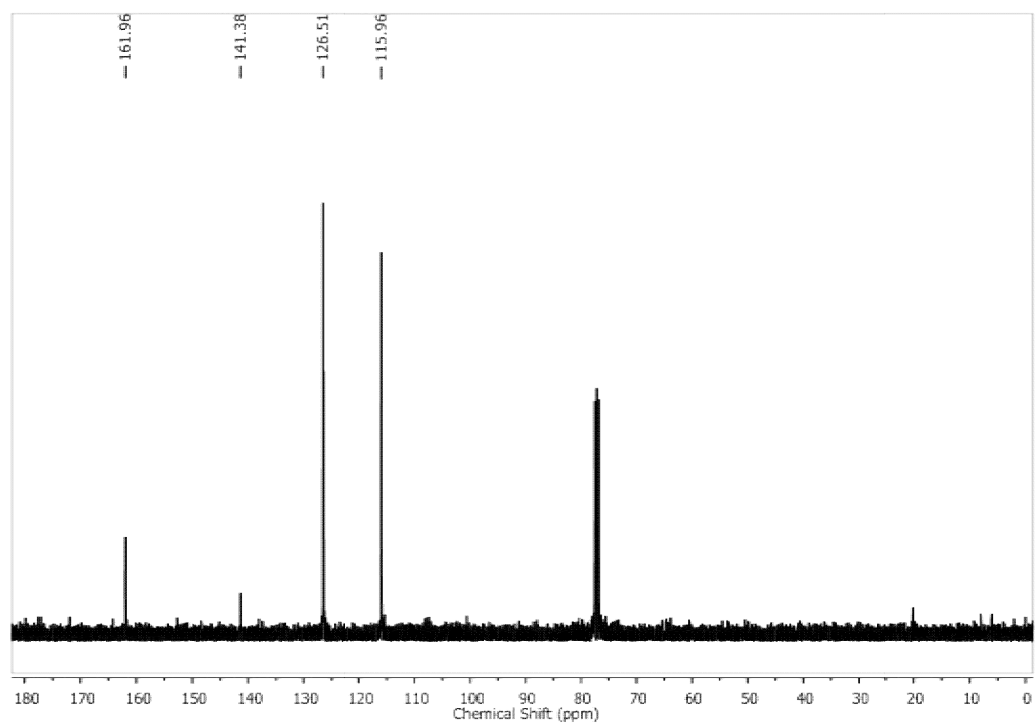
¹H NMR spectrum of phenol (Table 5B.3, Entry 1a):

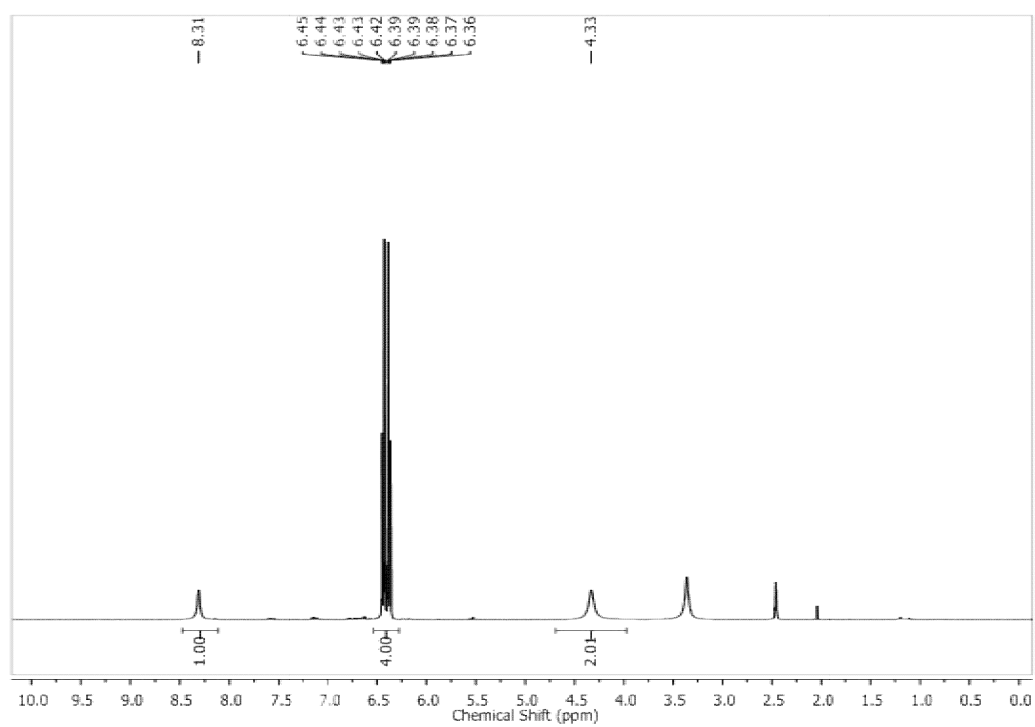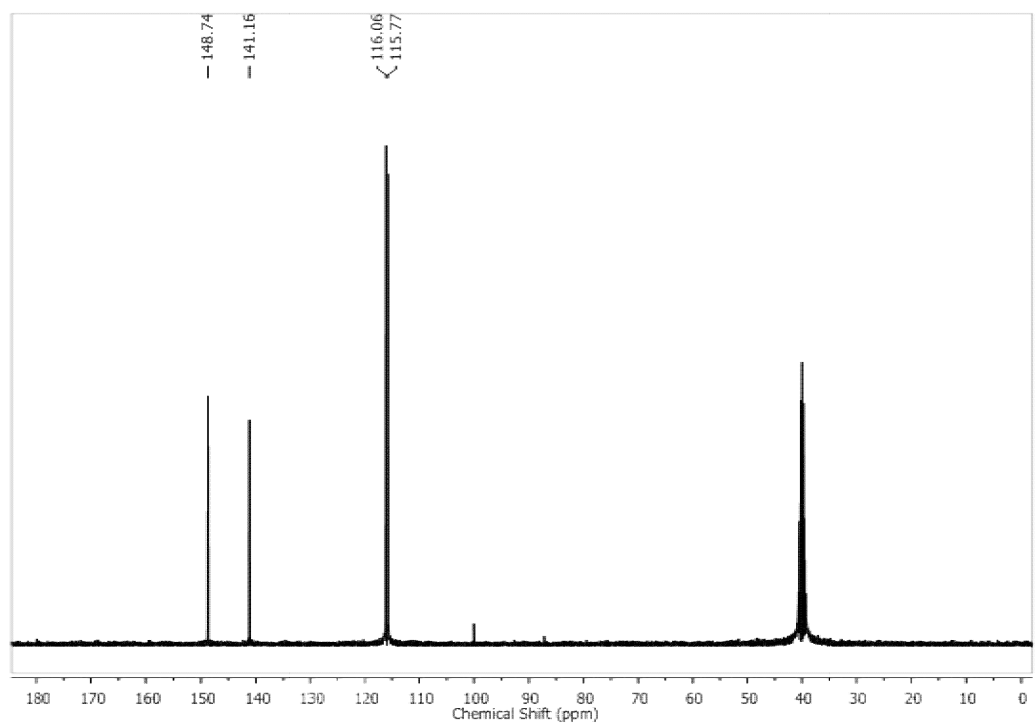**¹³C NMR spectrum of phenol (Table 5B.3, Entry 1a):**

¹H NMR spectrum of 4-methoxyphenol (Table 5B.3, Entry 1b):

¹³C NMR spectrum of 4-methoxyphenol (Table 5B.3, Entry 1b):

^{1}H NMR spectrum of 4-bromophenol (Table 5B.3, Entry 1c):

^{13}C NMR spectrum of 4-bromophenol (Table 5B.3, Entry 1c):
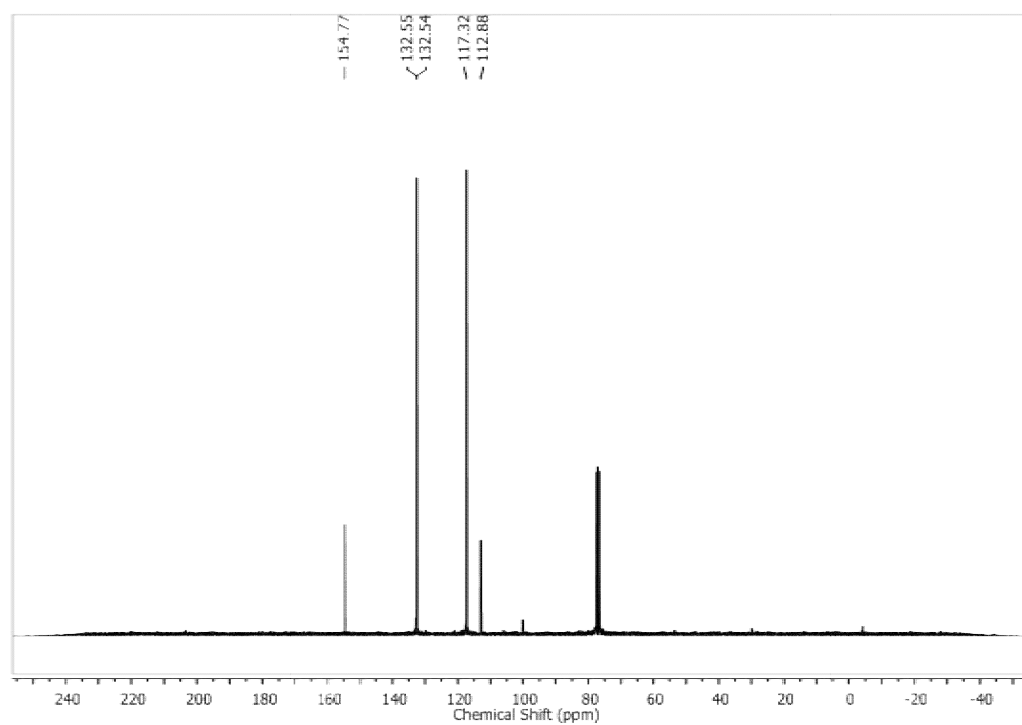
^{1}H NMR spectrum of 2-naphthol (Table 5B.3, Entry 1d):
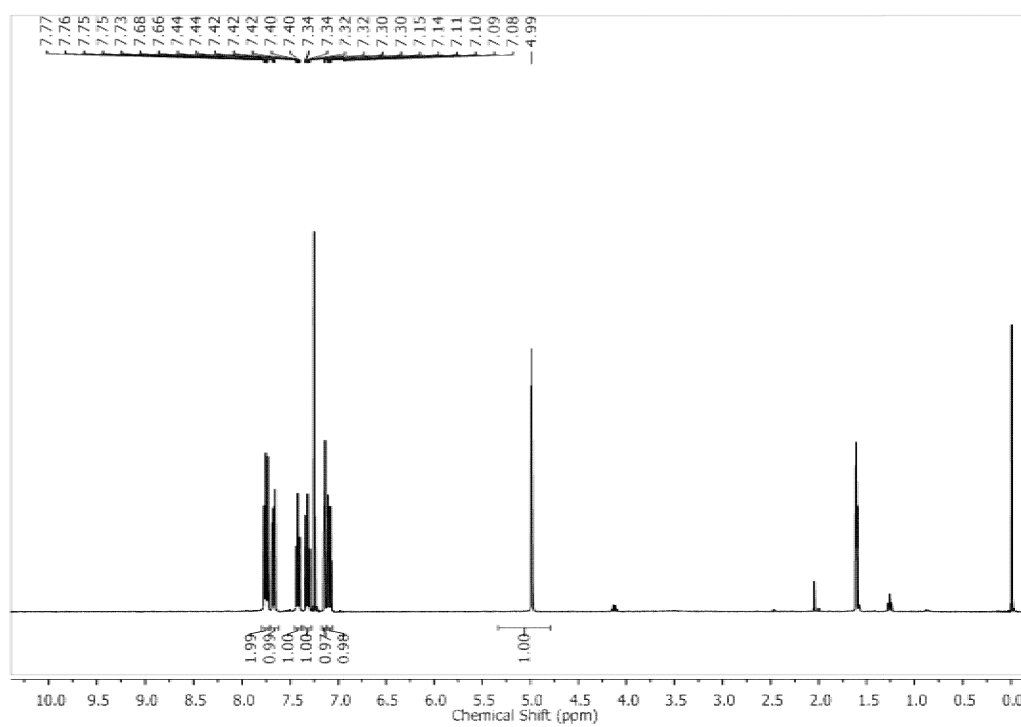
^{13}C NMR spectrum of 2-naphthol (Table 5B.3, Entry 1d):
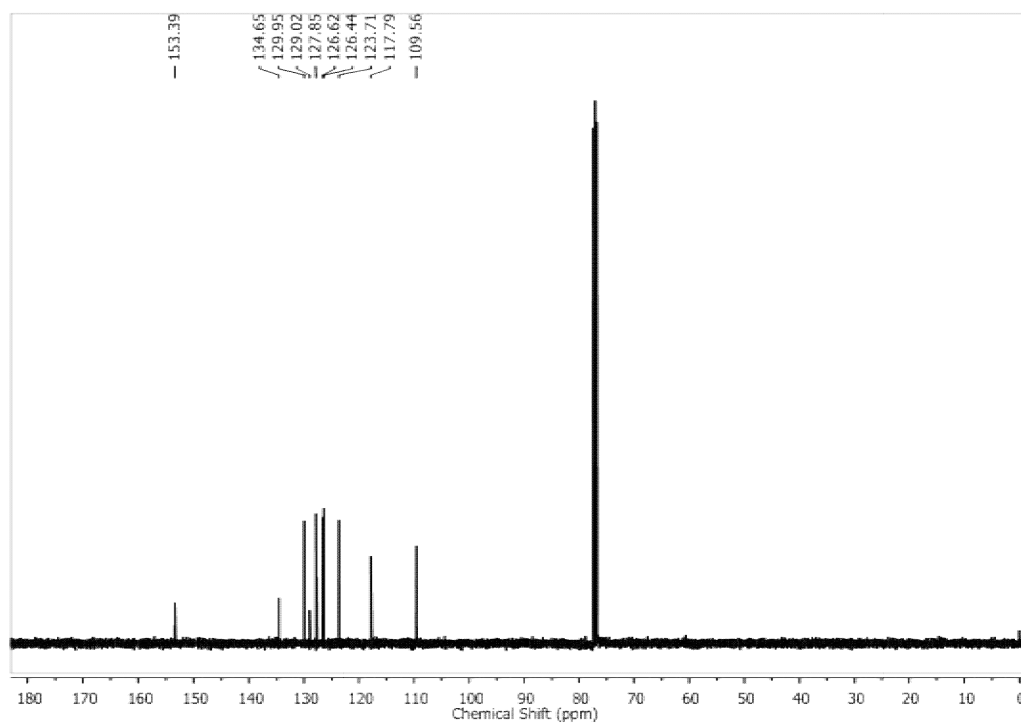
1H NMR spectrum of 3-nitrophenol (Table 5B.3, Entry 1e):
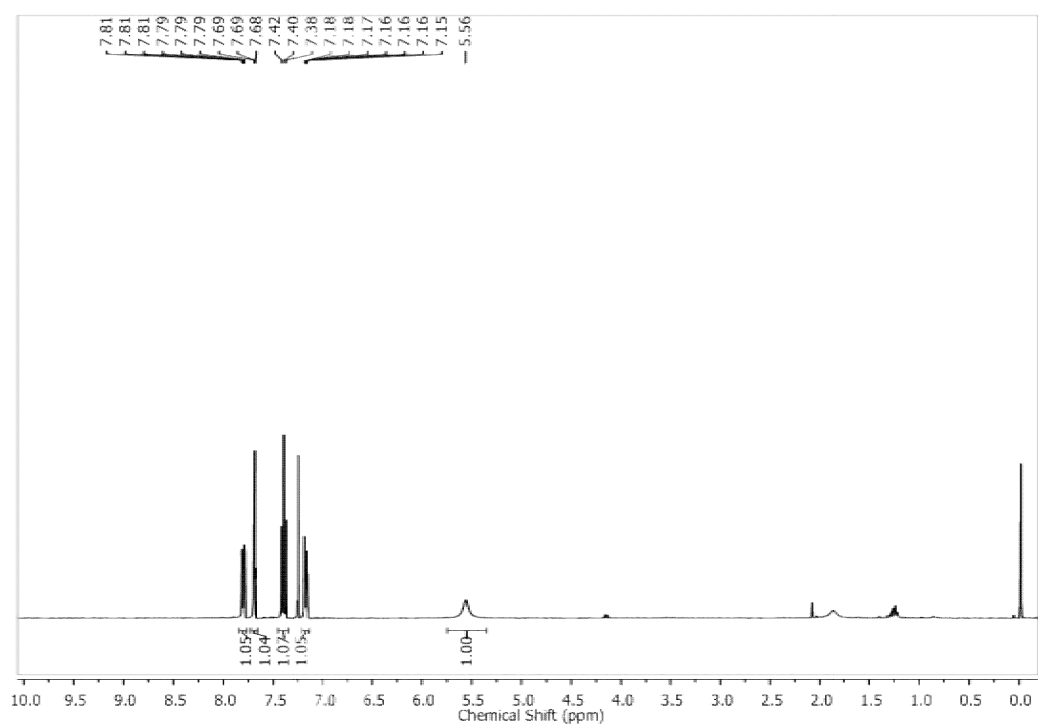
13C NMR spectrum of 3-nitrophenol (Table 5B.3, Entry 1e):
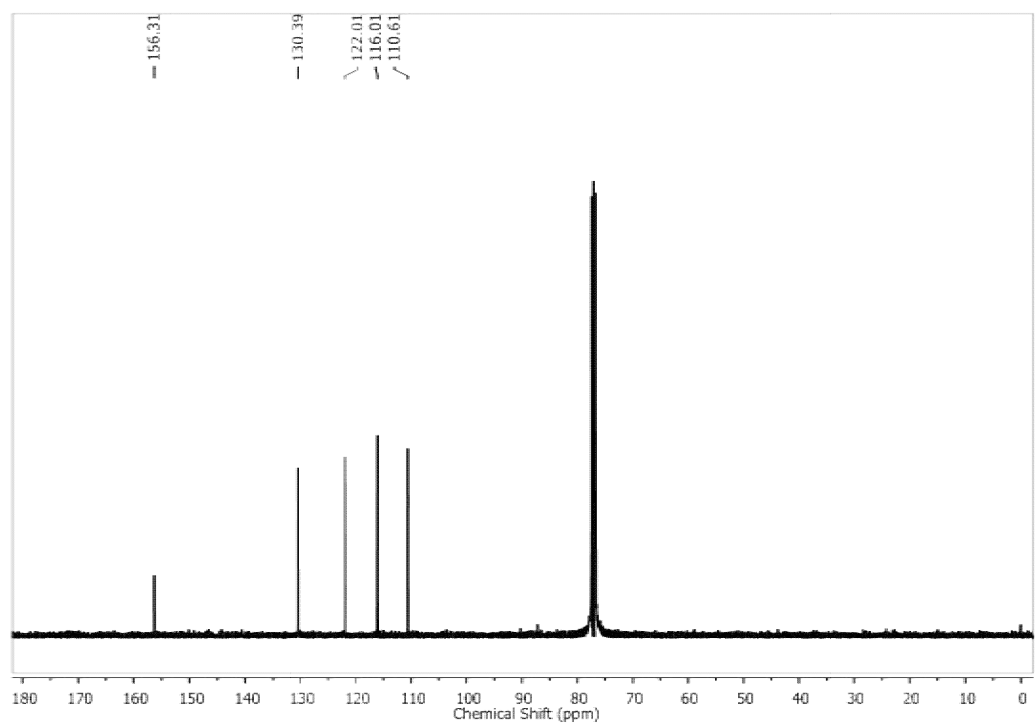
¹H NMR spectrum of 4-nitrophenol (Table 5B.3, Entry 1f):

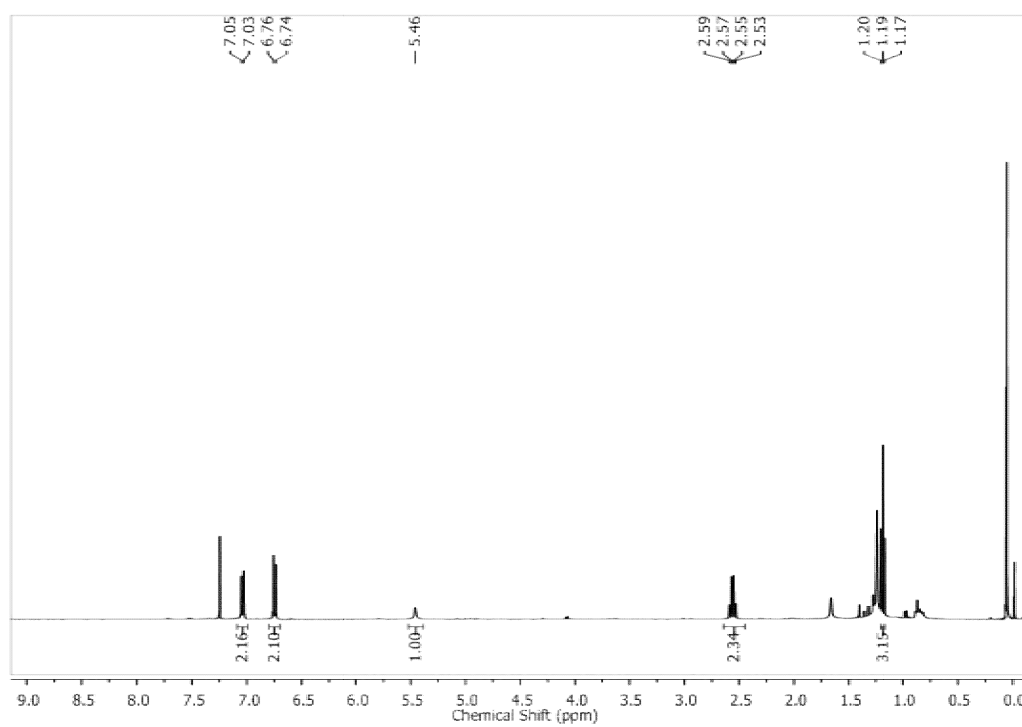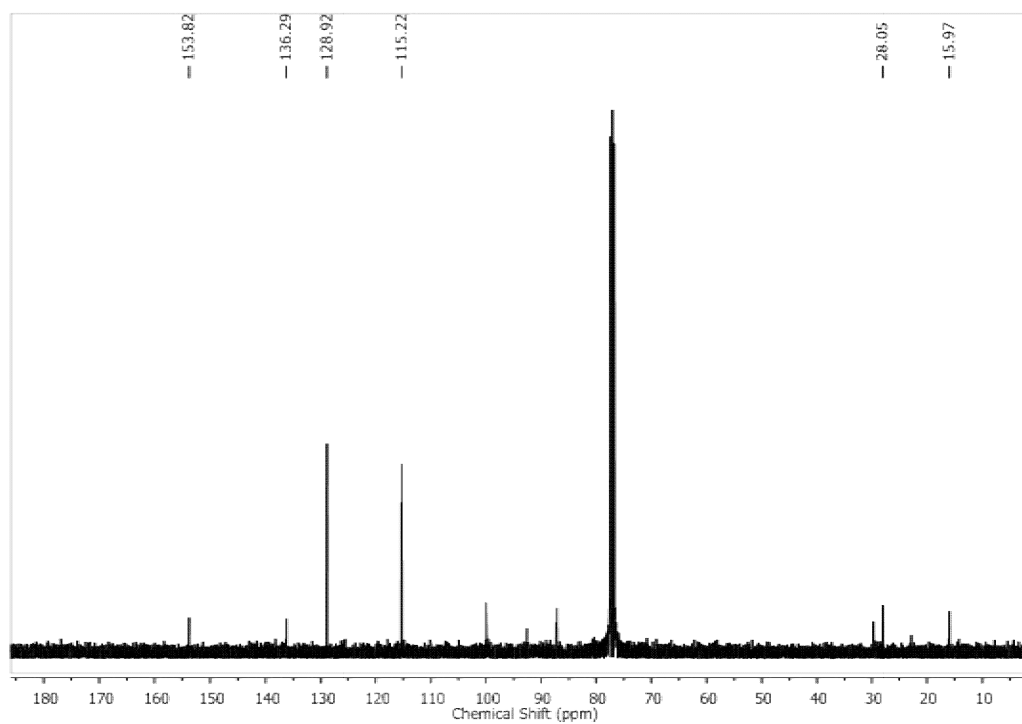**¹³C NMR spectrum of 4-nitrophenol (Table 5B.3, Entry 1f)**

^{1}H NMR spectrum of 4-aminophenol (Table 5B.3, Entry 1g):

^{13}C NMR spectrum of 4-aminophenol (Table 5B.3, Entry 1g):

¹H NMR spectrum of 4-ethylphenol (Table 5B.3, Entry 1h):

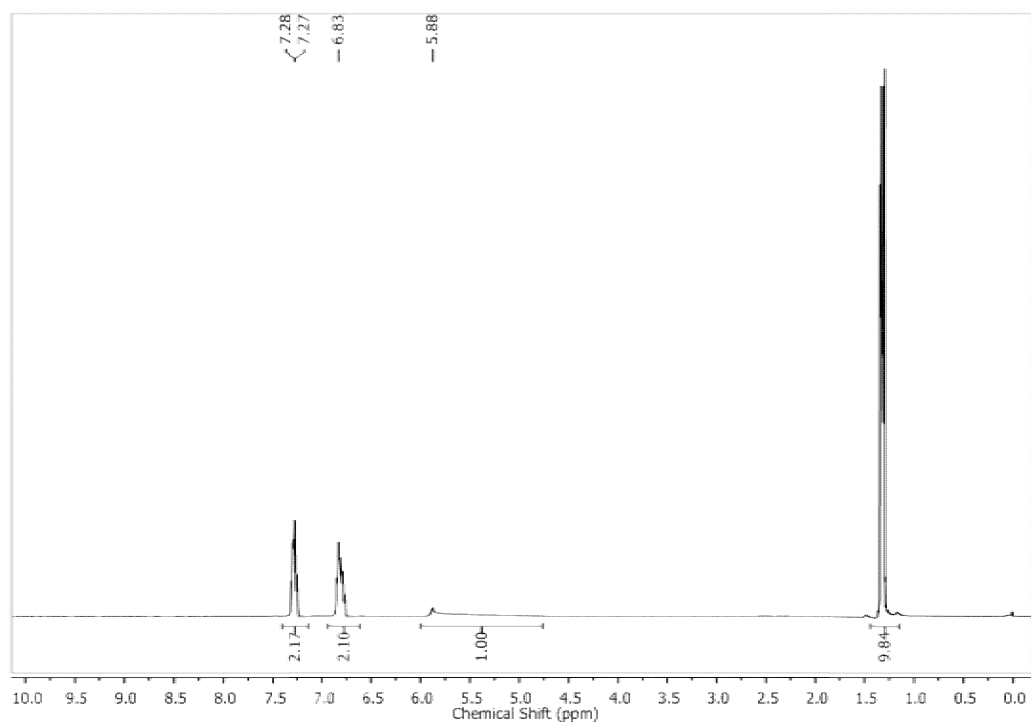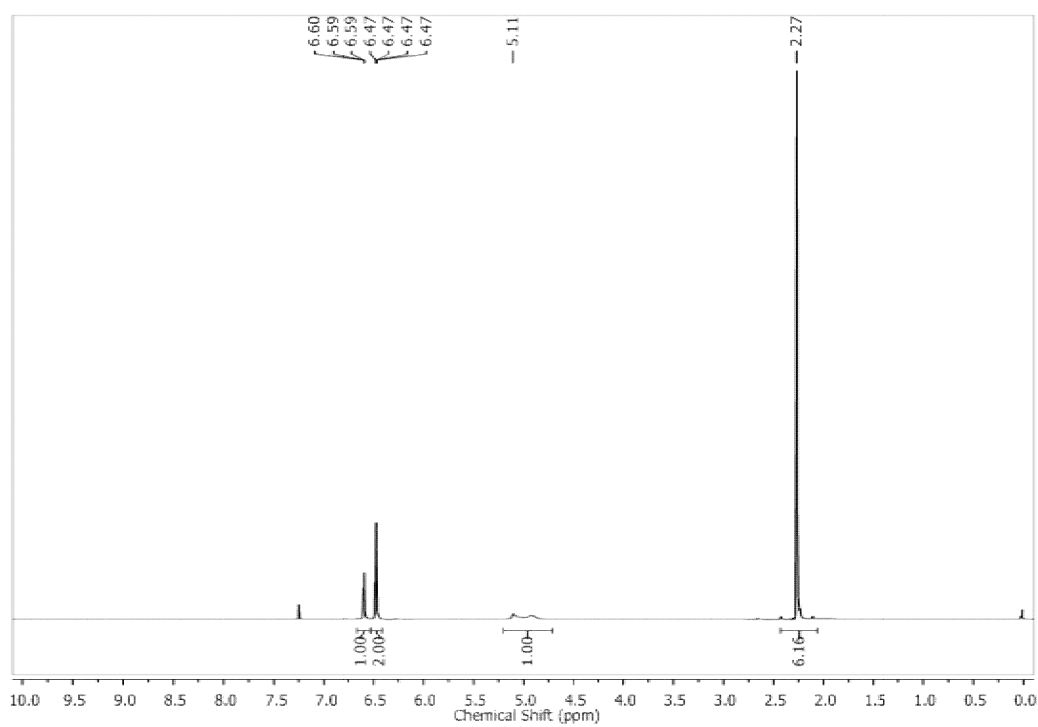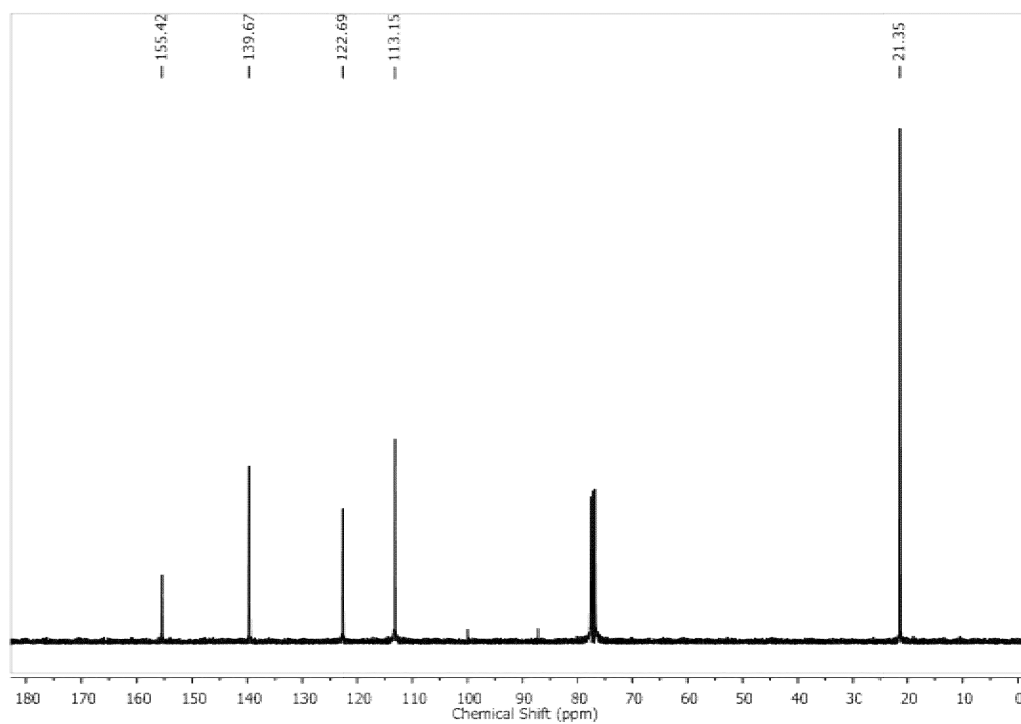**¹³C NMR spectrum of 4-ethylphenol (Table 5B.3, Entry 1h):**

¹H NMR spectrum of 4-*tert*-butylphenol (Table 5B.3, Entry 1i):

¹³C NMR spectrum of 4-*tert*-butylphenol (Table 5B.3, Entry 1i)
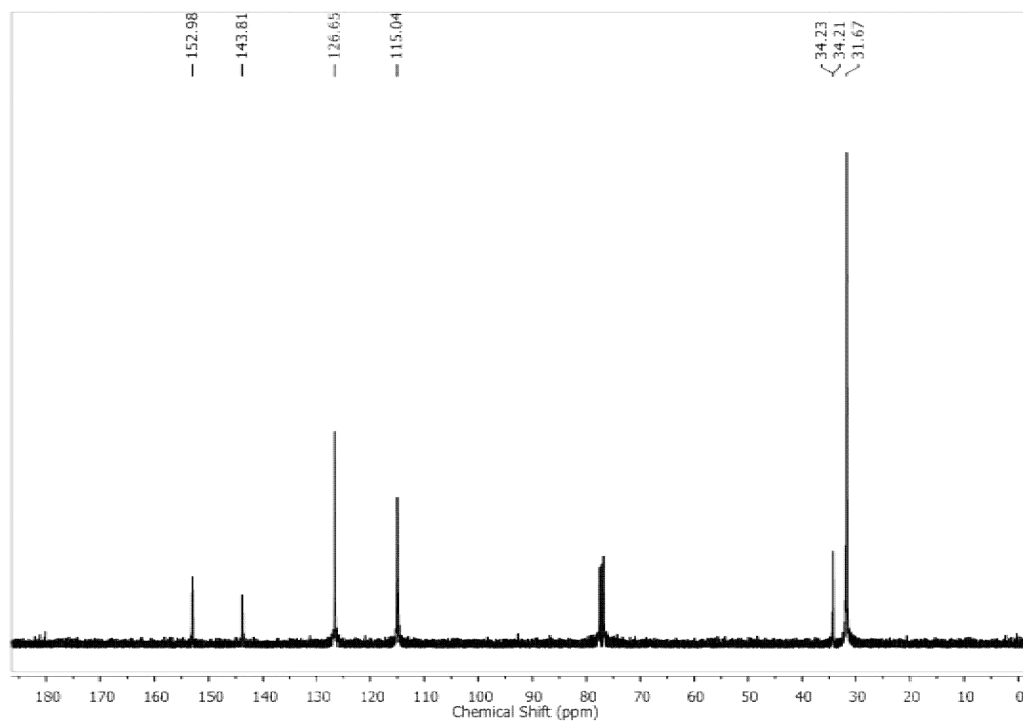
¹H NMR spectrum of 3,5-dimethoxyphenol (Table 5B.3, Entry 1j):

¹³C NMR spectrum of 3,5-dimethoxyphenol (Table 5B.3, Entry 1j):

References

[1]   Li, H., He, X., Kang, Z., Huang, H., Liu, Y., Liu, J., Lian, S., Tsang, C. H. A., Yang, X., and Lee, S. T. Water-soluble fluorescent carbon quantum dots and photocatalyst design. *Angewandte Chemie International Edition*, 49(26):4430-4434, 2010.

[2]   Wang, Y. and Hu, A. Carbon quantum dots: synthesis, properties and applications. *Journal of Materials Chemistry C*, 2(34):6921-6939, 2014.

[3]   Lim, S. Y., Shen, W., and Gao, Z. Carbon quantum dots and their applications. *Chemical Society Reviews*, 44(1):362-381, 2015.

[4]   Zhang, S., Wu, W., Xiao, X., Zhou, J., Xu, J., Ren, F., and Jiang, C. Polymer-supported bimetallic Ag@AgAu nanocomposites: synthesis and catalytic properties. *Chemistry–An Asian Journal*, 7(8):1781-1788, 2012.

[5]   Das, V. K., Gogoi, S., Choudary, B. M., and Karak, N. A promising catalyst for exclusive *para* hydroxylation of substituted aromatic hydrocarbons under UV light. *Green Chemistry*, 19(18):4278-4283, 2017.

[6]   Ma, R., Yang, P., and Bian, F. Magnetic dendritic polymer nanocomposites as supports for palladium: a highly efficient and reusable catalyst for Mizoroki–Heck and Suzuki–Miyaura coupling reactions. *New Journal of Chemistry*, 42(6):4748-4756, 2018.

[7]   Alonso, D. A., Nájera, C., Pastor, I. M., and Yus, M. Transition-metal-catalyzed synthesis of hydroxylated arenes. *Chemistry–A European Journal*, 16(18):5274-5284, 2010.

[8]   Tyman, J. H. P. *Synthetic and Natural Phenols*. Elsevier, New York, 1996.

[9]   Hanson, P., Jones, J. R., Taylor, A. B., Walton, P. H., and Timms, A. W. Sandmeyer reactions. Part 7. An investigation into the reduction steps of Sandmeyer hydroxylation and chlorination reactions. *Journal of the Chemical Society, Perkin Transactions*, 2(6):1135-1150, 2002.

[10]   Sergeev, A. G., Schulz, T., Torborg, C., Spannenberg, A., Neumann, H., and Beller, M. Palladium-catalyzed hydroxylation of aryl halides under ambient conditions. *Angewandte Chemie International Edition*, 48(41):7595-7599, 2009.

[11]   Mahanta, A., Adhikari, P., Bora, U., and Thakur, A. J. Biosilica as an efficient heterogeneous catalyst for *ipso*-hydroxylation of arylboronic acids. *Tetrahedron Letters*, 56(14):1780-1783, 2015.

[12]   Gogoi, A. and Bora, U. An iodine-promoted, mild and efficient method for the synthesis of phenols from arylboronic acids. *Synlett*, 23(07):1079-1081, 2012.

[13]   Gogoi, A. and Bora, U. A mild and efficient protocol for the *ipso*-hydroxylation of arylboronic acids. *Tetrahedron Letters*, 54(14):1821-1823, 2013.

[14]   Gohain, M., du Plessis, M., van Tonder, J. H., and Bezuidenhoudt, B. C. Preparation of phenolic compounds through catalyst-free *ipso*-hydroxylation of arylboronic acids. *Tetrahedron Letters*, 55(13):2082-2084, 2014.

[15]   Gogoi, P., Bezboruah, P., Gogoi, J., and Boruah, R. C. *ipso*-Hydroxylation of arylboronic acids and boronate esters by using sodium chlorite as an oxidant in water. *European Journal of Organic Chemistry*, 2013(32):7291-7294, 2013.

[16]   Kianmehr, E., Yahyaee, M., and Tabatabai, K. A mild conversion of arylboronic acids and their pinacolyl boronate esters into phenols using hydroxylamine. *Tetrahedron Letters*, 48(15):2713-2715, 2007.

[17]   Guo, S., Lu, L., and Cai, H. Base-promoted, mild and highly efficient conversion of arylboronic acids into phenols with *tert*-butyl hydroperoxide. *Synlett*, 24(13):1712-1714, 2013.

[18]   Xu, J., Wang, X., Shao, C., Su, D., Cheng, G., and Hu, Y. Highly efficient synthesis of phenols by copper-catalyzed oxidative hydroxylation of arylboronic acids at room temperature in water. *Organic Letters*, 12(9):1964-1967, 2010.

[19]   Gogoi, K., Dewan, A., Gogoi, A., Borah, G., and Bora, U. Boric acid as highly efficient catalyst for the synthesis of phenols from arylboronic acids. *Heteroatom Chemistry*, 25(2):127-130, 2014.

[20]   Saikia, E., Bora, S. J., and Chetia, B. H_2O_2 in WERSA: An efficient green protocol for *ipso*-hydroxylation of aryl/heteroarylboronic acid. *RSC Advances*, 5(124):102723-102726, 2015.

[21]   Mulakayala, N., Kumar, K. M., Rapolu, R. K., Kandagatla, B., Rao, P., Oruganti, S., and Pal, M. Catalysis by Amberlite IR-120 resin: a rapid and green method for the synthesis of phenols from arylboronic acids under metal, ligand, and base-free conditions. *Tetrahedron Letters*, 53(45):6004-6007, 2012.

[22]   Begum, T., Gogoi, A., Gogoi, P. K., and Bora, U. Catalysis by mont K-10 supported silver nanoparticles: a rapid and green protocol for the efficient *ipso*-hydroxylation of arylboronic acids. *Tetrahedron Letters*, 56(1):95-97, 2015.

[23]   Chatterjee, N. and Goswami, A. Organic hypervalent iodine (III) catalyzed *ipso*-hydroxylation of aryl-and alkylboronic acids/esters. *Tetrahedron Letters*, 56(12):1524-1527, 2015.

[24]   Yi, H. and Lei, A. Pd-catalyzed hydroxylation of aryl boronic acids using *in situ* generated hydrogen peroxide. *Chemistry–A European Journal*, 23(42):10023-10027, 2017.

[25]   Chng, L. L., Erathodiyil, N., and Ying, J. Y. Nanostructured catalysts for organic transformations. *Accounts of Chemical Research*, 46(8):1825-1837, 2013.

[26]   Liu, J., Gao, Y., Cao, D., Zhang, L., and Guo, Z. Nanoparticle dispersion and aggregation in polymer nanocomposites: insights from molecular dynamics simulation. *Langmuir*, 27(12):7926-7933, 2011.

[27]   De, B., Voit, B., and Karak, N. Transparent luminescent hyperbranched epoxy/carbon oxide dot nanocomposites with outstanding toughness and ductility. *ACS Applied Materials & Interfaces*, 5(20):10027-10034, 2013.

[28]   Gogoi, S., Kumar, M., Mandal, B. B., and Karak, N. High performance luminescent thermosetting waterborne hyperbranched polyurethane/carbon quantum dot nanocomposite with *in vitro* cytocompatibility. *Composites Science and Technology*, 118:39-46, 2015.

[29]   Hazarika, D. and Karak, N. Biodegradable tough waterborne hyperbranched polyester/carbon dot nanocomposite: approach towards an eco-friendly material. *Green Chemistry*, 18(19):5200-5211, 2016.

[30]   Bayan, R. and Karak, N. Renewable resource modified polyol derived aliphatic hyperbranched polyurethane as a biodegradable and UV-resistant smart material. *Polymer International*, 66(6):839-850, 2017.

[31]   Rana, S., Karak, N., Cho, J. W., and Kim, Y. H. Enhanced dispersion of carbon nanotubes in hyperbranched polyurethane and properties of nanocomposites. *Nanotechnology*, 19(49):495707, 2008.

[32]   Thakur, S. and Karak, N. Ultratough, ductile, castor oil-based, hyperbranched, polyurethane nanocomposite using functionalized reduced graphene oxide. *ACS Sustainable Chemistry & Engineering*, 2(5):1195-1202, 2014.

[33]   Ghosh, B., Gogoi, S., Thakur, S., and Karak, N. Bio-based waterborne polyurethane/carbon dot nanocomposite as a surface coating material. *Progress in Organic Coatings*, 90:324-330, 2016.

[34]   Bayan, R. and Karak, N. Photo-assisted synthesis of a Pd–Ag@CQD nanohybrid and its catalytic efficiency in promoting the Suzuki–Miyaura cross-coupling reaction under ligand-free and ambient conditions. *ACS Omega*, 2(12):8868-8876, 2017.

[35]   De, B., Voit, B., and Karak, N. Carbon dot reduced Cu_2O nanohybrid/hyperbranched epoxy nanocomposite: mechanical, thermal and photocatalytic activity. *RSC Advances*, 4(102):58453-58459, 2014.

[36]   Lennox, A. J. and Lloyd-Jones, G. C. Selection of boron reagents for Suzuki–Miyaura coupling. *Chemical Society Reviews*, 43(1):412-443, 2014.

[37]   Borah, R., Saikia, E., Bora, S. J., and Chetia, B. Banana pulp extract mediated synthesis of Cu_2O nanoparticles: an efficient heterogeneous catalyst for the *ipso*-hydroxylation of arylboronic acids. *Tetrahedron Letters*, 58(12):1211-1215, 2017.

[38]   Saikia, I., Hazarika, M., Hussian, N., Das, M. R., and Tamuly, C. Biogenic synthesis of $Fe_2O_3@SiO_2$ nanoparticles for *ipso*-hydroxylation of boronic acid in water. *Tetrahedron Letters*, 58(45):4255-4259, 2017.

[39]   Zheng, Y., Li, S., Weng, Z., and Gao, C. Hyperbranched polymers: advances from synthesis to applications. *Chemical Society Reviews*, 44(12):4091-4130, 2015.